



<https://theses.gla.ac.uk/>

Theses Digitisation:

<https://www.gla.ac.uk/myglasgow/research/enlighten/theses/digitisation/>

This is a digitised version of the original print thesis.

Copyright and moral rights for this work are retained by the author

A copy can be downloaded for personal non-commercial research or study, without prior permission or charge

This work cannot be reproduced or quoted extensively from without first obtaining permission in writing from the author

The content must not be changed in any way or sold commercially in any format or medium without the formal permission of the author

When referring to this work, full bibliographic details including the author, title, awarding institution and date of the thesis must be given

Enlighten: Theses

<https://theses.gla.ac.uk/>
research-enlighten@glasgow.ac.uk



UNIVERSITY
of
GLASGOW

Studies of the Cholesterol-Dependent Cytolysins

A thesis submitted to the University of Glasgow for the degree of
Doctor of Philosophy

by

Graeme James Macfarlane Cowan

Division of Infection and Immunity
Institute of Biomedical and Life Sciences
Glasgow Biomedical Research Centre
University of Glasgow
120 University Place
Glasgow G12 8TA

Submitted September 2006

© Graeme Cowan 2006

ProQuest Number: 10390613

All rights reserved

INFORMATION TO ALL USERS

The quality of this reproduction is dependent upon the quality of the copy submitted.

In the unlikely event that the author did not send a complete manuscript and there are missing pages, these will be noted. Also, if material had to be removed, a note will indicate the deletion.



ProQuest 10390613

Published by ProQuest LLC (2017). Copyright of the Dissertation is held by the Author.

All rights reserved.

This work is protected against unauthorized copying under Title 17, United States Code
Microform Edition © ProQuest LLC.

ProQuest LLC.
789 East Eisenhower Parkway
P.O. Box 1346
Ann Arbor, MI 48106 – 1346

GLASGOW
UNIVERSITY
LIBRARY:

Declaration

This thesis is the original work of the author except where otherwise stated.

Graeme Cowan

Abstract

The cholesterol-dependent cytolysins (CDCs) are a group of toxins produced by several genera of Gram-positive bacteria, that bind to and form large oligomeric pores in target cell membranes that contain cholesterol. In addition to cell lysis, a great number of other biological functions have been described for many members of the group, including induction of cytokine release and complement activation. Some of the CDCs have been shown to be critical virulence factors of their producing organisms and immunisation with a number of the CDCs has been shown to be protective against disease caused by those producing organisms. The CDCs are also being used in a diverse array of applications that utilise their pore-forming and toxic properties, including anti-cancer therapy, anti-viral therapy and cell biology.

Pneumolysin (PLY) is a member of the CDCs produced by *S. pneumoniae* and is an important virulence factor and vaccine candidate. A deletion mutant of PLY, $\Delta 6$ PLY, has been described (Kirkham *et al.*, 2006b), and this mutant is capable of cell binding but incapable of pore formation. Enhanced green fluorescent protein (eGFP) tagged forms of PLY and $\Delta 6$ PLY were produced and the tagged toxins had similar haemolytic and cytotoxic effects to the parent toxins. Toxin binding to host cells was visualised by epifluorescence microscopy and laser scanning confocal fluorescence microscopy. Binding of the tagged toxins to erythrocytes could also be measured by flow cytometry and an increase in the quantity of bound toxin could be detected in a dose-dependent manner over a large range of toxin concentrations. Rod-like structures were observed on membranes treated

with $\Delta 6eGFPPLY$ and these were further studied by SEM. These rod-like structures may be responsible for the strong aggregation effect observed upon $\Delta 6PLY$ treatment of erythrocytes.

Intermedilysin (ILY) is a member of the CDCs produced by *S. intermedius*. It is unique within the group in that it exhibits human-specific cytolysis and initial studies suggested that this is due to binding of a different cellular receptor to other toxins of the family and that this receptor was a protein (Nagamune *et al*, 1996).

eGFP-tagged forms of ILY and $\Delta 6ILY$ were produced to allow tracking of the localisation of ILY and for use in development of a quantitative binding assay. It was confirmed that these proteins could be easily visualised by fluorescence microscopy and that binding could be detected by flow cytometry. A two-hybrid screen was also used to screen for proteins from a human brain cDNA library that were capable of interaction with ILY in order to identify candidate protein receptors for ILY, however no likely receptor candidates were identified.

In order to determine which region is responsible for the human specificity of intermedilysin, a bank of chimeras between ILY and PLY was created. The chimeric toxins were expressed and purified and the specificity of the mutants was determined by haemolytic assay on human and rabbit erythrocytes. The specificity of the chimeric toxin was determined by the origin of the C-terminal 53/56 residues, indicating that the latter part of domain 4 is responsible for the human specificity of intermedilysin.

To further resolve the region involved in human specificity or cholesterol-binding, a series of small substitution mutants was created. These revealed that the promiscuous cell binding activity of the other CDCs was conferred by residues in the undecapeptide loop as this property could be transferred to ILY by introduction of the typical undecapeptide sequence. Surface-plasmon resonance analysis of substitutions of PLY was used to detect any mutants possessing reduced binding affinity. However, problems with aggregation of purified proteins prevented quantitative data from being collected.

Anthrolysin O (ALO) is a toxin produced by *Bacillus anthracis*, the causative agent of anthrax. It is a member of the cholesterol-dependent cytolysin (CDC) group of toxins, many of which are potential vaccine candidates that protect against their producing organisms.

Pore formation by ALO was studied by transmission electron microscopy and pores were found to be consistent with those formed by other members of this toxin family. A novel genetic toxoid of anthrolysin O, $\Delta 6mALO$, was constructed and characterised and was able to bind to cells but was incapable of pore-formation or haemolysis. The capacity of the haemolytic and non-haemolytic forms of ALO to protect against challenge with the toxin or *B. anthracis* was determined. Immunisation with both active and non-haemolytic forms of ALO elicited protection against lethal i.v. challenge with ALO but neither was protective against *B. anthracis* in a murine i.p. challenge model. Immunisation with another CDC, pneumolysin, did not confer cross-protection against challenge with ALO.

Histopathological investigation following lethal i.v. challenge with ALO revealed acute pathology in the lungs with occlusion of alveolar vessels by fibrin deposits.

Acknowledgements

I would like to thank my supervisor, Professor Tim Mitchell, for the opportunity to work on this project in his laboratory and for all the guidance along the way. I would also like to thank all members of the group formerly known as 'South Lab' for their support and help, particularly Lea-ann Kirkham, June Irvine, Gavin Paterson and Gordon Meiklejohn.

I am also grateful to those from within the University of Glasgow who have assisted me; Dr Laurence Tetley and Margaret Mullin for their help with the electron microscopy work and Alan Riboldi-Tunnicliffe for advice on protein purification. I'd also like to thank the numerous collaborators for their work in various aspects of this project; Professor Paul Morgan and Dr Tim Hughes from the University of Wales, Professor Hideaki Nagamune from the University of Tokushima, Professor Richard Titball and Dr Helen Atkins from DSTL Porton Down, Linda Johnson from the VLA, Dr Didier Dulong and his group from the University of Bordeaux and Dr. Ronald Anderson and his group at the University of Pretoria.

"The most exciting phrase to hear in science, the one that heralds new discoveries, is not 'Eureka!' (I found it!) but 'That's funny ...' "
Isaac Asimov (1920 - 1992)

Table of Contents

ABSTRACT.....	3
ACKNOWLEDGEMENTS.....	7
TABLE OF CONTENTS.....	8
INDEX OF TABLES.....	10
INDEX OF FIGURES.....	11
ABBREVIATIONS.....	13
CHAPTER 1: AN INTRODUCTION TO THE CHOLESTEROL-DEPENDENT CYTOLYSINS.....	15
STRUCTURE OF THE CDCs.....	17
<i>Primary Structure</i>	17
<i>Tertiary Structure</i>	21
<i>Quaternary Structure</i>	22
MODE OF ACTION OF THE CDCs.....	23
<i>Oligomerisation and Pore Formation</i>	26
<i>Problems with the prepore model</i>	30
<i>Role of the CDCs in Virulence</i>	33
BIOLOGICAL EFFECTS OF THE CDCs.....	34
<i>Protective vaccination with the CDCs</i>	42
<i>Other Applications of the CDCs</i>	43
AIMS OF THIS PROJECT.....	45
CHAPTER 2: MATERIALS AND METHODS.....	46
MATERIALS.....	47
<i>Primers</i>	47
<i>Plasmid Constructs</i>	47
<i>Bacterial Strains</i>	47
<i>Blood</i>	47
<i>Solutions, Buffers and Growth Media</i>	47
<i>DNA modifying enzymes</i>	48
METHODS.....	48
<i>Construction of pET33bEGFPPLY</i>	48
<i>Construction of pET33bDel6EGFPPLY</i>	48
<i>Construction of pET33bEGFP</i>	48
<i>Construction of TOPO-ALO</i>	49
<i>Construction of pET33b-mALO</i>	49
<i>Construction of pET33b-Δ6mALO</i>	49
<i>Construction of pET33bmILY</i>	50
<i>Construction of pET33bEGFPmILY</i>	50
<i>Construction of pET33bFGFPsILY</i>	50
<i>Construction of pET33bDel6EGFPsILY</i>	51
<i>Construction of vectors for expression of chimeric toxins between PLY and ILY</i>	51
<i>pDest32-D4ILY Yeast-2-hybrid bait vector</i>	52
<i>Gateway cloning</i>	52
<i>DNA sequencing</i>	53
<i>Protein Expression</i>	54
<i>Nickel-affinity purification of His-Tagged proteins</i>	54
<i>Hydrophobic interaction chromatography</i>	54
<i>SwellGel Tab purification</i>	55
<i>Anion Exchange Chromatography</i>	55
<i>UV Absorbance Scanning</i>	55
<i>LAL assay</i>	55
<i>Bradford Assay</i>	56
<i>Western Blotting</i>	56
<i>Epi-fluorescence microscopy of eGFP-tagged toxins</i>	56
<i>Laser Scanning Confocal Fluorescence microscopy</i>	57

<i>Scanning Electron Microscopy</i>	58
<i>Transmission Electron Microscopy</i>	58
<i>Detection of eGFP-tagged toxin binding by FACS</i>	59
<i>Transformation of Yeast – Simple Low-Efficiency Transformation</i>	60
<i>Transformation of Yeast – Library Transformation (60x)</i>	60
<i>Yeast-2-hybrid screen</i>	61
<i>Trypsin treatment of erythrocytes</i>	64
<i>Cell culture</i>	65
<i>L929 fibroblast cytotoxicity assay</i>	65
<i>Haemolysis Assay</i>	66
<i>Anthrolysin O binding assay</i>	67
<i>Determination of anti-ALO and anti-PLY IgG levels by ELISA</i>	67
<i>Determination of lethal dose of Anthrolysin O and histopathology</i>	68
<i>Immunisation studies with mALO, A6mALO and PLY</i>	69
<i>Surface Plasmon Resonance</i>	70
CHAPTER 3: PRODUCTION AND CHARACTERISATION OF EGFP-TAGGED PNEUMOLYSIN	71
SUMMARY.....	72
RESULTS.....	74
<i>Construction of eGFPPPLY, Δ6eGFPPPLY and eGFP expression vectors</i>	74
<i>Expression of eGFP-tagged PLY, Δ6eGFPPPLY and eGFP proteins</i>	76
<i>Comparison of haemolytic activity of eGFPPPLY and Δ6eGFPPPLY to PLY and A6PLY</i>	76
<i>Transmission Electron Microscopy of eGFPPPLY and Δ6eGFPPPLY</i>	77
<i>Comparison of cytotoxicity of eGFPPPLY, Δ6eGFPPPLY, PLY and A6PLY to L929 fibroblast cells</i>	79
<i>Visualisation of eGFPPPLY and Δ6eGFPPPLY binding to erythrocytes by fluorescence microscopy</i>	80
<i>Use of eGFPPPLY to study binding to cochlear hair cells of the rat</i>	82
<i>Visualisation of eGFPPPLY and Δ6eGFPPPLY binding by confocal fluorescence microscopy</i>	86
<i>Scanning Electron Microscopy of eGFPPPLY and Δ6eGFPPPLY</i>	90
<i>Detection of eGFPPPLY and Δ6eGFPPPLY binding to erythrocytes by flow cytometry</i>	92
APPLICATION OF THE eGFPPPLY BINDING ASSAY.....	93
DISCUSSION.....	95
<i>Rationale for using eGFP as a fusion partner</i>	95
<i>Comparison of the haemolytic and cytolytic properties of eGFP-tagged PLY to wild-type toxins</i>	98
<i>Comparison of pore formation by tagged and untagged toxins by TEM</i>	99
<i>Visualisation of toxin binding by epifluorescence microscopy</i>	100
BINDING OF eGFPPPLY TO COCHLEAR HAIR CELLS OF THE RAT.....	101
<i>Examination of toxin-treated erythrocytes by scanning electron microscopy</i>	103
<i>Confocal fluorescence microscopy of Detroit D562 cells treated with eGFP-tagged toxin</i>	104
<i>Expression of the eGFPPPLY fusion protein in the host organism</i>	105
<i>Development of a fluorescence-based quantitative binding assay for PLY</i>	106
CHAPTER 4: INTERMEDILYSIN – A ROGUE MEMBER OF THE CDC FAMILY	111
SUMMARY.....	112
RESULTS.....	114
<i>Construction of vectors for expression of chimeric toxins between PLY and ILY</i>	114
<i>Expression and purification of pneumolysin, intermedilysin and chimeric toxins</i>	116
<i>Haemolytic activities of chimeric toxins</i>	117
<i>Haemolytic activities of chimeric toxins G and H</i>	117
<i>PLY</i>	119
<i>Inhibition of action of chimeras G and H by ghost erythrocytes</i>	119
<i>Effect of trypsinisation of erythrocytes on susceptibility to PLY and ILY mediated lysis</i>	120
<i>Construction of pDest32-D4ILY Yeast-2-hybrid bait vector</i>	122
<i>Yeast-2-hybrid screen with pDest32-D4ILY against human brain cDNA library</i>	122
<i>Construction of eGFPMILY, eGFPILY and Δ6eGFPILY expression vectors</i>	126
<i>pET33bEGFPMILY</i>	126
<i>Expression and purification of eGFPMILY</i>	127

<i>Expression of eGFPsILY and Δ6eGFPsILY</i>	129
<i>Detection of eGFPsILY and Δ6eGFPsILY binding to erythrocytes and U937 cells by flow cytometry</i>	133
<i>Construction of vectors for expression of mutants with small substitutions within domain 4 of PLY and ILY</i>	135
<i>Expression of toxin mutants with small substitutions within domain 4 of PLY and ILY</i>	136
<i>Haemolytic activity of toxin mutants with small substitutions within domain 4 of PLY and ILY</i>	136
<i>Measurement of CD59 binding activity by Surface Plasmon Resonance</i>	138
DISCUSSION	141
CHAPTER 5: IMMUNISATION STUDIES WITH ANTHROLYSIN O, THE CDC FROM <i>BACILLUS ANTHRACIS</i>	150
SUMMARY	151
INTRODUCTION.....	152
RESULTS	155
<i>Construction of plasmid vectors</i>	155
<i>Δ6mALO is non-haemolytic but retains binding activity</i>	156
<i>Electron microscopy of erythrocyte membranes treated with mALO and Δ6mALO</i>	157
<i>Determination of the toxicity of mALO to A/J mice</i>	158
<i>Histopathological investigation of mice lethally challenged with Anthrolysin O</i>	159
<i>Determination of the effect of immunisation with mALO, Δ6mALO and PLY against challenge with the mALO toxin</i>	161
DISCUSSION	166
APPENDIX 1: SEQUENCE ALIGNMENT OF THE CDCS	173
APPENDIX 2: OLIGONUCLEOTIDES	178
APPENDIX 3: BUFFERS AND SOLUTIONS	181
PUBLICATIONS	185
REFERENCES	187

Index of Tables

TABLE 1.1: KNOWN MEMBERS OF THE CDC FAMILY.	16
TABLE 1.2: TABLE SHOWING SOME OF THE CYTOKINE AND INFLAMMATORY MEDIATORS INDUCED BY CDCs	39
TABLE 2.1: PRIMERS USED FOR AMPLIFICATION OF PLY AND ILY FRAGMENTS IN CONSTRUCTION OF CHIMERIC TOXINS.....	51
TABLE 4.1: CROSSOVER POSITIONS OF PLY/ILY CHIMERIC TOXINS	115
TABLE 4.2: HAEMOLYTIC ACTIVITY OF PLY, ILY AND CHIMERIC TOXINS A-H BY SEMI-QUANTITATIVE HAEMOLYSIS ASSAY.....	117
TABLE 4.3: SPECIFIC ACTIVITIES OF PLY, ILY, CHIMERA G AND CHIMERA H ON HUMAN OR HORSE ERYTHROCYTES.....	119
TABLE 4.4: CONFIRMATORY ASSAYS OF YEAST-2-HYBRID CLONES	125
TABLE 4.5: TOP BLAST HITS OF PROTEINS INTERACTING WITH D4ILY IN A YEAST-2-HYBRID SCREEN....	126
TABLE 4.6: DESIGN AND CREATION OF SMALL SUBSTITUTION MUTANTS OF PLY AND ILY	135

Index of figures

FIGURE 1.1: ALIGNMENT OF UNDECAPEPTIDE SEQUENCES OF THE CDCs	18
FIGURE 1.2: 3D SEQUENCE VARIABILITY MAP OF THE CDCs	19
FIGURE 1.3: GUIDE TREE INDICATING RELATIONSHIP BETWEEN THE CDCs.....	21
FIGURE 1.4: CRYSTAL STRUCTURES OF ILY AND PFO	22
FIGURE 1.5: SCHEMATIC DIAGRAM OF THE PREPORE MODEL.....	29
FIGURE 1.6: A HYBRID MODEL OF PORE-FORMATION BY THE CDCs BASED ON THAT PROPOSED BY GILBERT	33
FIGURE 2.1: OVERVIEW OF THE GATEWAY CLONING SYSTEM.....	53
FIGURE 2.2: SCHEMATIC DIAGRAM OF THE YEAST-2-HYBRID SYSTEM	63
FIGURE 3.1: SCHEMATIC DIAGRAMS OF PET33BEGFPPLY AND PET33BDEL6EGFPPLY PLASMIDS.....	75
FIGURE 3.2: COMPARISON OF THE HAEMOLYTIC ACTIVITY OF eGFPPLY, Δ6EGFPPLY, PLY AND Δ6PLY ON HUMAN ERYTHROCYTES.....	77
FIGURE 3.3: TRANSMISSION ELECTRON MICROGRAPHS OF HUMAN ERYTHROCYTE GHOST MEMBRANES TREATED WITH wtPLY, eGFPPLY, Δ6EGFPPLY OR NO TOXIN.....	78
FIGURE 3.4: CYTOTOXICITY OF eGFP-TAGGED TOXINS TO L929 FIBROBLAST CELLS.....	80
FIGURE 3.5: HUMAN ERYTHROCYTES TREATED WITH eGFPPLY OR Δ6EGFPPLY VIEWED BY EPHLUORESCENCE MICROSCOPY.....	81
FIGURE 3.7: BINDING OF PLY IN COCHLEAR HCS	83
FIGURE 3.8: ELEVATION OF EXTRACELLULAR CALCIUM PREVENTS BINDING OF eGFPPLY TO HCS.....	85
FIGURE 3.9: LASER SCANNING CONFOCAL MICROSCOPY OF DETROIT 562 CELLS TREATED WITH 700NM eGFPPLY.....	87
FIGURE 3.10: LASER SCANNING CONFOCAL MICROSCOPY OF DETROIT 562 CELLS TREATED WITH 700NM Δ6EGFPPLY.....	88
FIGURE 3.11: LASER SCANNING CONFOCAL MICROSCOPY OF DETROIT 562 CELLS TREATED WITH 700NM eGFP.....	89
FIGURE 3.12: SCANNING ELECTRON MICROGRAPHS OF ERYTHROCYTES TREATED WITH PLY, Δ6PLY, eGFPPLY OR Δ6EGFPPLY:	91
FIGURE 3.13: FLOW CYTOMETRY ANALYSIS OF ERYTHROCYTES TREATED WITH eGFPPLY OR Δ6EGFPPLY.....	93
FIGURE 3.14: EFFECTS OF DOCOSAHEXAENOIC ACID (DHA, 5 AND 10 MG/ML) ON THE BINDING OF THE eGFPPLY PROTEIN (500 NG/ML) TO NEUTROPHILS.....	94
FIGURE 4.1: SCHEMATIC DIAGRAM OF CHIMERIC PROTEINS BETWEEN PLY AND ILY	115
FIGURE 4.2: ALIGNMENT OF PLY AND mILY AMINO ACID SEQUENCES INDICATING CONSERVED REGIONS SELECTED AS CROSS-OVER JUNCTIONS IN ILY/PLY CHIMERAS	116
FIGURE 4.3: HAEMOLYSIS ASSAYS OF PLY, ILY, CHIMERA G AND CHIMERA H.....	118
FIGURE 4.4: INHIBITION OF THE HAEMOLYTIC ACTIVITY OF CHIMERAS G AND H BY HUMAN OR RABBIT ERYTHROCYTE GHOSTS.....	119
FIGURE 4.5: THE EFFECT OF TRYPSINISATION OF HUMAN ERYTHROCYTES ON LYSIS BY mILY AND PLY.....	121
FIGURE 4.6: COOMASSIE-STAINED SDS-PAGE GEL OF PURIFIED PROTEIN FROM eGFPmILY PURIFICATION.....	127
FIGURE 4.7: PLASMID MAPS OF PET33BEGFPsILY AND PET33BDEL6EGFPsILY.....	129
FIGURE 4.8: COOMASSIE-STAINED SDS-PAGE GEL OF eGFPsILY AND Δ6EGFPsILY IN PBS OR TRIS BUFFER.....	130
FIGURE 4.9: HAEMOLYTIC ACTIVITIES OF mILY, eGFPsILY AND Δ6EGFPsILY.....	130
FIGURE 4.10: LASER SCANNING CONFOCAL MICROSCOPY OF HUMAN AND HORSE ERYTHROCYTES TREATED WITH eGFPsILY, Δ6EGFPsILY OR eGFP.....	132
FIGURE 4.11: FLOW CYTOMETRY ANALYSIS OF eGFPsILY BINDING TO HUMAN AND HORSE ERYTHROCYTES.....	134
FIGURE 4.12: DIAGRAM SHOWING LOCATION OF MUTATIONS OF ILY AND PLY PRESENT IN ILY AND PLY SUBSTITUTION MUTANTS	136
FIGURE 4.13: HAEMOLYTIC ACTIVITIES OF ILY SUBSTITUTIONS 1-15 AND PLY SUBSTITUTIONS 8-10.....	137
FIGURE 4.14: BIACORE SENSORGRAM FOR ANALYSIS OF ILY AND PLY SUBSTITUTION MUTANT BINDING TO CD59.....	139
FIGURE 4.15: BIACORE SENSORGRAM ANALYSIS OF ILY AND PLY BINDING TO CD59.....	139

FIGURE 5.1: HAEMOLYSIS ASSAY OF PURIFIED MALO AND Δ6MALO TOXINS ON HUMAN AND HORSE ERYTHROCYTES.	156
FIGURE 5.2: BINDING ASSAY OF MALO AND Δ6MALO TO HUMAN ERYTHROCYTES.	157
FIGURE 5.3: TRANSMISSION ELECTRON MICROGRAPHS OF HUMAN ERYTHROCYTE GHOST MEMBRANES TREATED WITH MALO OR Δ6MALO.	158
FIGURE 5.4: SURVIVAL OF A/J MICE AFTER I.V. CHALLENGE WITH DIFFERENT CONCENTRATIONS OF MALO TOXIN.	159
FIGURE 5.5: LIGHT MICROSCOPY OF HISTOLOGICAL SECTIONS OF LUNGS TAKEN FROM MICE LETHALLY CHALLENGED WITH MALO OR A NAÏVE CONTROL MOUSE	160
FIGURE 5.6: ANTI-MALO AND ANTI-PLY ELISAs SHOWING TITRES OF ANTI-MALO IGG ANTIBODY DETECTED FOR EACH IMMUNISED GROUP OF ANIMALS SUBSEQUENTLY CHALLENGED WITH MALO	161
FIGURE 5.7: NEUTRALISATION OF MALO OR PLY ACTIVITY BY POOLED SERA FROM EACH IMMUNISED GROUP.	162
FIGURE 5.8: SURVIVAL OF MICE IMMUNISED WITH MALO, Δ6MALO, PLY OR ADJUVANT ALONE AFTER CHALLENGE WITH MALO.	163
FIGURE 5.9: SURVIVAL OF IMMUNISED A/J MICE FOLLOWING I.P. CHALLENGE WITH 10^5 <i>B. ANTHRACIS</i> STRAIN ST1 SPORES.	164
FIGURE 5.10: DETERMINATION OF LEVELS OF ANTI-MALO IGG IN SERA FROM GROUPS OF MICE IMMUNISED WITH MALO, Δ6MALO, PLY AND ADJUVANT, PRIOR TO CHALLENGE WITH <i>B. ANTHRACIS</i>.	165

Abbreviations

°C	Degrees Celsius
µl	Microlitre
µM	Micromolar
µm	Micrometre
5FOA	5-Fluoroorotic Acid
A	Absorbance
AEC	Anion exchange chromatography
ALO	Anthrolysin O
ALY	Alveolysin
APS	Ammonium Persulphate
AUC	Analytical Ultracentrifugation
BSA	Bovine Serum Albumin
CDC	Cholesterol-Dependent Cytolysin
cds	Coding sequence
cDNA	complementary deoxyribonucleic acid
CIAP	Calf Intestinal Alkaline Phosphatase
CLY	Cereolysin
CSF	Cerebral Spinal Fluid
DAPI	4',6-Diamidino-2-phenylindole
DHA	Docosahexaenoic acid
DMEM	Dulbecco's Modified Eagle's Medium
DNA	Deoxyribonucleic acid
DTT	Dithiothreitol
EDTA	Ethylene Diamine Tetra Acetic Acid
EF	Edema (Oedema) Factor
eGFP	Enhanced Green Fluorescent Protein
ELISA	Enzyme-Linked Immunosorbent Assay
ECM	Erythrocyte Medium
FACS	Fluorescence Activated Cell Sorting
FBS	Foetal Bovine Serum
FITC	Fluorescein isothiocyanate
FIAsH	Fluorescein Arsenical Hairpin
FPLC	Fast Protein Liquid Chromatography
FRET	Fluorescence resonance energy transfer
HIC	Hydrophobic interaction chromatography
His-Tag	Poly-Histidine Tag
HRP	Horse Radish Peroxidase
i.p.	intraperitoneal
i.v.	intravenous
IgG	Immunoglobulin G
ILO	Ivanolysin O
ILY	Intermedilysin
IPTG	Isopropyl-β-D-Thiogalactopyranoside
kb	Kilobase(s)
LAL	Limulus Amebocyte Lysate
LB broth	Luria Bertani Broth

LF	Lethal Factor
LLO	Listeriolysin O
LPS	Lipopolysaccharide
LSO	Seeligeriolysin O
M	Molar
MTT	3-[4,5-Dimethylthiazol-2-yl]-2,5-diphenyltetrazoliumbromide
NBD	<i>N,N</i> -dimethyl- <i>N</i> -(iodoacetyl)- <i>N</i> -(7-nitrobenz-2-oxa-1,3-diazolyl)ethylene-diamine
orf	Open Reading Frame
PA	Protective Antigen
PBS	Phosphate Buffered Saline
PCR	Polymerase Chain Reaction
PFO	Perfringolysin O
PLO	Pyolysin
PLY	Pneumolysin
Rpm	Revolutions per minute
SDS-PAGE	Sodium Dodecyl Sulphate-Polyacrylamide Gel Electrophoresis
SEM	Scanning Electron Microscopy
SLO	Streptolysin O
smhPAF	Streptococcus mitis-derived human platelet aggregation factor
TB	Terrific Broth
TEM	Transmission Electron Microscopy
TLO	Thuringiolysin O
TLR	Toll-like receptor
TLY	Tetanolysin O
YPAD	Yeast extract-peptone-adenine-dextrose medium

Chapter 1: An introduction to the cholesterol-dependent cytolysins

The cholesterol-dependent cytolysins (CDCs) are a group of toxins produced by particular members from seven genera of Gram-positive bacteria. At least 25 members are currently known (Table 1.1) and the family continues to grow with the discovery of novel members through traditional screening processes (Ohkuni *et al.*, 1997) and the completion of bacterial genome sequencing projects (Read *et al.*, 2003).

Table 1.1: Known members of the CDC family.

Genus	Species	CDC produced	Abbreviation	Genbank Accession
<i>Arcanobacterium</i>	<i>pyogenes</i>	Pyolysin	PLO	AB027461
<i>Bacillus</i>	<i>anthracis</i>	Anthrolysin O	ALO	AE017034 (from genome BA3355)
<i>Bacillus</i>	<i>cereus</i>	Cereolysin	CLY	AY818309
<i>Bacillus</i>	<i>thuringiensis</i>	Thuringiolysin O	TLO	AE017355 (from genome BT9727_3086)
<i>Brevibacillus</i>	<i>laterosporus</i>	Laterosporolysin	LSL	
<i>Paenibacillus</i>	<i>alvei</i>	Alveolysin	ALY	M62709
<i>Clostridium</i>	<i>bifermentans</i>	Bifermentolysin	BFL	
<i>Clostridium</i>	<i>chauvoei</i>	Chauveolysin	CVL	
<i>Clostridium</i>	<i>botulinum</i>	Botulinolysin	BLY	
<i>Clostridium</i>	<i>histolyticum</i>	Histolyticolysin	HLO	
<i>Clostridium</i>	<i>novyi (type A)</i>	Novyilysin	NVL	
<i>Clostridium</i>	<i>perfringens</i>	Perfringolysin O	PFO	M36704
<i>Clostridium</i>	<i>septicum</i>	Septicolysin O	SPL	
<i>Clostridium</i>	<i>sordellii</i>	Sordellilysin	SDL	
<i>Clostridium</i>	<i>tetani</i>	Tetanolysin O	TLY	AE015927 (from genome CTC01888)
<i>Listeria</i>	<i>ivanovi</i>	Ivanolysin O	ILO	X60461
<i>Listeria</i>	<i>monocytogenes</i>	Listeriolysin O	LLO	M24199
<i>Listeria</i>	<i>seeligeri</i>	Seeligeriolysin O	LSO	X60462
<i>Streptococcus</i>	<i>canis</i>	Streptolysin O	SLO	
<i>Streptococcus</i>	<i>equisimilis</i>	Streptolysin O	SLO	
<i>Streptococcus</i>	<i>intermedius</i>	Intermedilysin	ILY	AB029317
<i>Streptococcus</i>	<i>pneumoniae</i>	Pneumolysin	PLY	X52474
<i>Streptococcus</i>	<i>pyogenes</i>	Streptolysin O	SLO	M18638
<i>Streptococcus</i>	<i>suis</i>	Suilysin	SLY	AF043556
<i>Streptococcus</i>	<i>mitis</i>	<i>Streptococcus mitis</i> - derived human platelet aggregation factor	smhPAF	AB051299

The group was formerly referred to as the thiol-activated cytolysins (TACYs) since these toxins were observed to lose their haemolytic activity through oxidation of a thiol-group, and regain activity upon addition of reducing agents such as

dithiothreitol or β -mercaptoethanol (Iwamoto *et al.*, 1987; Johnson, 1972; Van Epps & Andersen, 1971). This effect was originally thought to indicate reduction of intra-molecular di-sulphide bonds, however gene sequencing showed that many members had only a single cysteine residue that occurred within the conserved 'undecapeptide' region of the molecule (Kehoe *et al.*, 1987; Mengaud *et al.*, 1987; Tweten, 1988; Walker *et al.*, 1987).

Highly purified preparations of CDCs do not demonstrate thiol-activation (Alouf, 1980; Boulnois *et al.*, 1991) and substitution of the cysteine residue with alanine leads to only a small reduction in haemolytic activity of PLY, PFO and LLO indicating that the thiol group is not essential for the activity of the toxins (Michel *et al.*, 1990; Pinkney *et al.*, 1989; Saunders *et al.*, 1989). It is thought that the effect may be attributed to association of the cysteine residue with cysteine-containing impurities causing steric hindrance to critical residues contained within this region (Pinkney *et al.*, 1989).

Structure of the CDCs

Primary Structure

Gene sequences of the CDCs published to date range from 1416 to 1998 base pairs in length, corresponding to mature proteins with predicted molecular weights of 51 – 70kDa. The most variable region between the CDCs is the N-terminal end, where both SLO and smhPAF possess an additional domain, although these domains are dissimilar between the two proteins.

All CDCs sequenced to date, with the exception of PLY, carry a putative N-terminal secretion signal that targets the protein for secretion from the bacterium. PLY does not carry a secretion signal (Walker *et al.*, 1987), and it is thought to be released from the cell through autolysin (LytA) mediated degradation of the cell wall (Benton *et al.*, 1997; Paton *et al.*, 1993). The toxin has also been shown to be released from some strains during log-phase growth and in an autolysin-independent manner suggesting that in some cases PLY may be released by an as yet undefined mechanism (Balachandran *et al.*, 2001).

Alveolysin	(460)	ECTGLAWEWWR
Anthrolysin O	(471)	ECTGLAWEWWR
Cereolysin O	(468)	ECTGLAWEWWR
Thuringiolysin O	(471)	ECTGLAWEWWR
Perfringolysin O	(458)	ECTGLAWEWWR
Streptolysin O	(532)	FCTGLAWEWWR
Tetanolysin	(484)	ECTGLAWEWWR
Ivanolysin C	(482)	ECTGLAWEWWR
Listeriolysin C	(483)	ECTGLAWEWWR
Pneumolysin	(427)	ECTGLAWEWWR
Sullysin	(455)	ECTGLAWEWWR
Seelegeriolysin O	(484)	ECTGLAWEWWR
Pyolysin	(491)	EATGLAWCPWW
smhPAF	(666)	FKTGLAWEWWR
Intermedilysin	(485)	GATGLAWEWWR

Figure 1.1: Alignment of undecapeptide sequences of the CDCs

Alignment of available sequences of the CDCs using the ClustalW algorithm (Appendix 1) indicates amino acid sequence similarity ranging from 40-97% and there are a number of regions of sequence that are highly conserved between the CDCs (Appendix 1, Figure 1.1 and Figure 1.2).

In addition to sequence variation between members of the CDCs, there can also be sequence variation between alleles of a single CDC. A number of alleles of pneumolysin have been described in clinical isolates of *Streptococcus pneumoniae*, including some alleles in *S. pneumoniae* ST306 that were non-haemolytic (Kirkham *et al.*, 2006a).

Sequence variability was calculated from an amino acid sequence alignment (ClustalW) of ALY, ALO, CLY, PFO, SLO, TLY, ILO, LLO, PLO, ILY and PLY using the AA_Frequency excel macro from http://www.biochem.unizh.ch/antibody/Macros/Macros/AA_Frequency.html.

The frequency of an amino acid at a particular position is calculated as the number of times the amino acid occurs at that position divided by the number of sequences in the alignment. The sequence variability is defined as the number of different amino acids in a given position divided by the frequency of the most abundant amino acid in that position (Kabat *et al.*, 1977).

Values potentially range from 1 (no variability) to 400 (Highest variability – i.e. all 20 amino acids occurring with equal frequency) but in this 11 sequence comparison the maximum possible sequence variability is 121. Amino acids that did not align with a corresponding residue in the structure of PFO were excluded.

Sequence variability was mapped onto the crystal structure of perfringolysin O (Rossjohn *et al.*, 1997) using the colours shown in the table below and rendered with WebLab Viewer Lite 5.0 (Accelrys Software, Cambridge, UK).

Sequence Variability	Colour
1	Red
1-3	Orange
3-10	Green
>10	Blue



Figure 1.2: 3D sequence variability map of the CDCs

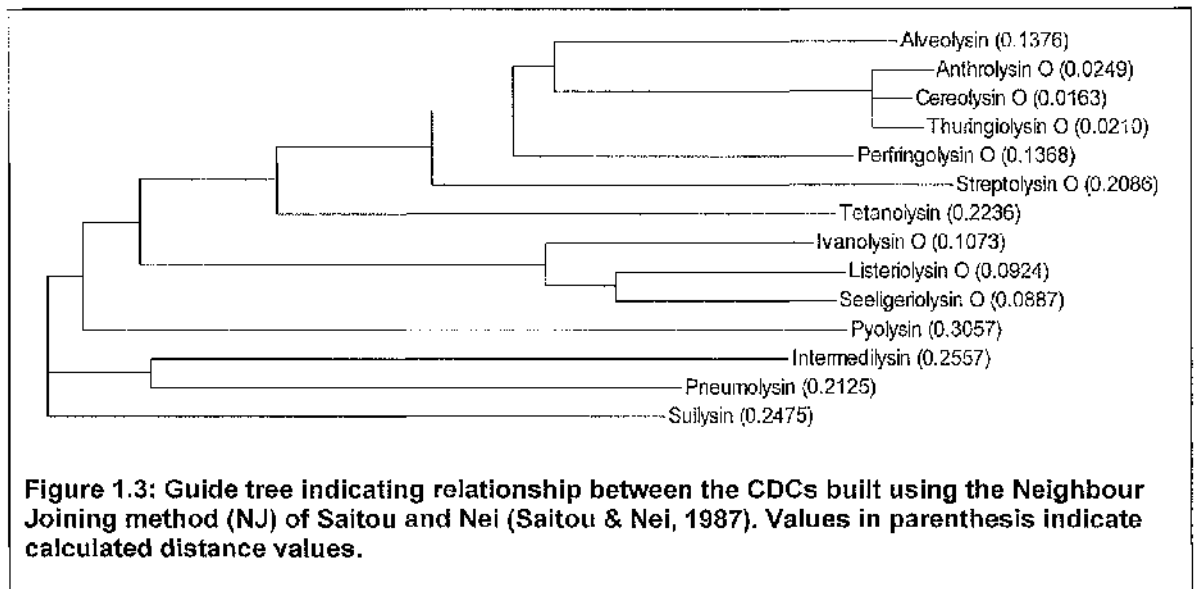
The variation between different alleles of a CDC can equal the variation found between CDCs from different bacterial species: for example alignment of anthrolysin O and cereolysin produces a similarity score of 97%, equal to the similarity score calculated between different PLY alleles produced by *S. pneumoniae* (sequences obtained from Dr. Johanna Jefferies and Mr. Calum Johnson, University of Glasgow, unpublished results). This is perhaps not surprising when you take into account the difficulty in defining species limits and in particular the indistinct boundary between *B. anthracis* and *B. cereus* (Hoffmaster *et al.*, 2004).

The most prominent and well-studied highly conserved region is the 'undecapeptide' motif consisted of 11 contiguous amino acid residues. The undecapeptide region is completely conserved in all CDCs sequenced to date with the exception of ILY, PLO, LSO and smhPAF, which have variation in up to 4 of the 11 amino acid residues (Figure 1.1).

The cysteine residue within the undecapeptide region has been shown to be non-critical to activity, since substitution of this residue in PLY with alanine, C428A did not affect the haemolytic activity of the protein, but this residue is in an important region of PLY, since mutations C428G and C428S reduced the activity of the toxin (Saunders *et al.*, 1989).

A number of other conserved regions occur in the alignment and these map to residues throughout the crystal structure of PFO. Conserved residues mostly oppose other conserved residues within β -sheets and highly variable residues

occur opposite other highly variable residues, possibly indicating the occurrence of co-ordinated or compensatory mutations (Figure 1.2).



Tertiary Structure

X-ray crystal structures of two members of the cholesterol-dependent cytolysins, ILY and PFO, have been solved (Polekhina *et al.*, 2005; Rossjohn *et al.*, 1997). Although ILY and PFO have two of the most dissimilar sequences when compared on a dendrogram of the CDCs (Figure 1.3), their tertiary structures are very similar (Polekhina *et al.*, 2005). Both PFO and ILY have an elongated shape and are composed of four domains (Figure 1.4). The molecules are rich in β -sheet in all domains, but particularly domains 2 and 4 which contain no α -helices.

The most distinct differences between the PFO and ILY structures occur within domain 4. The curved undecapeptide loop of PFO is in a straightened conformation in ILY and a hairpin loop centred on E418 at the opposing end of domain 4 of PFO is folded over in ILY (Polekhina *et al.*, 2005). The angle formed

between domain 4 and domains 1-3 in the crystal structure of ILY is more pronounced than that of PFO giving this molecule an overall bent shape. However, this angle is different for each of the two monomers within the crystal cell of ILY suggesting that this junction may be flexible and the apparent differences may be an artefact of crystallisation.

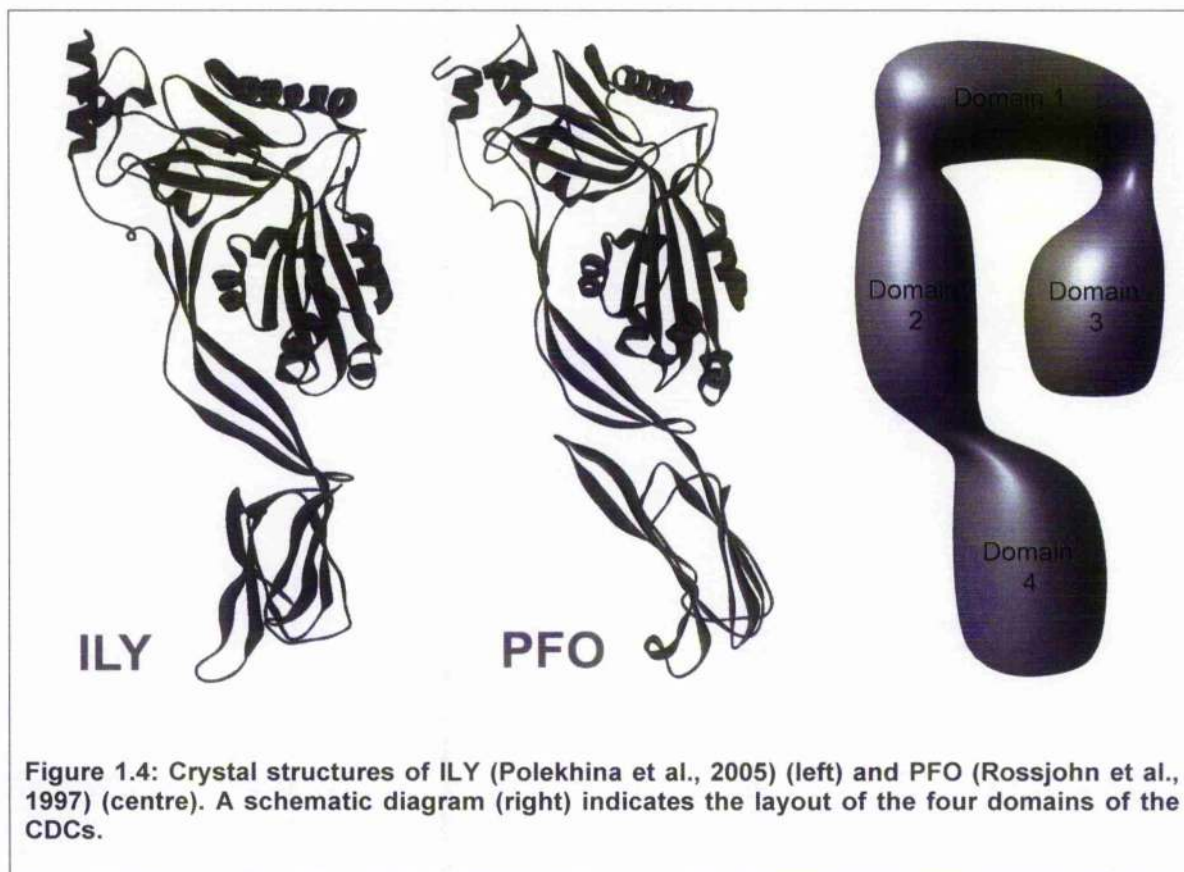


Figure 1.4: Crystal structures of ILY (Polekhina et al., 2005) (left) and PFO (Rossjohn et al., 1997) (centre). A schematic diagram (right) indicates the layout of the four domains of the CDCs.

Quaternary Structure

It has been shown using analytical ultracentrifugation (AUC) and small-angle X-ray scattering combined with ab-initio modelling that PFO forms anti-parallel dimers in solution (Solovyova *et al.*, 2004). PFO also occurs as an anti-parallel dimer in the crystal cell in all of the crystal forms solved to date (Gilbert, 2005). In contrast, PLY

did not form dimers in solution (Solovyova *et al.*, 2004) and this toxin has been shown to be capable of oligomerisation in solution (Gilbert *et al.*, 1998; Gilbert *et al.*, 1999; Solovyova *et al.*, 2004). Solovyova *et al* suggest that formation of dimers is a method of preventing untimely pore formation prior to membrane contact and that the different oligomerisation states of the two toxins may reflect the different mechanisms of release from the bacteria (Solovyova *et al.*, 2004). PFO is secreted across the plasma membrane and this may require a dimeric structure to allow transport across the membrane, whereas PLY appears to remain in the cytoplasm until cell lysis in at least some strains of *S. pneumoniae*.

Mode of Action of the CDCs

The mechanism of pore formation by the CDCs remains largely controversial despite years of study. It is now generally agreed that the mode of action involves binding of the monomeric toxin to the host cell membrane followed by oligomerisation and insertion to form a pore, however many of the finer points remain unclear.

Target Cell Binding

The first event in the mode of action is binding of the CDC monomer to the target cell membrane. With the exception of one member of the group – ILY – the CDCs are able to bind to cells from a wide range of animal species. ILY is specific for human cells – it was shown to be fully active on human erythrocytes and retained 1% activity on erythrocytes from chimpanzees and cynomolgus monkeys, but it was inactive on erythrocytes from all of the other mammalian species tested

(Nagamune *et al.*, 1996). ILY binds to human CD59, a cell surface protein that protects the host from complement-mediated lysis by the membrane-attack complex, but was found to be incapable of binding to rabbit CD59 (Giddings *et al.*, 2004). Binding is thought to involve an α -helical region contained within residues 40-66, the region responsible for CD59 binding to C8 α and C9 complement proteins, since exchange of residues 42-58 between human and rabbit CD59 expressed in SV-T2 cells also transferred susceptibility to lysis by ILY.

For the other CDCs, a number of lines of evidence suggest that cholesterol is the binding receptor. Cholesterol inhibition of CDC haemolysis has been realised for a long time (Johnson, 1972). It has also been demonstrated that CDCs are capable of binding to artificial membranes containing cholesterol (Ohno-Iwashita *et al.*, 1991) and that chemical modification of cholesterol inhibits cytolysis by streptolysin O (Prigent & Alouf, 1976).

Since it is clear that for members of the family other than ILY, binding to cholesterol is sufficient to allow toxin binding and insertion into model lipid bilayers, it is commonly stated that cholesterol acts as the cell binding receptor for these CDCs.

However, studies on LLO have shown that pre-incubation of the toxin with cholesterol inhibited haemolysis but did not inhibit LLO from binding to erythrocyte membranes, eukaryotic cells or artificial membranes, suggesting that another cell binding site may exist on LLO (Jacobs *et al.*, 1998). Toxin fragments composed of either domains 1-3 or domain 4 of LLO were both independently capable of

binding to cells, judged both by immunoblot of erythrocyte membranes and immunohistochemistry of epithelial cells incubated with D123 LLO or D4 LLO (Dubail *et al.*, 2001). The authors suggest that this indicates that more than one binding site exists for these toxins. It is therefore possible that in the work by Jacobs *et al.* (Jacobs *et al.*, 1998), the LLO pre-incubated with cholesterol bound to cells by the binding site on domain 1-3 and that this was a non-productive binding event for pore formation.

Giddings *et al.*, 2003 used a combination of FRET to detect oligomerisation and labelling of transmembrane β -hairpin 1 with the NBD fluorophores to detect membrane insertion (Giddings *et al.*, 2003). They demonstrated that cholesterol depletion of erythrocyte membranes did not prevent binding and oligomerisation of PLY, PFO or ILY but prevented insertion of the toxins into the membrane. Like the LLO data discussed above, this suggests that the role of cholesterol is not in the initial binding step but it is involved in insertion of the pore into the membrane, perhaps being required for a second binding step, to enable conformational change or to maintain membrane fluidity.

Further evidence was provided by Billington *et al.*, who showed that a number of mutants in the undecapeptide region of PLO which greatly reduced haemolytic and cholesterol binding activities retained erythrocyte membrane binding activity (Billington *et al.*, 2002). PLO is also more active on erythrocytes from some species (e.g. rabbit) than others (e.g. bovine) (Funk *et al.*, 1996), suggesting that toxin action may involve more than just a cholesterol-containing membrane.

Given these observations, it seems plausible that although cholesterol is sufficient to act as a receptor for membrane binding and insertion of the CDCs in artificial systems, another receptor may be involved in whole-cell systems.

Oligomerisation and Pore Formation

Following binding to the cell membrane, toxin monomers are thought to come together through transverse movement in the cell membrane and oligomerise to form a prepore complex. Shepard *et al* showed by SDS-agarose gel electrophoresis that PFO predominantly occurred as a single size of oligomer on liposomal membranes, although small amounts of lower molecular weight oligomers were detected by immunoblot analysis (Shepard *et al.*, 2000). Following incubation of PFO with cholesterol-containing liposomes for 90 minutes at 4°C, nearly 80% of the PFO was found to have oligomerised to the typical oligomerisation mass. However, insertion of the oligomers into the membrane appeared to be limited, as only a 5-28% change in fluorescence of NBD-labelled residues within the transmembrane helices was detected (Shepard *et al.*, 2000).

Hotze *et al* used a di-sulphide trapped mutant of PFO, PFO^{C190-C57} to separate the processes of oligomerisation and membrane insertion (Hotze *et al.*, 2001). Using FRET to monitor toxin oligomerisation and PFO containing residues of the transmembrane hairpin labelled with NBD to indicate membrane insertion, the authors showed that oligomerisation proceeded to form large ring-shaped oligomers in non-reducing conditions but upon reduction of the di-sulphide bond the transmembrane hairpin was able to insert into the membrane.

These lines of evidence indicate that oligomerisation can occur without insertion of the toxin into the membrane.

Monomer-monomer interactions are thought to initially involve domain 4 since PLY derivatised with TMB at C428 in domain 4 was rendered incapable of self association (Gilbert *et al.*, 1998) and domain 4 of SLO was found to interact reversibly with the whole toxin to inhibit pore formation (Weis & Palmer, 2001). However, in the prepore state, contact between subunits occurs between domain 1 and domain 3 (Ramachandran *et al.*, 2002; Tilley *et al.*, 2005; Weis & Palmer, 2001). A hidden β -strand that forms the monomer-monomer interface is reported to be exposed upon cell binding (Ramachandran *et al.*, 2004). In this work, crosslinking of the β 4 and β 5 strands by introduction of a disulphide bridge inhibited toxin oligomerisation and pore formation but upon addition of a reducing agent, oligomerisation and pore formation were able to proceed.

The size of the CDC oligomers appears to be variable (Olofsson *et al.*, 1993; Sekiya *et al.*, 1993) and the number of molecules per oligomer have been reported as 40-50 (Morgan *et al.*, 1995), ~33 (Gilbert *et al.*, 1999), 34-36 (Czajkowsky *et al.*, 2004) or 31 (prepore) and 38-44 (pore) (Tilley *et al.*, 2005). The conformation of toxin monomers in the prepore complex is thought to be similar to that of the x-ray crystallographic structure (Czajkowsky *et al.*, 2004; Tilley *et al.*, 2005).

The next step involves a conformational change of the oligomer to insert into the membrane. One predominant model, the prepore model (Rossjohn *et al.*, 1997;

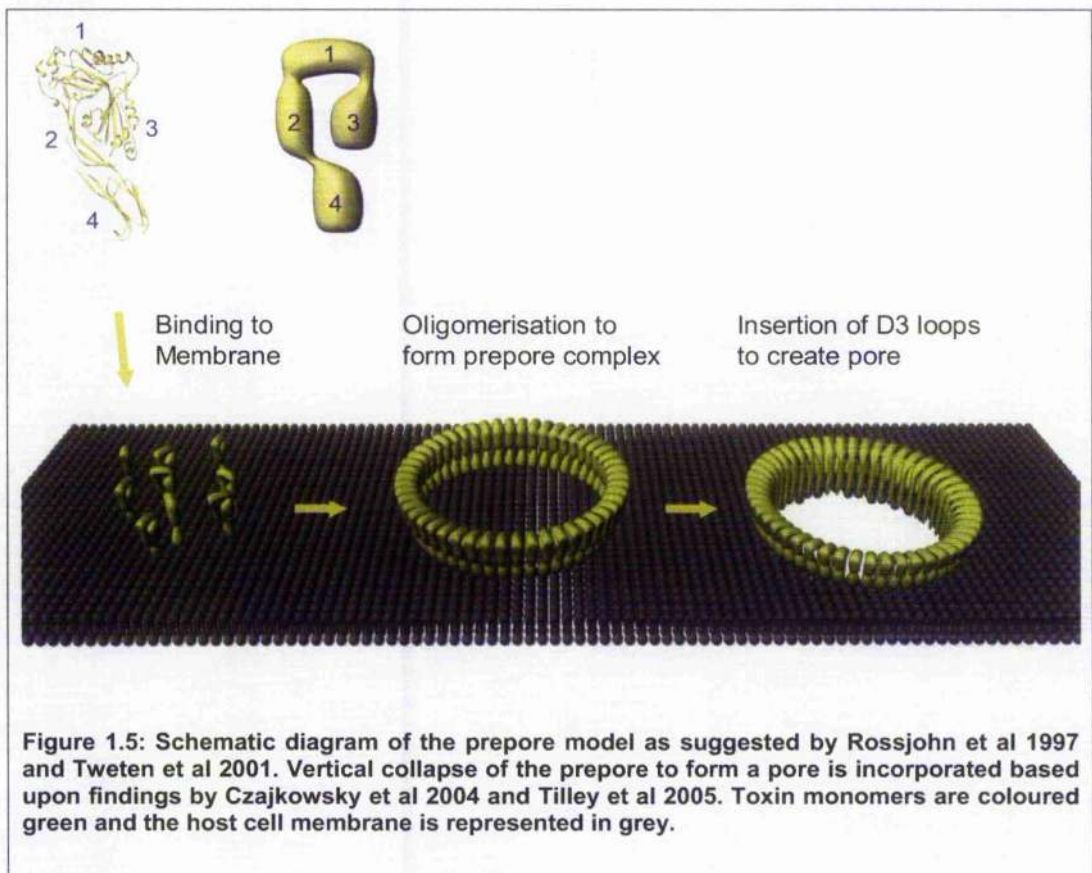
Tweten *et al.*, 2001), requires that oligomerisation into ring structures must be complete prior to membrane insertion.

It is thought that insertion of the oligomers to form a pore is a co-ordinated process suggesting that conversion involves monomer-monomer interactions (Hotze *et al.*, 2002). Hotze *et al* showed that a mutant of PFO, Y181A was not able to insert its transmembrane hairpins but these hairpins were inserted when PFO was added to create mixed oligomers. Insertion of the transmembrane helices was found to be an 'all or nothing' process and it was therefore suggested that monomer-monomer interactions drive the insertion of the transmembrane hairpins.

Prepore to pore conversion involves a huge conformational change of the toxin subunits that form the oligomeric ring. Domain 3 inserts into the membrane by conversion of six helices to β -hairpins (Heuck *et al.*, 2000; Ramachandran *et al.*, 2004; Ramachandran *et al.*, 2005; Shepard *et al.*, 1998).

Prepore to pore conversion is accompanied by a 'vertical collapse' of the prepore structure, with most height loss due to a shortening of domain 2. This has now been illustrated by a number of techniques. Czajkowsky *et al* used atomic force microscopy to visualise a change in height of the di-sulphide trapped PFO^{C190-C57} mutant upon reduction of the disulphide bond allowing insertion of the transmembrane helices (Czajkowsky *et al.*, 2004). Tilley *et al* used cryo-electron microscopy and image processing to determine the structures of prepore and pore configurations of PLY and showed a large conformational change and shortening of domain 2 upon membrane insertion (Tilley *et al.*, 2005) (Figure 1.5).

Ramachandran et al used FRET to detect re-arrangement of PFO domains upon membrane insertion whereby parts of domain 3 enter the membrane, domain 1 moves closer to the membrane, domain 4 remains in approximately the same position perpendicular to the membrane and, by inference, domain 2 undergoes a shortening or re-configuration.



Problems with the prepore model

The prepore model described above (Figure 1.5) is the currently prevailing model in most texts, however it has a number of discrepancies with research findings.

In addition to ring-shaped structures, arc structures are frequently observed by electron microscopy on membranes treated with CDC toxins (Bhakdi *et al.*, 1985; Morgan *et al.*, 1994; Sekiya *et al.*, 1996; Sekiya *et al.*, 1998) but the role of arcs in pore formation remains largely unresolved. It has been shown by the use of an oligomerisation-deficient, arc-forming mutant of SLO, SLO T250C, that arcs were capable of forming small pores allowing passage of NaCl and calcein but not large dextran molecules (Palmer *et al.*, 1998).

A study on PLY-induced channels in artificial bilayers showed that a range of different sizes of PLY-induced channels were present based on conductance measurements (Korchev *et al.*, 1992). The smallest channels exhibited cation selectivity whereas the larger channels were not ion selective. Small and medium sized channels were subject to closure by divalent cations to a greater degree than larger channels (Korchev *et al.*, 1992). The existence of a number of sizes of pore would be in accordance with the idea that in addition to fully circular pores, smaller arc-mediated pores may be present. Their gated nature could be a result of the bounding of part of the pore by an edge of lipid, as interpreted from TEM images of streptolysin O (Bhakdi *et al.*, 1985; Palmer *et al.*, 1998).

As mentioned earlier, Czajkowsky *et al* used atomic force microscopy to visualise a change in height of ring structures resulting from insertion into the membrane (Czajkowsky *et al.*, 2004). However in the images of pore complexes of PFO inserted into the lipid bilayer that accompany the work, ring and arc structures occur in approximately equal numbers. On these images and on a graph of cross-sectional relief, the arc structures are of similar relief to the ring structures, i.e. they appear to protrude from the membrane by approximately 73Å and not 113Å like the prepore structures. The presence of arcs is mentioned in the figure legend but no other mention or discussion of their relevance is made in this work (discussed in Gilbert, 2005).

Another study used a form of PFO that has an introduced disulphide bond within domain 3 which prevents insertion until the disulphide bond is reduced, termed dsPFO (Dang *et al.*, 2005). This work was performed on cholesterol-lipid bilayers and both pores and arcs are present in the negative-staining TEM images presented. Inserted ring structures observed in samples treated with DTT possess an inner ring of density that is absent on those in the prepore state (DTT untreated). However, the arcs present in the DTT treated sample also appear to possess a corresponding area of density, in contrast to the untreated sample. The presence of arcs is not acknowledged within the text and their potential significance appears to have been overlooked.

The observation of different sizes of arc-like structures gave rise to the model of Palmer *et al*, 1998 whereby oligomerisation and pore formation are simultaneous and semi-circular arcs form a pore lined by a free-edge of lipid membrane that

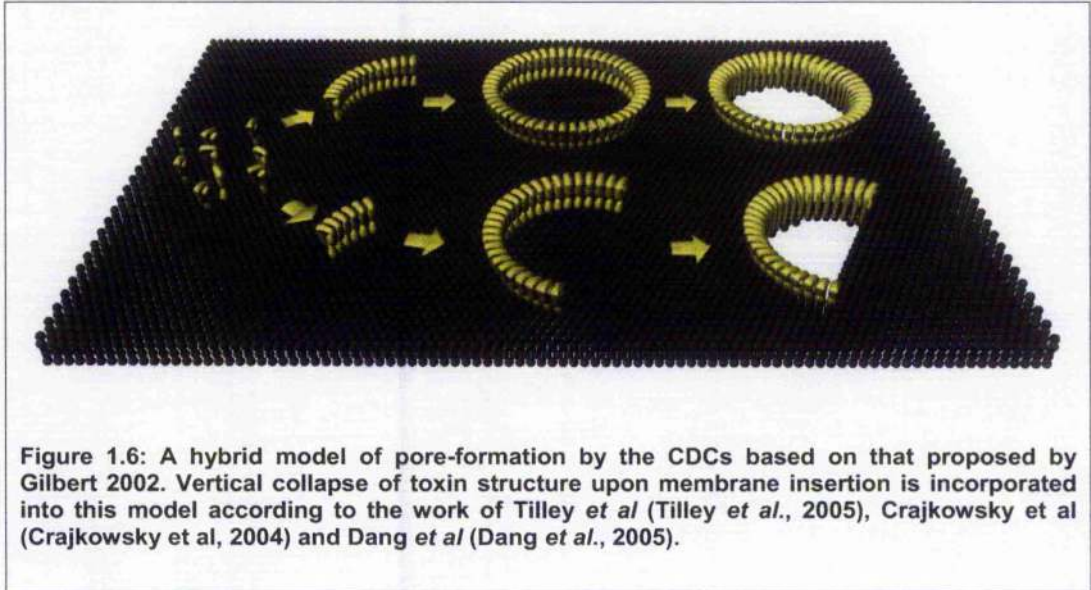
grows sequentially until a complete circular pore is formed (Palmer *et al.*, 1998). This model does not account for the observation of un-inserted arcs and prepore complexes (Czajkowsky *et al.*, 2004; Shepard *et al.*, 2000; Tilley *et al.*, 2005) and is in direct conflict with the prepore model.

A hybrid model

Given the inconsistencies above, there is evidence for alteration of prepore model presented above (Gilbert, 2005). A hybrid model, as previously proposed by Gilbert (Gilbert, 2002), is capable of fitting the discrepancies that cast doubt on the prepore model. In this combined model, toxin monomers bind to the target membrane and commence oligomerisation. Oligomeric structures can be triggered to insert their transmembrane loops either when fully formed as a ring structure or in the form of a semi-circular arc. The result is a mixture of inserted arc and ring structures, which is consistent with the results provided in the work by Czajkowsky *et al* and Dang *et al* (Czajkowsky *et al.*, 2004; Dang *et al.*, 2005). This model also allows for the formation of the double arc structures that are commonly observed by electron microscopy of treated membranes (Bhakdi & Tranum-Jensen, 1985).

Despite the great amount of work that has been done to elucidate the mechanism of action of the CDCs, even the combined hybrid model requires further experimental support. It is still to be shown whether arcs are able to insert as a coordinated process as shown in the hybrid model and whether the pores formed by arcs are responsible for the cation-gated pores that have been observed at low

toxin concentrations. Another highly active area is investigation of the role of the CDCs in virulence of their producing organisms in infections and infection models.



Role of the CDCs in Virulence

A number of members of the CDC family have been implicated in the virulence of their producing organisms.

Deletion of the *ply* gene of *Streptococcus pneumoniae* led to reduced virulence in a murine i.p. challenge model of infection. The median survival time for mice injected with the PLY knockout strain was 13.8 days, compared with 0.9 days for the wild-type D39 strain (Berry *et al.*, 1999). Another study found that a PLY knockout strain caused chronic bacteraemia lasting several days whereas the wild-type D39 strain caused acute sepsis leading to death within 24 to 38 hours post-infection (Benton *et al.*, 1995).

LLO has been shown to be essential for the virulence of *Listeria monocytogenes* as Tn917 transposon insertion mutants of the *hly* gene encoding LLO were avirulent but full virulence was returned upon gene complementation (Cossart *et al.*, 1989). Similarly, insertional inactivation of the *ply* gene of *Arcanobacterium pyogenes* lead to reduced virulence in murine models of infection (Jost *et al.*, 1999).

Whereas the reduction in virulence of *S. pneumoniae* resulting from inactivation of PLY is substantial, loss of PFO from *C. perfringens* has only a minor effect on the overall virulence of the organism (Awad *et al.*, 2001), indicating the CDCs can have a range of importance to their producing organisms. However, experimental evidence suggests that the role and importance of the toxin can vary depending on the infection model used. For example, a PLY knockout strain, PLN-A, was found to cause chronic bacteraemia rather than acute sepsis in a mouse model of bronchopneumonia (Benton *et al.*, 1995), the knockout strain was ten times less virulent than the wild-type in a mouse model of lobar pneumonia (Rubins *et al.*, 1995) but in a chinchilla model of otitis media, toxin positive and negative *S. pneumoniae* produced similar amounts of inflammation (Sato *et al.*, 1996).

Biological effects of the CDCs

The cholesterol-dependent cytolysins were initially described as haemolysins, but for many their biological effects are now recognised to be much more complex and diverse than solely cytolytic activity. A great number of other biological effects in addition to pore formation have been described in a wide array of CDCs however

for many of these, the degree of contribution to pathogenesis of the producing organism has not been well defined.

Complement activation

PLY and SLO have both been shown to activate complement (Bhakdi & Tranum-Jensen, 1985; Paton *et al.*, 1984). Activation of complement by PLY occurred in the absence of specific antibodies and introduction of a D385N mutation to PLY reduced non-specific antibody binding and abolished complement activation (Mitchell *et al.*, 1991). It has been suggested that activation occurs via a β -sandwich region of domain 4 similar to that of the Fc region of IgG (Rossjohn *et al.*, 1998).

A strain of *S. pneumoniae* expressing a PLY mutant deficient in complement activation, D385N, had reduced virulence in a murine pneumonia model (Alexander *et al.*, 1998). Another *S. pneumoniae* mutant expressing D385N PLY showed greater clearance from the blood and reduced mortality compared with wild-type *S. pneumoniae* following *i.v.* injection in cirrhotic rats (Alicantara *et al.*, 1999). This group also demonstrated complement depletion during *S. pneumoniae* infection of cirrhotic and control rats that was directly attributed to the complement activating activity of PLY (Alicantara *et al.*, 2001). An *S. pneumoniae* mutant carrying the D385N mutation of PLY that reduces complement activation activity was found to have lower virulence in a rabbit model of corneal infection, although it was less attenuated than a PLY knockout strain indicating that complement

activation may play a role in the activity of the protein during ocular infection (Johnson *et al.*, 1995).

Phagosomal escape and intra-cellular growth

LLO is a major virulence factor that is responsible for the escape of *L. monocytogenes* from phagosomes to the cytosolic space within macrophages (Cossart *et al.*, 1989; Portnoy *et al.*, 1988). LLO, in conjunction with two other proteins, phosphatidylinositol-specific phospholipase C (PI-PLC) and phosphatidylcholine phospholipase C (PC-PLC) lead to a escape of the bacterium through the phagosomal membrane (Camilli *et al.*, 1993; Gedde *et al.*, 2000; Portnoy *et al.*, 1992).

LLO has an acidic pH optimum to enable disruption of the phagosomal membrane at low endosomal pH but prevent damage to the host cell plasma membrane. LLO also contains a 26 amino acid region rich in proline, glutamate, serine and threonine which is similar to PEST sequence motifs that target eukaryotic proteins for degradation. This motif is critical to the virulence of *L. monocytogenes* and was first thought to target the toxin for degradation thereby preventing damage to the host cell (Decatur & Portnoy, 2000; Lety *et al.*, 2001). However mutational studies have cast doubt that the PEST-like sequence is acting to promote degradation as previously thought (Lety *et al.*, 2002). Recent results showed that mutation of the PEST sequence did not change intracellular half-life but did lead to higher LLO levels, suggesting that the sequence may have a role in translational control of the toxin in the host cell cytosol (Schnupf *et al.*, 2006aa; Schnupf *et al.*, 2006bb).

Introduction of LLO to the soil-resident bacterium *B. subtilis* enabled escape of the bacterium from the phagosome and growth within macrophages (Bielecki *et al.*, 1990).

Another bacterium that employs escape from within the phagosome as a virulence mechanism is *B. anthracis*. During inhalation anthrax, *B. anthracis* spores are phagocytosed by alveolar macrophages which transport the bacterium across the alveolar barrier upon migration to the lymph nodes (Guidi-Rontani *et al.*, 1999). The spores then germinate within the phagolysosome of the macrophage, and escape from the macrophage allowing the bacterium to proliferate within the bloodstream.

Given the similar requirement of *B. anthracis* to *L. monocytogenes* to escape from the phagosome of macrophages, it is possible that ALO plays a role in the disruption of the phagosomal and/or plasma membranes. Recombinant strains of *L. monocytogenes* expressing anthrolysin O were capable of escape from the phagocytic vacuole but unlike LLO also damaged the plasma membrane of the cell (Wei *et al.*, 2005), highlighting the essential role of the low pH optimum of LLO in selectively damaging the endosomal membrane without cell lysis (Glomski *et al.*, 2002; Schuerch *et al.*, 2005).

SLO has been shown to allow group A Streptococci to evade uptake and killing within pharyngeal epithelial cells by preventing internalisation into lysosomes. On

the other hand, SLO-negative mutants were readily taken up and killed within the lysosomes of epithelial cells (Hakansson *et al.*, 2005).

Cytolysin-mediated translocation

SLO has been shown to be capable of translocating a small effector molecule, *S. pyogenes* NAD-glycohydrolase (SPN) across the host membrane (Madden *et al.*, 2001). This process has been likened to a Gram-positive version of the well-described type-III secretion systems of gram-negative bacteria. SPN produces the secondary messenger cyclic-ADP-ribose that contributes to the cytotoxic effect of *S. pyogenes* on HaCaT keratinocytes (Madden *et al.*, 2001). SPN has been shown to enhance the cytotoxic activity of Group-A Streptococcal lysate in combination with SLO and leading to depletion of NAD⁺, ATP and cell death (Michos *et al.*, 2006).

Translocation of SPN is dependent on a 66 amino acid domain of SLO not present in other CDCs but addition of this domain to PFO was insufficient to confer SPN-translocating ability on it (Meehl & Caparon, 2004). None of the other CDCs sequenced to date has such a large N-terminal extension with the exception of smhPAF, although no translocational activity has been attributed to this domain and its function remains unknown.

Cytokines and inflammatory mediators

CDCs have been demonstrated to potentiate release of a number of cytokines and are very potent inflammatory mediators. A selection of the broad range of inflammatory mediators produced by cells upon exposure to CDCs *in vitro* is shown in Table 1.2. C-terminal truncations of PLY which are not capable of cell binding or pore formation are still capable of inducing interferon γ and TNF- α , indicating that cell binding may not be required for these effects (Baba *et al.*, 2001).

Table 1.2: Table showing some of the cytokine and inflammatory mediators induced by CDCs

CDC	Cell Type	Cytokine or mediator induced	Reference
PLY ALO SLO	Epithelial cells (D562 cells & A549 cells)	Activation of p38 MAPK leading to release of IL-8	(Ratner <i>et al.</i> , 2006)
PLY	Primary Murine Spleen Cells	γ -interferon and nitric oxide induced by PLY and two C-terminal truncations, PLY426 and PLY437	(Baba <i>et al.</i> , 2002)
PLY	Human Monocytes	TNF- α and IL-1 β	(Houldsworth <i>et al.</i> , 1994)
PLY	Murine Macrophages	Nitric Oxide	(Braun <i>et al.</i> , 1999)
PLY	Human neutrophils	IL-8 but not TNF- α	(Cockeran <i>et al.</i> , 2002)
LSO	Primary Murine Spleen Cells	γ -interferon induced by LSO and a truncated derivative, LSO 483	(Ito <i>et al.</i> , 2003)
LLO	Murine peritoneal macrophage	IL-1	(Yoshikawa <i>et al.</i> , 1993)
LLO	Murine Spleen Cells	γ -interferon and IL-12	(Nishibori <i>et al.</i> , 1996) (Nomura <i>et al.</i> , 2002)
LLO	Human umbilical vein endothelial cells (HUVECs)	Activation of NF-kappaB and IL-8 secretion	(Kayal <i>et al.</i> , 1999)
LLO	Caco-2 cells	IL-6 production	(Tsuchiya <i>et al.</i> , 2005)
SLO	Human monocytes	TNF- α and IL-1 β production	(Hackett & Stevens, 1992)
SLO	Human Keratinocytes (HaCat) and Endothelial cells	NF-kappaB activation and release of IL-6 and IL-8	(Walev <i>et al.</i> , 2002)

The results of such experiments vary greatly by cell-lines used, many of which may not be relevant as toxin exposure may not occur to all cell types in the body during infections. The situation is further complicated by cascade effects of activation when multiple cell types are present. For example, it has been shown that co-cultures of U937 and NK cells produce interferon- γ on stimulation with PLY but this is not observed on individual cultures of either cell type (Kerr *et al.*, 2005).

The induction of pro-inflammatory mediators such as IL-1 β , IL-6 and TNF- α is thought to have a role in inflammation *in vivo*. PLY production by *S. pneumoniae* has been linked to inflammation and histological examination of rats indicated that administration of PLY directly to the lung can cause pulmonary inflammation effects on the lung similar to those observed in infection with *S. pneumoniae* (Feldman *et al.*, 1991).

Recent work has shown that in mice some of these effects can be caused by a direct interaction of CDCs with Toll-like receptor 4 (TLR-4).

Activation of TLR-4

Toll-like receptors are transmembrane proteins that recognise conserved microbial structures as part of the innate immune system (Kawai & Akira, 2005).

A number of components of Gram-positive bacteria have been shown to activate TLRs including peptidoglycan and teichoic acid, mainly through TLR2 (Schwandner *et al.*, 1999). The responses generated by these components are

generally weaker than the responses produced by activation of TLR-4 by LPS from Gram-negative bacteria. It has now been shown that a number of CDCs, including PLY, ALO, PFO, LLO and SLO (Malley *et al.*, 2003; Park *et al.*, 2004) are also capable of activation of TLR-4.

In the study by Malley and colleagues, they found that signalling through TLR-4 was responsible for the stimulation of IL-6 and TNF- α in macrophages by PLY, and that mice with a mutation in TLR-4 that reduced activation by PLY were more susceptible to intranasal infection by *S. pneumoniae* (Malley *et al.*, 2003). They also showed that mice with a mis-sense mutation that makes TLR-4 hyporesponsive to stimulation by PLY and LPS were more susceptible to lethal infection after intra-nasal colonisation with *S. pneumoniae*. It was therefore suggested that interaction between PLY and TLR-4 is important in preventing pneumococcal colonisation from progressing to invasive pneumococcal disease (Malley *et al.*, 2003).

Activation of TLR-4 by ALO in combination with another toxin from *B. anthracis*, lethal toxin (LT), can induce apoptosis of macrophages and it is suggested that ALO is required for the induction of macrophage apoptosis by *B. anthracis* (Park *et al.*, 2004). The ability to activate TLR-4 was also shared by PFO, SLO and LLO (Park *et al.*, 2004).

Protective vaccination with the CDCs

Immunisation with some members of the cholesterol-dependent cytolysin family, or genetic toxoids or peptides derived from them, can be protective against disease caused by the producing organisms.

Paton *et al* first demonstrated that PLY can protect against infection with *S. pneumoniae* (Paton *et al.*, 1983) and this has been subsequently confirmed by a number of studies. Immunisation of mice with a partial toxoid of PLY containing a single mutation causing greatly reduced haemolytic activity, W433F, protected mice against i.p. or i.n. challenge with a number of strains of *S. pneumoniae* (Alexander *et al.*, 1994). Recently it has been shown that i.p. immunisation with wild-type PLY or a novel non-toxic genetic toxoid, $\Delta 6$ PLY, increases the survival of mice after i.p. challenge with *S. pneumoniae* (Kirkham *et al.*, 2006b).

Immunisation of mice with PLO or genetically-toxoided PLO showed complete protection against i.p. challenge with *A. pyogenes* (Billington *et al.*, 2001; Jost *et al.*, 2003). Vaccination of mice with SLY has also been demonstrated to protect against its producing organism, *Streptococcus suis* (Jacobs *et al.*, 1994).

Vaccination with CDCs can also produce a response that is protective against an intracellular bacterium. A number of studies have demonstrated that immunisation with LLO can produce a response protective against *Listeria monocytogenes*. Vaccination with *L. monocytogenes* strains producing LLO causes protective immunity whereas LLO-negative or LLO-attenuated mutants fail to protect against

L. monocytogenes infection (Berche *et al.*, 1987; Michel *et al.*, 1990). Cytotoxic T-lymphocytes (CTLs) specific for LLO are generated by immunisation, particularly directed toward the class I MHC-restricted epitope LLO₉₁₋₉₉ (Pamer *et al.*, 1991) and these lymphocytes are protective against *L. monocytogenes in vivo* (Harty & Bevan, 1992).

Intramuscular DNA vaccination with a plasmid containing the coding sequence for LLO W492A, a mutant of LLO with 100-1000 fold reduced haemolytic activity, was also effective at producing a protective response against *L. monocytogenes* (Cornell *et al.*, 1999). Prime-boost DNA gene gun vaccination with a plasmid containing the *hly* gene for LLO is also capable of protection against listeriosis (Fensterle *et al.*, 1999).

The efficacy of particular formulations of antigen and routes of administration may vary between CDCs and with the type of infection. While vaccination with a purified pneumolysin toxoid protected against lethal intraperitoneal challenge with *S. pneumoniae*, DNA vaccination with the same toxoid did not provide protection (Ferreira *et al.*, 2006).

Other Applications of the CDCs

The cholesterol-dependent cytolysins are finding uses in a number of applications. The most common application of the CDCs is the use of SLO as a cell permeabilisation reagent in cell biology, although other CDCs including TLY have also been used in this way (Bhakdi *et al.*, 1993).

The human-specific cell-binding domain of ILY has been shown to be capable of use as an adaptor molecule to bind substances conjugated to the N-terminus of domain 4 to human cells. An initial trial of this technology proposes use of domain 4 of ILY as a cell-targeting molecule in cancer immunotherapy (Nagamune *et al.*, 2004b). This 'proof of principle' demonstrated that domain 4 of intermedilysin linked to Fab of an anti-carcinoembryonic antigen monoclonal antibody was capable of delivering erythrocytes to carcinoembryonic cancer cells in vitro, although the potential for cancer therapy in a clinical setting is not elaborated upon.

The cytotoxic activity of the CDCs may also prove therapeutically useful when specifically targeted to kill problematic cells. One approach being investigated is using ALO in anti-viral therapy against HIV (Yuntao, 2004). Delivery of a lentiviral vector for HIV-1 Tat and Rev promoter driven expression of ALO to cells may limit the toxicity of ALO to selectively kill HIV-1-infected cells.

Another approach, pioneered by Yang *et al.*, utilises SLO as a 'suicide gene' in cancer therapy. This group created an adenovirus and injected the virus directly into human cervical cancer cell-derived tumours grown in a nude mouse model. The average size of the tumours reduced to 26.3% of that of a PBS control group after 21 days, demonstrating that tools derived from CDCs could prove useful in cancer therapy (Yang *et al.*, 2006).

Aims of this project

The aims of this work were:

- Construction of a fluorescently-tagged form of pneumolysin to enable detection and visualisation of toxin localisation.
- Determination of the protein receptor for intermedilysin and analysis of the region of intermedilysin responsible for this interaction through mutational studies.
- Cloning of anthrolysin O and creation of a genetic toxoid for immunisation studies. Investigation of the potential of ALO and detoxified derivatives for immunisation against anthrax.

Chapter 2: Materials and Methods

Materials

Primers

All primers used in these experiments are shown in appendix 2. Primers were obtained from Sigma-Genosys Ltd, UK. All primers were ordered desalted with no further purification steps.

Plasmid Constructs

The pET33b(+) plasmid was obtained from Novagen Inc, pQE9mILY was a kind gift from H. Nagamune, University of Tokushima and pNF320 was from N. Freitag of Wayne State University School of Medicine, Detroit, Michigan, USA.

Bacterial Strains

Chemically competent *E. coli* strains TOP10 and DH5 α were purchased from Invitrogen, and chemically-competent *E. coli* strains XL-1-blue and BL21(DE3) were purchased from Stratagene. *B. anthracis* ST1 was from the strain library at DSTL, Porton Down, UK and all *B. anthracis* experimental work was performed by DSTL staff at the facility.

Blood

Human blood was obtained from the Scottish Blood Transfusion Service. Horse and sheep blood were obtained from E&O laboratories and rabbit blood was from the Central Research Facility, University of Glasgow.

Solutions, Buffers and Growth Media

The composition of solutions, buffers and growth media, and protocols for their production are given in appendix 3.

DNA modifying enzymes

T4 DNA Ligase and Calf Intestinal Alkaline Phosphatase (CIAP) was obtained from Promega. All restriction enzymes were obtained from Promega except for *PciI*, which was obtained from New England Biolabs.

Methods

Construction of pET33bEGFPPLY

The GFP coding sequence was amplified from pNF320 (Freitag *et al.*, 1999) by PCR using primers 20G and 20H. The PCR product was cut with *NheI* and *BglII*, ligated into *NheI/BamHI* digested pET33bPLY and transformed into TOP10 *E. coli*. Mutations F64L and S65T (Cormack *et al.*, 1996) were introduced into the GFP cds to make eGFP by site-directed mutagenesis (Quikchange SDM Kit, Stratagene) with primers 24W and 24X.

Construction of pET33bDel6EGFPPLY

pET33bDel6EGFPPLY was created by site directed mutagenesis (Quikchange SDM Kit, Stratagene) of pET33bEGFPPLY using primers 23B and 23C to introduce the $\Delta 6$ mutation (Deletion of A146 and R147, (Kirkham *et al.*, 2006b)) within the *ply* coding sequence.

Construction of pET33bEGFP

The coding sequence for eGFP was amplified by PCR from pET33bEGFPPLY using primers 20G and 45L. The resulting product was cut with *NheI* and *SacI*, gel purified and ligated into *NheI/SacI* cut, CIAP-treated pET33b. The ligation reaction was transformed into XL-1 *E. coli* (Stratagene).

Construction of TOPO-ALO

A 2433bp genomic segment containing the anthrolysin O coding sequence and flanking regions was amplified by PCR from *B. anthracis* Ames strain genomic DNA using primers 32G and 32H. The resulting PCR product was cloned into pCR2.1-TOPO and transformed into TOP10 *Escherichia coli* using the TOPO-TA cloning kit (Invitrogen) according to the manufacturer's recommended protocol. This cloning step was performed by Prof. Richard Titball, DSTL, Porton Down, UK.

Construction of pET33b-mALO

The coding sequence of mature ALO (mALO), encoding residues E35-H512 of whole ALO, was amplified by PCR from TOPO-ALO using primers 43X and 41P. The amplified product was digested with *Bam*HI and *Sac*I, gel purified, ligated into *Bam*HI/*Sac*I cut, calf-intestinal alkaline phosphatase-treated pET33b and transformed into chemically-competent XL-1 *E. coli* (Stratagene, Amsterdam Zuidoost, Netherlands).

Construction of pET33b- Δ 6mALO

The Δ 6 mutation (Kirkham *et al.*, 2006b), which corresponds to deletion of residues A190 R191 of whole ALO or A156 R157 of mALO, was introduced to pET33bmALO by site-directed mutagenesis (SDM) (Stratagene Quikchange XL kit) using primers 42S and 42T.

Construction of pET33bmILY

The *mILY* cds was amplified by PCR from pQE9mILY using primers 26W and 26X. The amplified fragment was gel purified, digested with *Bam*HI and *Sac*I and ligated with a *Bam*HI/*Sac*I digested, CIAP-treated pET33b purified plasmid. The ligation reaction was transformed into XL-1 blue *E. coli*.

Construction of pET33bEGFPmILY

The eGFP and mILY coding sequences were amplified by PCR using primer sets 31T vs 31V and 31U vs 26X respectively. The PCR products were purified and an overlap PCR was performed to join the two products using primers 31T vs 26X. The resulting PCR product was digested with *Spe*I and *Sac*I and ligated with *Nhe*I/*Sac*I digested pET33b plasmid. The ligation mixture was transformed into TOP10 *E. coli* and plated on LB agar containing kanamycin.

Construction of pET33bEGFPsILY

The eGFP cds was amplified from pET33bEGFPPLY using 31T vs 36D and the sILY fragment was amplified from pET33bILY using primers 26X vs 36C. PCR products were gel purified and an overlap PCR reaction was performed using primers 31T and 26X to join the two products. The resulting PCR product was digested with *Spe*I and *Sac*I, gel purified and ligated into *Nhe*I/*Sac*I cut, CIAP-treated pET33b and the ligation reaction was transformed into TOP10 *E. coli*. The sequence of the cds and flanking regions of the plasmid were confirmed by DNA sequencing.

Construction of pET33bDel6EGFPsILY

The $\Delta 6$ mutation (deletion of residues equivalent to A204 and R205 of ILY precursor) was introduced to pET33bEGFPsILY using primers 31W vs 31X) by SDM (Stratagene Quikchange XL SDM kit). The sequence over the mutated region was checked by DNA sequencing and confirmed to be correct.

Construction of vectors for expression of chimeric toxins between PLY and ILY

Fragments of ILY and PLY were amplified by PCR using the primer sets shown in Table 2.1. Each pair of amplified fragments was gel purified and joined by overlap PCR using the overlap primers shown on the right hand side of Table 2.1. The resulting product was gel purified, digested with *Bam*HI and *Sac*I and ligated into *Bam*HI/*Sac*I cut, CIAP-treated pET33b. Ligations were transformed into TOP10 *E. coli* and plated on LB containing kanamycin.

Chimera	5' primer set (template)	3' primer set (template)	Overlap Primer set
A	26F vs 9Y (PLY)	26C vs 26X (ILY)	9Y vs 26X
B	26D vs 26W (ILY)	26E vs 9Z (PLY)	26W vs 9Z
C	26J vs 9Y (PLY)	26G vs 26X (ILY)	9Y vs 26X
D	26I vs 26W (ILY)	26H vs 9Z (PLY)	26W vs 9Z
E	26N vs 9Y (PLY)	26K vs 26X (ILY)	9Y vs 26X
F	26L vs 26W (ILY)	26M vs 9Z (PLY)	26W vs 9Z
G	26R vs 9Y (PLY)	26O vs 26X (ILY)	9Y vs 26X
H	26P vs 26W (ILY)	26Q vs 9Z (PLY)	26W vs 9Z

Table 2.1: Primers used for amplification of PLY and ILY fragments in construction of chimeric toxins

pDest32-D4ILY Yeast-2-hybrid bait vector

The D4ILY coding sequence was amplified from pQE9mILY using primers 40T and 40U. These primers were designed to add Gateway Att-B1 and Att-B2 sites to the ends of the coding sequence.

A one-tube gateway cloning reaction was performed according to the Invitrogen Pro-Quest manual to clone the D4ILY PCR product into pDEST32 (DNA binding domain fusion vector) via pDONR221. The reaction was transformed into DH5 α *E. coli* and plated on LB agar containing gentamycin.

Gateway cloning

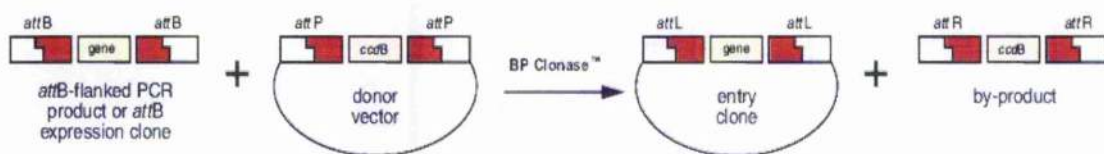
Gateway cloning was performed according to the Gateway Cloning Manual provided by Invitrogen. All reagents for gateway cloning were obtained from Invitrogen.

Gateway Cloning is a technology for cloning of DNA sequences which relies on site-specific recombination rather than traditional restriction and ligation cloning techniques (Figure 2.1). This provides a rapid and highly efficient method of moving DNA sequences into and between cloning and expression vector systems that ensures reading frame and ORF orientation are maintained.

The Gateway system is based on a modification of the bacteriophage lambda site-specific recombination system. Gateway components are modified from those of bacteriophage lambda to increase specificity and efficiency (Bushman *et al.*, 1985). A BP (attB-attP) reaction clones an attB-flanked PCR product or coding

sequence from a Gateway expression clone into a Gateway entry clone. This entry clone can then be combined with a Gateway destination vector in an LR reaction (*attL*-*attR*) to produce a Gateway expression clone containing the gene of interest (Figure 2.1).

- **BP Reaction:** Facilitates recombination of an *attB* substrate (*attB*-PCR product or a linearized *attB* expression clone) with an *attP* substrate (donor vector) to create an *attL*-containing entry clone (see diagram below). This reaction is catalyzed by BP Clonase™ enzyme mix.



- **LR Reaction:** Facilitates recombination of an *attL* substrate (entry clone) with an *attR* substrate (destination vector) to create an *attB*-containing expression clone (see diagram below). This reaction is catalyzed by LR Clonase™ enzyme mix.

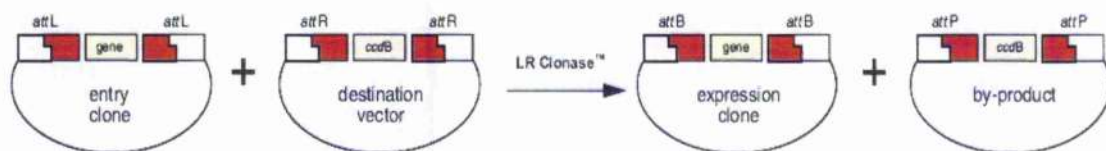


Figure 2.1: Overview of the Gateway Cloning system. Diagram taken from the Invitrogen Gateway Manual.

DNA sequencing

DNA sequencing was provided by the Molecular Biology Support Service, University of Glasgow. Sequence analysis was performed using the Contig Express component of Vector NTI Software version 9 or 10 (Invitrogen).

Protein Expression

Recombinant *E. coli* containing the expression plasmids were grown to mid-log phase in terrific broth (Tartof & Hobbs, 1987) containing an antibiotic appropriate to maintain plasmid selection. IPTG was added to a final concentration of 1mM to induce expression and cultures were incubated shaking at 30°C or 37°C for 3, 6 or 18 hours. Bacteria were harvested from the broth by centrifugation at 13000 x G for 3 minutes. Bacterial pellets were resuspended in PBS containing Dnase I (Sigma) and Benzamidine (Sigma) and cells were disrupted by sonication or using a One-Shot Cell Disruptor (Constant Systems). Cell lysates were centrifuged at 18000 x G and 4°C for 30 minutes and the supernatant was passed through a 0.2µM syringe filter to remove remaining cell debris.

Nickel-affinity purification of His-Tagged proteins

His-tagged proteins were purified from crude cell extracts by FPLC on a Nickel-charged NTA column (Qiagen Superflow resin) with elution on a 0-300mM continuous imidazole gradient in PBS. Purified proteins were dialysed at least three times against a greater than 50-fold volume of PBS and concentrated using Amicon Ultra Centrifugal Concentration columns with 10 or 30kDA molecular weight cut-off membranes.

Hydrophobic interaction chromatography

Hydrophobic interaction chromatography of PLY and eGFPLY was performed as described (Kirkham *et al.*, 2006b) using a Bio-Cad 700E chromatography workstation.

SwellGel Tab purification

Purification of poly-histidine tagged proteins using SwellGel Ni-NTA tabs (Pierce Biotechnology, Rockford, IL, US) was performed according to the 'batch purification' protocol provided by the manufacturer.

Anion Exchange Chromatography

Following nickel-affinity purification or hydrophobic interaction chromatography, proteins were dialysed into PBS and then further purified by passage through an anion exchange (HQ) column on a BioCad 700E Workstation (Applied Biosystems Ltd, Warrington, UK). In this purification step, DNA and contaminants were retained on the column and purified proteins were present in the flow through. Eluted proteins were immediately dialysed into PBS and concentrated using Amicon Ultra centrifugal concentrators (Millipore, Watford, UK).

UV Absorbance Scanning

Absorbance scans from 220-320nm were performed on purified proteins using a Unicam UV2 spectrophotometer.

LAL assay

Endotoxin levels were measured in protein samples using the Limulus Amoebocyte Lysate (LAL) Kinetic-QCL kit from BioWhittaker. LPS causes the conversion of a proenzyme in the LAL lysate into the active form and the rate of activation is proportional to the amount of LPS present. This enzyme then cleaves p-nitroaniline (pNA) from Ac-Ile-Ala-Arg-pNA increasing the absorbance of the solution at 405nm. LPS concentration is calculated by comparison to a standard curve generated from known standards.

Bradford Assay

Bradford assays were performed according to the technique of Bradford (Bradford, 1976). Known standards of BSA (Sigma) were made up in PBS covering a range of concentrations from 23-1500 $\mu\text{g/ml}$. 10 μl of standard, blank (PBS) or protein sample were added to a flat-bottomed 96-well plate (Nunc) and 200 μl Bradford reagent (Sigma) was added to each well. The absorbance at 570nm was read on a plate reader (Dyner Revelation) and protein concentrations were interpolated on graphs of standard curves generated using Graphpad Prism software.

Western Blotting

Western Blotting was performed by routine methods as originally described (Burnette, 1981; Renart *et al.*, 1979). Optimal antibody concentrations varied according to the reaction and are described in the appropriate results section.

Epi-fluorescence microscopy of eGFP-tagged toxins

The following protocol was devised to visualise eGFP-tagged toxin binding to human erythrocytes. Fresh human blood was washed three times by resuspension in PBS followed by centrifugation at 900 x G for 5 minutes. After the final wash, the human erythrocyte suspension was diluted to 4% v/v in PBS. 250 μl of 1.4 μM eGFP-tagged toxin solution in PBS was added to 250 μl 4% hRBC solution to give 500 μl of 700nM eGFP-tagged toxin in a 2% hRBC solution and the suspension was incubated at 37°C for 30 minutes.

10 μl of reaction solution was applied to the surface of a glass microscope slide and a glass coverslip was gently applied. Slides were viewed immediately by

fluorescence microscopy using a Zeiss Axioskop 20 Fluorescence Microscope fitted with a #09 FITC filter set (Excitation 488nm, Emission 530nm bandpass). Images were captured using a Coolsnap CCD camera (Photometrics) and Openlab software (Improvision).

The protocols for the epifluorescence microscopy work described in Beurg et al, 2005 are described in that work (Beurg *et al.*, 2005).

Laser Scanning Confocal Fluorescence microscopy

Tissue culture cells were grown to 30-50% confluence on 8-well chamber slides (Nunc ref. 154534). The growth medium was removed from each well and replaced with 300µl pre-warmed growth medium containing toxin at test concentration, or PBS for control wells. Slides were incubated at 37°C, 5% CO₂ and 100% humidity for 30 minutes. The growth medium was removed from each well and cells were washed with 300µl pre-warmed growth medium. Cells were fixed by addition of 300µl 3.8% w/v paraformaldehyde in growth medium, corrected to pH 7 and pre-warmed to 37°C, for 20 minutes at room temperature. Fixed cells were washed with PBS. Where appropriate, cells were also stained by addition of 6.6µM (200units/mL) rhodamine-phalloidin (Invitrogen) in PBS for 20 minutes and/or 0.1µg/ml DAPI (Sigma Chemicals) in PBS for 1 minute, both at room temperature. Cells were rinsed three times in PBS, slide chambers were removed using the tool provided and cells were mounted using Pro-long Gold anti-fade reagent (Invitrogen) according to the manufacturer's instructions.

Scanning Electron Microscopy

Toxin solutions were centrifuged for 5 minutes at 17000 x G to remove any large aggregates of protein. 250 μ l of 1.4mM toxin in erythrocyte medium (ECM) was added to 250 μ l 0.4% human erythrocyte solution in ECM and each reaction was incubated at 37°C for 10 minutes. 500 μ l 5% Glutaraldehyde in ECM was added to each tube and incubated for 1 hour at room temperature. Erythrocytes were then washed three times in ECM by centrifugation at 17000 x G for 1 minute and resuspended in 100 μ l ECM. 20 μ l erythrocyte suspension was applied to a poly-lysine coated 10mm glass coverslip and incubated at room temperature for 20 minutes. Coverslips were rinsed three times with ECM solution and fixed with 1% OsO₄ for 1 hour. After rinsing in dH₂O three times for 10 minutes, samples were dehydrated by passage through an ethanol series. Samples were processed using a critical point drier then coated twice with gold/paladium using a Polaron SC515 diode sputter coater. Sample dehydration and gold coating was done by Margaret Mullen.

Coverslips were mounted on aluminium studs using double-sided tape and viewed on a Jeol JSM 6400 Scanning Electron Microscope.

Transmission Electron Microscopy

Fresh human blood was washed three times in PBS by centrifugation for 3 minutes at 100 x G in a microcentrifuge. Washed erythrocytes were diluted to 2% v/v with PBS. Toxins were diluted to a concentration of 20 μ g/ml in 200 μ l PBS and added to 1000 μ l 2% human erythrocyte solution. Samples were incubated for 5 minutes at 37°C and washed three times in 0.5M Tris 150mM NaCl pH7.4.

Formvar/Carbon-coated 200 mesh copper grids were glow discharged and specimens in distilled water were dried from suspension onto the support film. A droplet of 1% aqueous methylamine vanadate (Nanovan; Nanoprobes, Stony Brook, NY, USA) or 10% uranyl formate (appendix 3) stain was applied and allowed to dry. Specimens were imaged with a LEO 912AB energy filtering transmission electron microscope at 120kV. Contrast enhanced, zero-loss electron energy filtered images were recorded with a 14 bit /2K Proscan CCD camera. Scale bars were derived from calibration against the lattice plane spacings of a catalase crystal grid (Agar Scientific Ltd, Stansted, UK).

Detection of eGFP-tagged toxin binding by FACS

Human blood was washed three times by centrifugation at 3000 x G for 1 minute and resuspension in PBS. The pellet was resuspended in PBS to give a 4% erythrocyte solution. 250 μ l 4% v/v human blood solution in PBS was added to 250 μ l toxin at 2 times final concentration in PBS and the solution was incubated at 37°C for 10 minutes before being placed on ice. Erythrocytes were either pelleted at 10000 x G for 3 minutes then resuspended in 3mL PBS or diluted to 3mL with PBS.

Cell suspensions were analysed by flow cytometry using a Becton-Dickinson FACScalibur flow cytometer and Cell-Quest software recording forward scatter, side scatter and FL-1 channels (Excitation 488nm, Emission 530nm). Flow cytometry charts were generated using WinMDI v2.8 (<http://facs.Scripps.edu>) and axis labels were added manually using Adobe Photoshop CS software.

The experimental work and data analysis for the flow cytometry binding assay published with Dr. R Anderson's group at the University of Pretoria, South Africa is described in that work (Fickl *et al.*, 2005).

Transformation of Yeast – Simple Low-Efficiency Transformation

This protocol is based on that described by Grey and Brendel (Grey & Brendel, 1992).

Yeast strain MAV203 was grown to large single colonies on YPAD agar by incubation at 28°C for 3 days. One colony of approximately 20µL volume was picked using a sterile toothpick. The pellet was resuspended and washed three times by centrifugation at 17000 x G in 1mL of sterile 20mM HEPES buffer containing 1M Sorbitol. After the final centrifugation, the pellet was resuspended in 250µl sterile buffer containing 20mM HEPES and 1M Sorbitol. 0.5µg plasmid DNA in 5µl sterile distilled water was added to 40µl yeast suspension and the solution was transferred to a pre-cooled 0.2cm gap electroporation cuvette. The sample was electroporated using BioRad Genepulser electroporation apparatus set to 1.6kV, 25µF and 200Ω, 0.2mL 1M sorbitol was added and the sample was plated immediately on selective SC agar media.

Transformation of Yeast – Library Transformation (60x)

MAV203 yeast containing the DB-X plasmid were inoculated into 25mL SC-leu medium and incubated at 30°C overnight. The number of cells were counted with a haemocytometer and 1.5×10^9 cells were pelleted by centrifugation at 3000 x G

for 5 minutes at room temperature. Cells were resuspended in 300mL pre-warmed YPAD broth, transferred to a sterile culture flask and incubated at 30°C shaking at 200 rpm until the cell titre reached 2×10^7 cells/mL. Cells were harvested by centrifugation at 3000 x G for 5 minutes at room temperature then the cell pellet was washed by resuspension in 150mL sterile distilled water followed by centrifugation at 3000 x G for 5 minutes. The pellet was resuspended in 6mL of sterile 100mM Lithium Acetate, transferred to a sterile 15mL centrifuge tube and incubated for 15 minutes at 30°C. Cells were pelleted again by centrifugation at 3000 x G for 5 minutes and the supernatant was removed.

The following reagents were added, in order, to a separate tube and mixed thoroughly by vortexing: 14.4 mL 50% PEG, 2.16mL 1.0 M Lithium Acetate, 3.0mL 0.5 mL Single-Stranded Carrier DNA, 50µg plasmid cDNA library in 2.04mL distilled water. The transformation mix was added to the cell pellet and vortexed vigorously until the cell pellet was resuspended. The transformation mix was incubated at 30°C for 30 minutes then heat-shocked at 42°C for 50 minutes, with inversion for 15 seconds every 5 minutes. Cells were pelleted by centrifugation at 3000 x G for 5 minutes then resuspended in 40mL sterile distilled water and spread onto 200 SC-leu-trp-ura plates. The number of transformants screened was calculated by spreading dilutions of the mixture onto four SC-leu-trp plates.

Yeast-2-hybrid screen

With the aim of finding candidates which may be the protein receptor for ILY, a yeast-2-hybrid assay was used to determine proteins from a human cDNA library were able to interact with ILY.

The yeast-2-hybrid system is a yeast-based assay to identify protein:protein interactions (Figure 2.2). Two yeast plasmid vectors are constructed: one fuses a 'bait' protein (X) to the DNA-binding domain (DB) of the GAL-4 transcription factor and the other fuses a library of 'prey' proteins (Y) to the activation domain (AD) of GAL-4 transcription factor. Interaction of the DB-X and AD-Y proteins leads to reconstitution of an active transcription factor and transcription of genes under the control of GAL4 promoters. After transformation with the plasmids, the yeast are screened for multiple reporter genes and transcription of these genes suggests an interaction between the prey and bait proteins. The potential interacting proteins can then be confirmed by other means such as co-immunoprecipitation, surface plasmon resonance or knockout experiments in model biological systems.

For this study, a yeast-2-hybrid system was used to screen for proteins from a human brain cDNA library that are capable of interaction with domain 4 of intermedilysin.

A yeast-2-hybrid screen was performed with pDest32-D4ILY against a human foetal brain cDNA library (Invitrogen 11396-018) using the Invitrogen Pro-Quest Yeast-2-hybrid system.

The pDest32-D4ILY plasmid was transformed into MAV203 yeast using the plate transformation method. The presence of the plasmid in a resulting clone was confirmed by PCR using primers 42P and 42R.

MAV203 yeast containing the pDest32-D4ILY bait vector were grown up and a 60x library-efficiency yeast transformation was performed to introduce a human brain cDNA Gal4-AD-fusion library. Cells were plated onto SC-leu-trp-his+25mM 3AT. Plates were incubated at 28°C for 3 days.

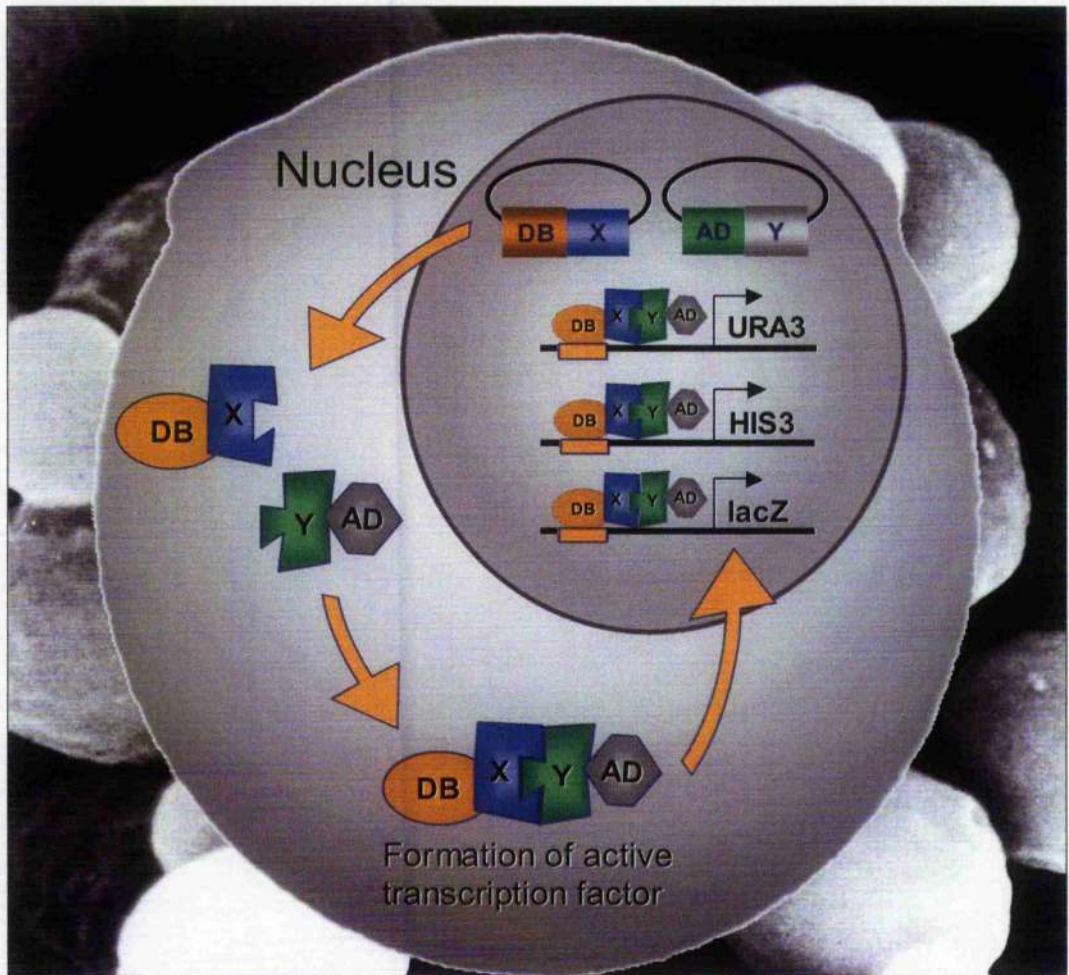


Figure 2.2: Schematic diagram of the Yeast-2-hybrid system. Interaction of the bait protein (X) fused to the Gal4 DNA-binding domain (DB) with the prey protein (Y) fused to the Gal4 activation domain (AD) causes reconstitution of an active transcription factor. This leads to expression of the *ura3*, *his3* and *lacZ* reporter genes. Initial Screens select colonies capable of growth on histidine-deficient agar medium and these clones are further characterised for growth on uracil-deficient medium, β -galactosidase activity using X-GAL and inhibition of growth on 5FOA-containing medium.

Trypsin treatment of erythrocytes

An assay was developed to determine the effect of trypsin treatment of erythrocytes on susceptibility to lysis by ILY and PLY.

A 5mg/ml solution of trypsin in PBS (Sigma T-1426) and solutions of trypsin inhibitor containing 10mg/mL chicken egg-white trypsin inhibitor (Sigma T-4385) and 1% w/v BSA in PBS were made up. Human blood was washed three times by centrifugation at 3000 x G for 1 minute and resuspension in PBS. The pellet was resuspended in PBS to give a 2% v/v erythrocyte solution.

Six 15mL centrifuge tubes were set up, each containing 2.5mL 2% human erythrocyte solution. 0.25mL trypsin solution was added to five tubes and 0.5mL PBS was added to the other tube (no trypsin control). 0.25mL trypsin inhibitor solution was added to the five tubes containing trypsin either immediately or after 1 hour, 2 hours, 4 hours or 8 hours.

The erythrocytes in each tube were pelleted by centrifugation at 3000 x G for 5 minutes and resuspended in 2.5mL PBS. The colour of the supernatants was monitored to ensure no haemolysis had occurred at this stage. Erythrocytes were used in a standard quantitative haemolytic assay as described in this chapter to determine their susceptibility to lysis by PLY or ILY. Lysis of erythrocytes causes release of haemoglobin into the supernatant in the assay well causing an increase in absorbance at 540nm.

Cell culture

BHK C13 cells (ATCC ref. CRL-1632) and Detroit 563 cells (ATCC ref. CCL-138) were maintained by standard cell culture techniques. Detroit 562 cells were grown in RPMI medium (Sigma) without phenol red, and for BHK C13 cells the growth medium used was DMEM (Sigma) without phenol red. Both media were supplemented with 2mM glutamine (Sigma) and 10% foetal bovine serum (Sigma). 1x Trypsin-EDTA solution (Cambrex) was used to detach the cells for cell passage.

L929 fibroblast cytotoxicity assay

The L929 fibroblast cytotoxicity was performed as described by Mosmann (Mosmann, 1983). The MTT [3-(4,5-dimethylthiazol-2-yl)-2,5-diphenyltetrazolium bromide] assay is based on the ability of the mitochondrial dehydrogenase enzyme of viable cells to cleave the tetrazolium rings of pale yellow MTT forming dark blue formazan crystals which are impermeable to cell membranes, thus resulting in accumulation within healthy cells. Addition of a detergent to the cells results in the liberation of the crystals, which are then dissolved. The number of surviving cells is directly proportional to the level of the formazan product created and this colour can be quantified using a simple colorimetric assay read on a multiwell spectrophotometer (ELISA reader).

Haemolysis Assay

Haemolysis assays were performed using human blood (Scottish Blood Transfusion Service) and horse blood (E&O laboratories, Bonnybridge, Scotland) by a modification of the technique described by Walker *et al.*, 1987 (Walker *et al.*, 1987). Following the incubation step, plates were centrifuged at 1000 x G using a Sigma 4K15 bench top centrifuge, and 50µl supernatant from each well was transferred to a new plate. The absorbance at 540nm was measured using a Dynex Revelation microplate reader and the A_{540} for percentage lysis was calculated by expression of each absorbance reading as a percentage of the A_{540} for a positive control well containing erythrocytes lysed by addition of 0.1mg/mL PLY.

Data were imported into Graphpad Prism 4 (GraphPad Software Inc.) and an XY scatterplot of Log_{10} toxin concentration against percentage haemolysis was produced. A variable slope sigmoidal response curve was plotted using the analysis component of the software and the concentration of toxin that would cause 50% lysis was calculated by interpolation using the fitted line on the graph. The specific activity was then determined by taking the reciprocal of the concentration that would cause 50% lysis (in mg/mL). 1 haemolytic unit is the amount of toxin that produces 50% lysis of a well containing 1% erythrocyte solution and specific activity is expressed in HU/mg.

Anthrolysin O binding assay

Human erythrocyte ghost membranes were produced by washing of 1mL of human blood in 5mM sodium phosphate buffer three times by centrifugation at 17000 x G for 1 minute followed by resuspension in 1mL PBS. 200 μ L of human erythrocyte ghost membrane solution was mixed with 50 μ L toxin at 20 μ g mL⁻¹ and the reaction was incubated at 37°C for 10 minutes. Ghost membranes were pelleted by centrifugation at 17000 x G and washed three times in PBS. Pellets were resuspended in SDS-PAGE buffer (without β -mercaptoethanol), incubated at 70°C for 10 minutes and run on a 10% SDS-PAGE gel. An immunoblot was performed by standard techniques using pooled mouse anti-mALO anti-serum from the ALO vaccination experiments of this work as the primary antibody and an anti-mouse IgG HRP-linked secondary antibody (Amersham Biosciences).

Determination of anti-ALO and anti-PLY IgG levels by ELISA

ELISA plates were coated with 100 μ L of 2.5 μ g/mL mALO or PLY in 50mM bicarbonate coating buffer (pH9.6) per well and incubated for 18h at 4°C. Plates were washed five times with PBS containing 0.01% Tween 20 (PBS-T) then 200 μ L 1% bovine serum albumen (Sigma) in coating buffer was applied to each well and plates were incubated for 3 hours at 37°C. Plates were washed five times with PBS-T then 1:5 serial dilutions of control or test serum in assay buffer (coating buffer containing 1% bovine serum albumin + 0.25% Tween 20) were made across the plate with a final volume of 100 μ L.

Following incubation for 2 hours at 37°C, plates were washed five times in PBS-T. 100µL of 1:2000 dilution of anti-mouse IgG HRP-linked antibody from sheep (Amersham Biosciences) in assay buffer was added to each well and plates were incubated at 37°C for 1 hour. Plates were washed five times in PBS-T and 100µL/well TMB substrate solution was added (KPL, Maryland, USA). After development, reactions were stopped by addition of 50µl 0.4M H₂SO₄ to each well.

The absorbance at 450nm was measured using an ELX808 Ultra microplate reader (Bio-Tek Instruments Inc, Winooski, VT, USA) and titres were calculated using Kineticalc v2.7 software (Bio-Tek Instruments Inc, Winooski, VT, USA). Absorbance readings were corrected for background by subtraction of values obtained from wells containing pooled serum from naïve animals and the A₄₅₀ was plotted against dilution for each serum sample. Titres were calculated as the dilution of serum calculated by interpolation to give an A₄₅₀ value of 0.3, which was within the linear part of the curve. Serum from each mouse was tested in duplicate and the mean value for each mouse was calculated.

Determination of lethal dose of Anthrolysin O and histopathology

This work was performed as part of a collaboration with DSTL, Porton Down, UK. Five groups of 8-12 week old female A/J mice were injected intravenously (i.v.) with single doses of 0.1µg (n=7), 0.5µg (n=7), 1µg (n=7), 2µg (n=7) or 5µg (n=3) mALO protein in 100µl PBS. Survival of each group of mice was monitored.

Tissues (spleen, heart, kidney, liver and lung) were harvested from 2 mice that died immediately after injection with 1µg mALO and from a naïve mouse. Organs were fixed with 10% neutral-buffered formalin (Sigma) and embedded in paraffin. Sections were stained with haematoxylin and eosin and Martius Yellow-Brilliant Crystal Scarlet-Soluble Blue (MSB) (Lendrum *et al.*, 1962).

Immunisation studies with mALO, Δ6mALO and PLY

This work was performed as part of a collaboration with DSTL, Porton Down, UK. For each challenge study, five groups of 8 female A/J mice were immunised via the intra-peritoneal (i.p.) route with 10µg mALO, Δ6mALO, or PLY in 100µl PBS containing 25% v/v alhydrogel (2%) adjuvant (Superfos Biosector a/s, Vedback, Denmark). Control groups were administered the adjuvant alone, or left untreated. For the *B. anthracis* challenge experiment, a sixth group was immunised with recombinant protective antigen (rPA; obtained from DSTL). Immunisations were performed on day 0, day 14 and day 28. Mice were bled on day 40 for determination of anti-mALO and anti-PLY IgG titres.

Animals were challenged on day 49 by i.v. administration of 5µg mALO in 100µl PBS for the anthrolysin O challenge study or inoculated with 10⁵ *B. anthracis* STI spores (obtained from DSTL) via the i.p. route (previously calculated to be approximately equivalent to 100 MLD (Beedham *et al.*, 2001)) and survival was monitored.

All *in vivo* experiments were performed in accordance with the UK Animals (Scientific Procedures) Act 1986.

Surface Plasmon Resonance

Surface plasmon resonance (SPR) was performed using a Biacore 3000 (Biacore AB, Uppsala, Sweden). CM5 sensor chips were coated with thiol-coupled CD59. The binding assay was developed and performed by Dr. Tim Hughes, UWCM, Wales.

Chapter 3: Production and characterisation of eGFP-tagged pneumolysin

Summary

Pneumolysin is a toxin produced by virtually all clinical isolates of *Streptococcus pneumoniae* (Paton *et al.*, 1993) and is a member of the cholesterol-dependent cytolysins. PLY has been shown to be a key virulence factor (Berry *et al.*, 1999; Rubins *et al.*, 1995; Wellmer *et al.*, 2002) and the toxin has a range of biological effects including pore formation, complement activation and induction of cytokine production *in vitro* and *in vivo*. A deletion mutant of PLY, $\Delta 6$ PLY, has been described (Kirkham *et al.*, 2006b), and this mutant is capable of cell binding but incapable of pore formation.

The aim of this study was to produce an enhanced green fluorescent protein (eGFP) labelled form of PLY that could be detected quantitatively and in real time. It was hoped that this would allow direct visualisation of the localisation of the toxin as an aid to studies of cellular tropism, potential internalisation into host cells, and the binding capabilities of toxin mutants.

PLY and $\Delta 6$ PLY were fused to the C-terminus of eGFP to produce eGFPPLY and $\Delta 6$ eGFPPLY. Both fluorescently labelled proteins were shown to have similar haemolytic and cytotoxic properties to their parent toxins as measured by quantitative haemolytic assay and MTT-cytotoxicity assay on L929 fibroblasts.

Fluorescence microscopy of eGFPPLY and $\Delta 6$ eGFPPLY treated erythrocytes and Detroit 562 cells showed the toxins bound to the plasma membranes.

eGFPPLY and $\Delta 6$ eGFPPLY binding of erythrocytes could be measured by flow cytometry and the fluorescence of cells was found to increase with the concentration of toxin added over a 100-fold range from 0.7nM up to 70nM.

Finally, rod-like structures were observed on membranes treated with $\Delta 6$ eGFPPLY and these were further studied by SEM. These structures were found to be caused only by the $\Delta 6$ mutant of PLY as they were present on cells treated with $\Delta 6$ eGFPPLY and $\Delta 6$ PLY but not those treated with PLY or eGFPPLY.

Results

Construction of eGFPPLY, $\Delta 6$ eGFPPLY and eGFP expression vectors

Plasmid vectors were constructed containing the coding sequence for eGFP alone (pET33bEGFP), as an N-terminal fusion to PLY (pET33bEGFPPLY) or as an N-terminal fusion to $\Delta 6$ PLY (pET33b $\Delta 6$ EGFPPLY). The pET33b expression vector (Novagen) was selected to allow high-level inducible expression with the addition of a poly-histidine tag to facilitate protein purification. Initial cloning was confirmed by PCR using primers for the T7 promoter and T7 terminator sequences flanking the multiple cloning site (primer references 7F and 7G).

The construction of all plasmids was checked by DNA sequencing. The sequence was confirmed to be as expected with no mutations present. Plasmid maps of pET33bEGFPPLY and pET33b $\Delta 6$ EGFPPLY plasmids are shown in Figure 3.1. Constructs were transformed into BL21(DE3) *E. coli* for protein expression.

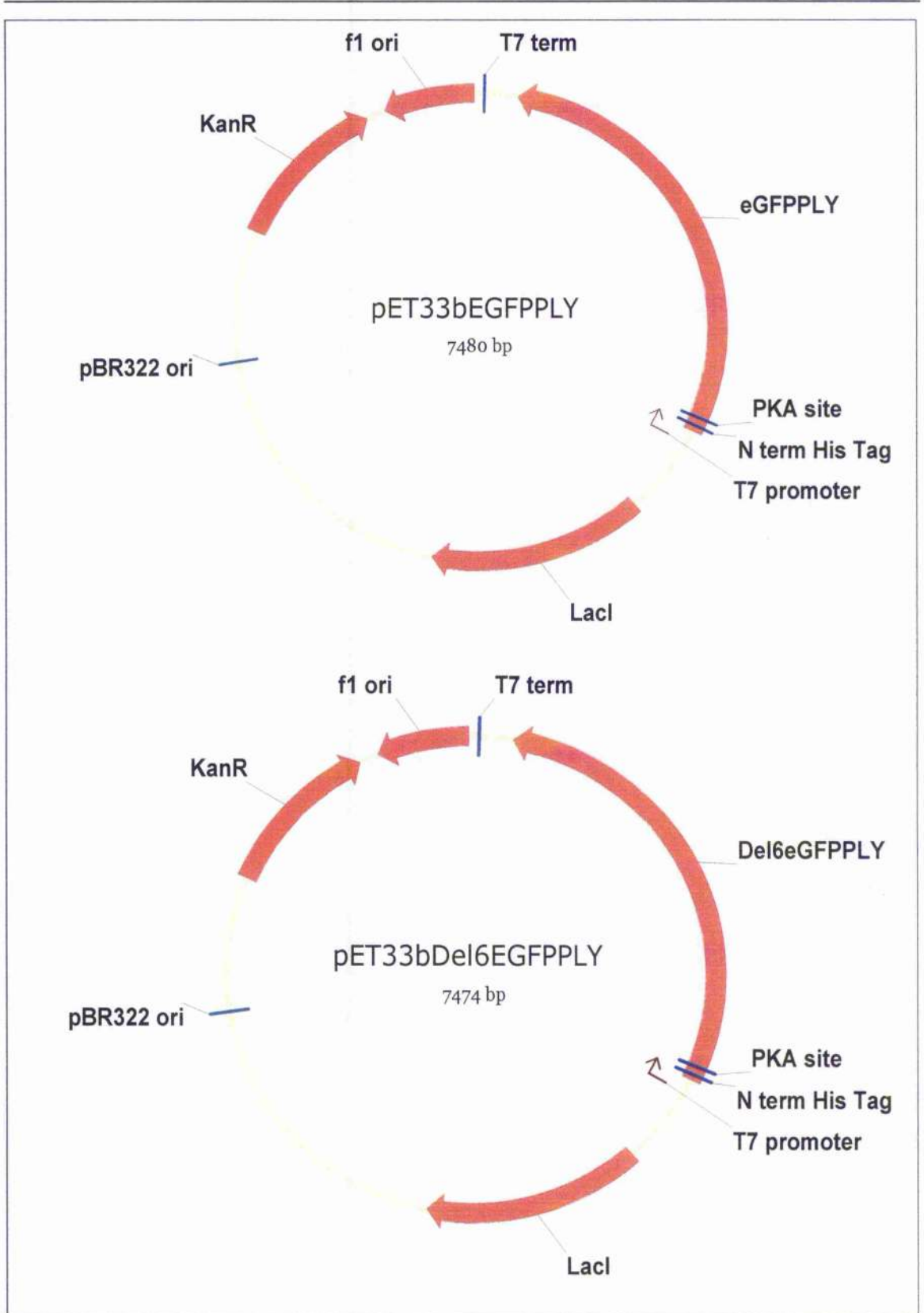


Figure 3.1: Schematic diagrams of pET33bEGFPPLY and pET33bDel6EGFPPLY plasmids

Expression of eGFP-tagged PLY, $\Delta 6$ eGFPPLY and eGFP proteins

Recombinant eGFPPLY, $\Delta 6$ eGFPPLY and eGFP were expressed in *E. coli* and purified by nickel-affinity chromatography or hydrophobic interaction chromatography (HIC), then further purified by anion exchange chromatography (AEC). Protein preparations were estimated by Coomassie-blue-stained SDS-PAGE to be greater than 98% pure and protein concentrations were determined by Bradford assay.

All experiments used nickel-affinity chromatography / AEC purified toxins, except for the MTT cytotoxicity assay, which used HIC / AEC purified toxins. This alternative purification strategy was used to allow comparison with PLY and $\Delta 6$ PLY proteins which had previously been purified by this method.

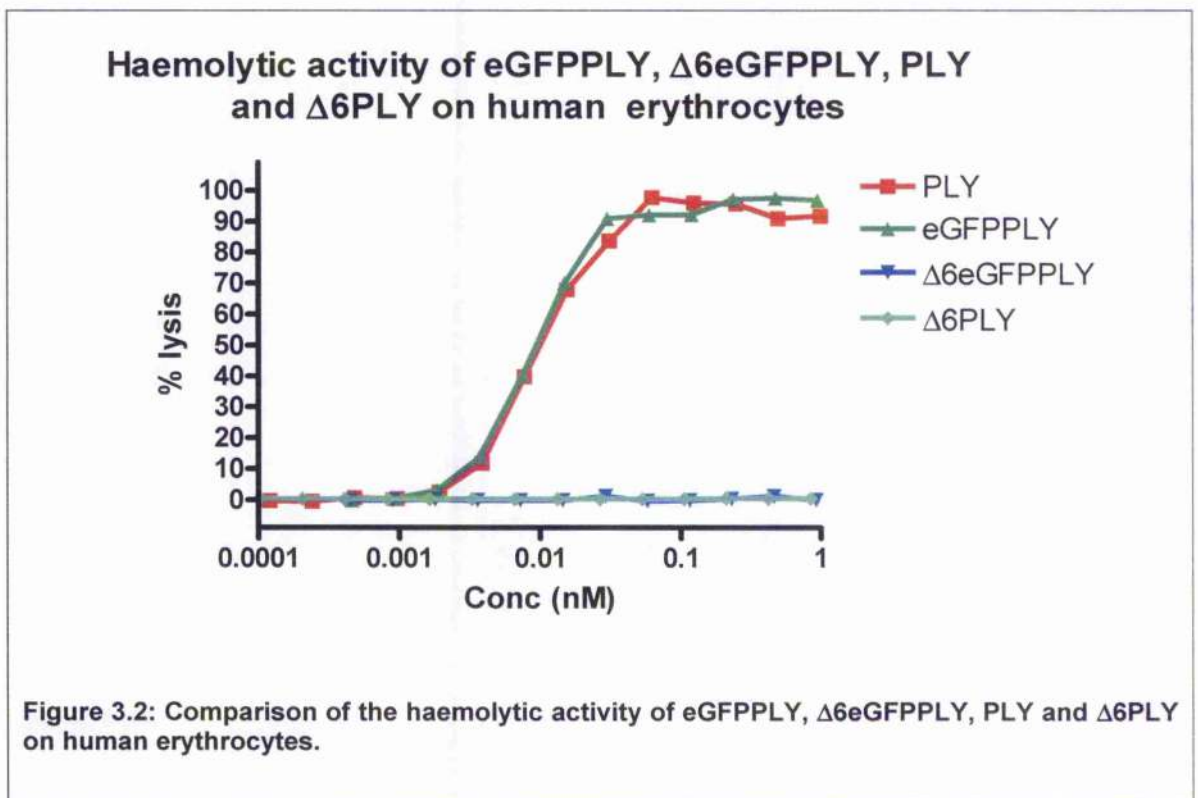
The levels of lipopolysaccharide (LPS) in the HIC and AEC eGFPPLY and $\Delta 6$ eGFPPLY preparations were measured by LAL endotoxin assay. The LPS concentration was calculated to be 93IU/mg for eGFPPLY and 308IU/mg for $\Delta 6$ eGFPPLY.

Comparison of haemolytic activity of eGFPPLY and $\Delta 6$ eGFPPLY to PLY and $\Delta 6$ PLY

A quantitative haemolysis assay was performed to compare the activities of PLY, eGFPPLY and $\Delta 6$ eGFPPLY on human erythrocytes (Figure 3.2). Toxin concentration was calculated using molarity to enable a comparison in terms of the

number of toxin molecules present that was not influenced by the much higher molecular weight of the eGFP-tagged toxins.

PLY and eGFPPLY were both similarly haemolytic on human erythrocytes with calculated specific haemolytic activities of 1×10^8 HU/M. $\Delta 6$ eGFPPLY was not haemolytic even up to a concentration of 4mM.



Transmission Electron Microscopy of eGFPPLY and $\Delta 6$ eGFPPLY

In order to compare pores formed by eGFPPLY to those formed by wild-type PLY, erythrocyte membranes were treated with eGFPPLY or PLY and examined by negative staining TEM. Membranes treated with $\Delta 6$ eGFPPLY were also examined

to determine whether any oligomeric structures were visible on the membranes. Electron micrographs are shown in Figure 3.3.

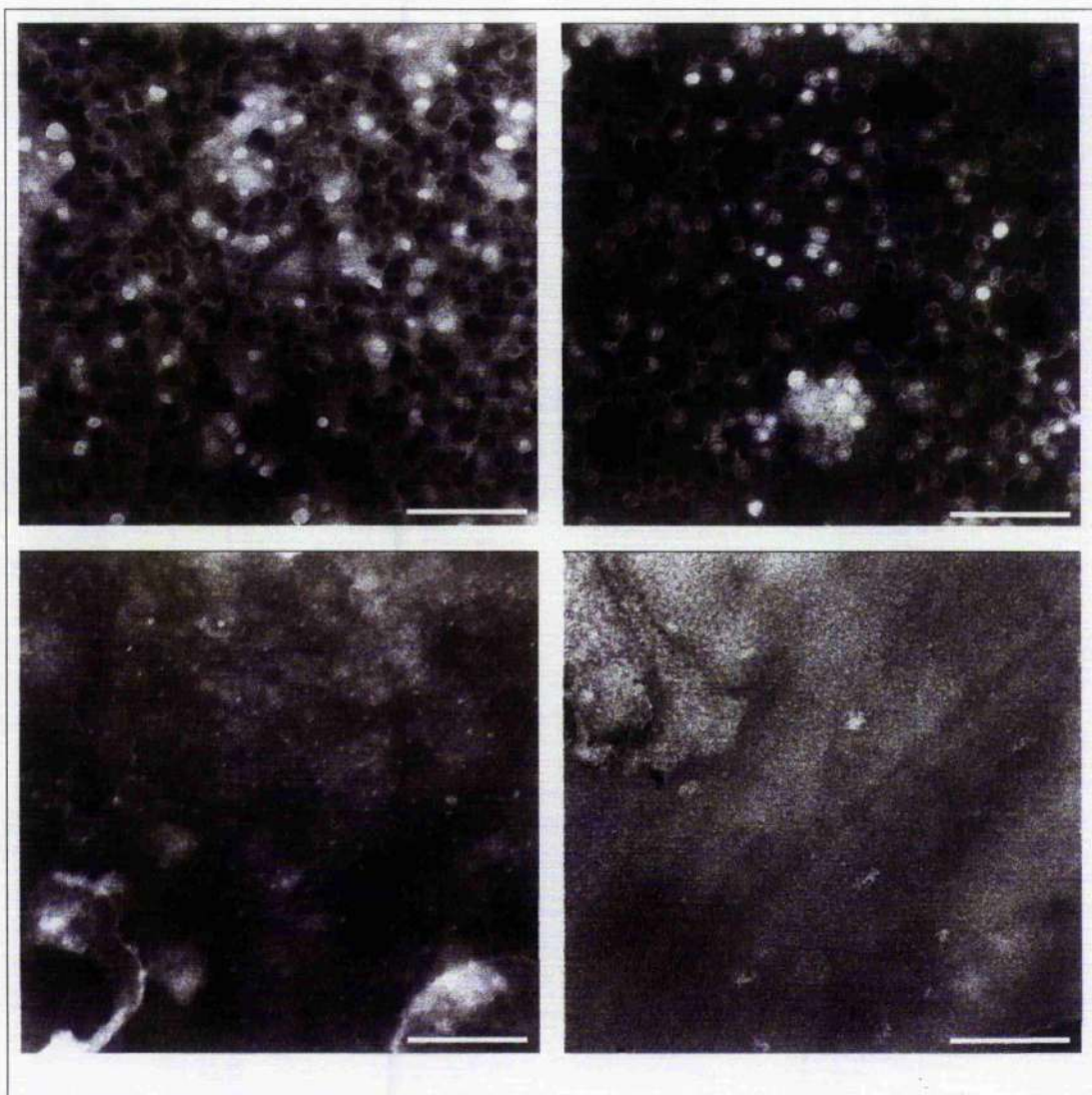


Figure 3.3: Transmission electron micrographs of human erythrocyte ghost membranes treated with A: wtPLY B: eGFPLY C: $\Delta 6$ eGFPLY D: No toxin. Samples were stained with Nanovan negative staining reagent. Magnification x25000, white horizontal scale bar represents 200nm.

Full rings, arcs and double arcs were present on membranes treated with PLY. All of these structures were also observed on membranes treated with eGFPPLY and were similar to those formed by PLY. No rings or arcs were observed on membranes treated with $\Delta 6$ eGFPPLY.

Comparison of cytotoxicity of eGFPPLY, $\Delta 6$ eGFPPLY, PLY and $\Delta 6$ PLY to L929 fibroblast cells

An L929 fibroblast cytotoxicity assay was performed by Lea-ann Kirkham using eGFPPLY, $\Delta 6$ eGFPPLY, PLY, $\Delta 6$ PLY and eGFP purified proteins to determine whether addition of the eGFP tag affected the cytotoxicity of the parent toxin. High A_{540} indicates viability of the cells as the active mitochondria are capable of conversion of MTT into a purple product whereas loss of viability is indicated by a low A_{540} where the MTT solution remains yellow.

Both PLY and eGFPPLY caused a loss of viability to L929 fibroblasts and their toxicities were found to be similar. $\Delta 6$ eGFPPLY, $\Delta 6$ PLY and eGFP were not toxic to L929 fibroblast cells at the concentrations tested (Figure 3.4).

L929 fibroblast cytotoxicity assay on eGFP tagged toxins

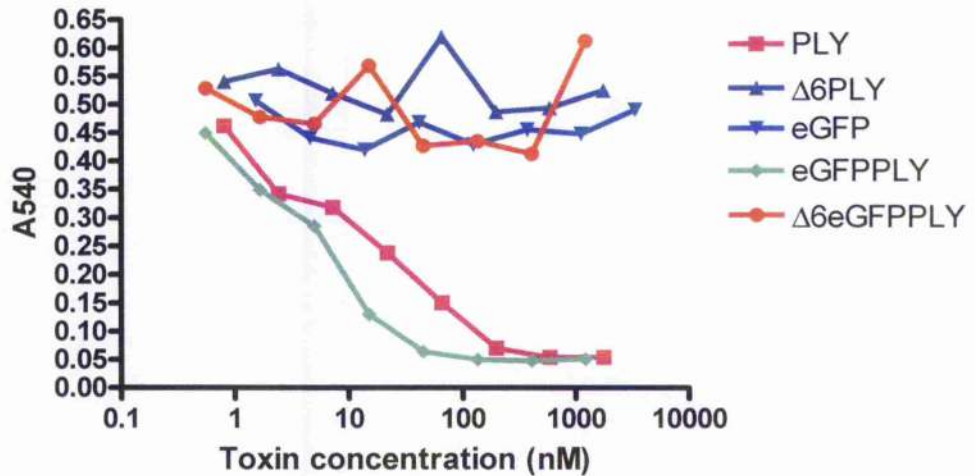


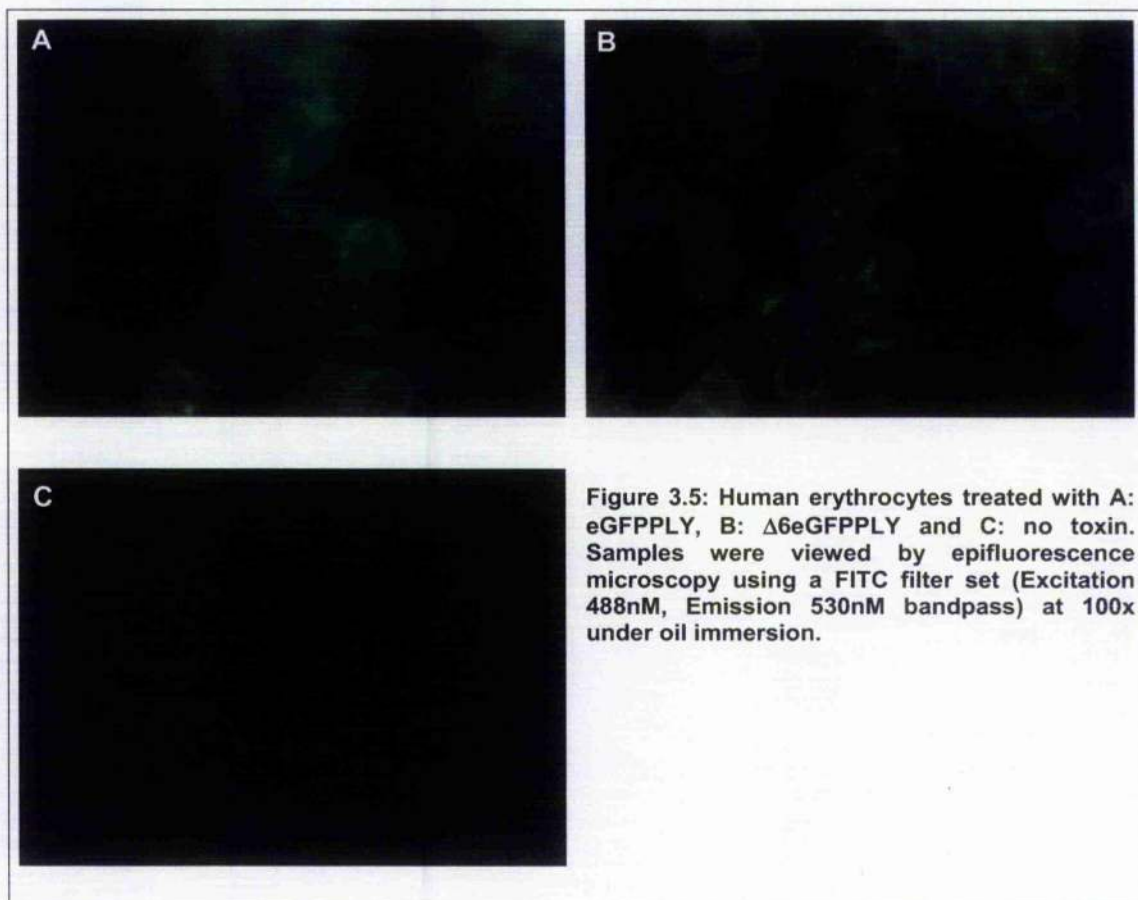
Figure 3.4: Cytotoxicity of eGFP-tagged toxins to L929 fibroblast cells. L929 fibroblasts were treated with a range of concentrations of PLY, $\Delta 6$ PLY, eGFP, eGFPPLY or $\Delta 6$ PLY and the cell viability was measured by MTT assay.

Visualisation of eGFPPLY and $\Delta 6$ eGFPPLY binding to erythrocytes by fluorescence microscopy

In order to determine whether eGFPPLY and $\Delta 6$ eGFPPLY were capable of cell binding, erythrocytes treated with each of two toxins were visualised by fluorescence microscopy. Slides of treated erythrocytes were viewed using a Zeiss Axioskop 20 fluorescence microscope fitted with Zeiss FITC filter set 09, which provides excitation of 450-490nm with a 520nm high-pass emission filter.

Erythrocytes treated with eGFPPLY and $\Delta 6$ eGFPPLY were fluorescent whereas no fluorescence was observed on samples treated with eGFP (Figure 3.5). For both eGFPPLY and $\Delta 6$ eGFPPLY-treated erythrocytes, fluorescence appeared to

localise to the plasma membrane of the erythrocytes. The morphology of erythrocytes treated with the wild-type or $\Delta 6$ forms of the toxins were different: erythrocytes treated with eGFPPLY were flattened ghost membranes whereas erythrocytes treated with $\Delta 6$ eGFPPLY maintained their rounded bi-concave shape and were not lysed, as revealed by the red colour observed on brightfield images of these cells (images not shown).



Small foci of fluorescence were observed on erythrocytes treated with eGFPPLY. Very pronounced foci were observed on erythrocytes treated with $\Delta 6$ eGFPPLY and these were much more distinct than those observed for eGFPPLY.

Owing to the shallow depth of field obtained when viewing samples with the 100x oil-immersion lens, it was possible to limit the focal plane to the upper membrane of the erythrocytes (Figure 3.6). This revealed that the punctate localisation observed when the focal plane was set to view the centre of the erythrocytes in the Z-plane was a cross-section of fluorescent rod-like structures on the cell membrane (Figure 3.6).

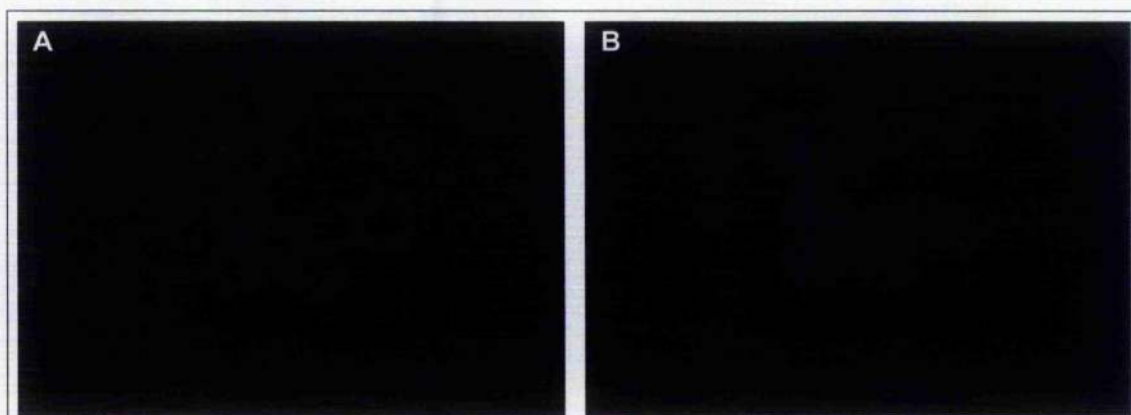


Figure 3.6: $\Delta 6eGFPPLY$ treated human erythrocytes viewed by epifluorescence microscopy. Figure A shows the cells viewed with the focal plane set to the Z-centre of the erythrocytes whereas figure B shows the same cells with the focal plane set to view the upper surface of the erythrocytes. Samples were viewed by epifluorescence microscopy using a FITC filter set (Excitation 488nm, Emission 530nm bandpass) at 100x under oil immersion.

Use of eGFPPLY to study binding to cochlear hair cells of the rat

In collaboration with Dr. Didier Dulon's group at the University of Bordeaux , we used tagged toxin to study the binding of eGFPPLY to rat cochlear hair cells by epifluorescence microscopy (Beurg *et al.*, 2005). The toxicity of eGFPPLY was evaluated in an organ of corti (OC) explant culture model and was found to be similar to that of PLY (Beurg *et al.*, 2005).

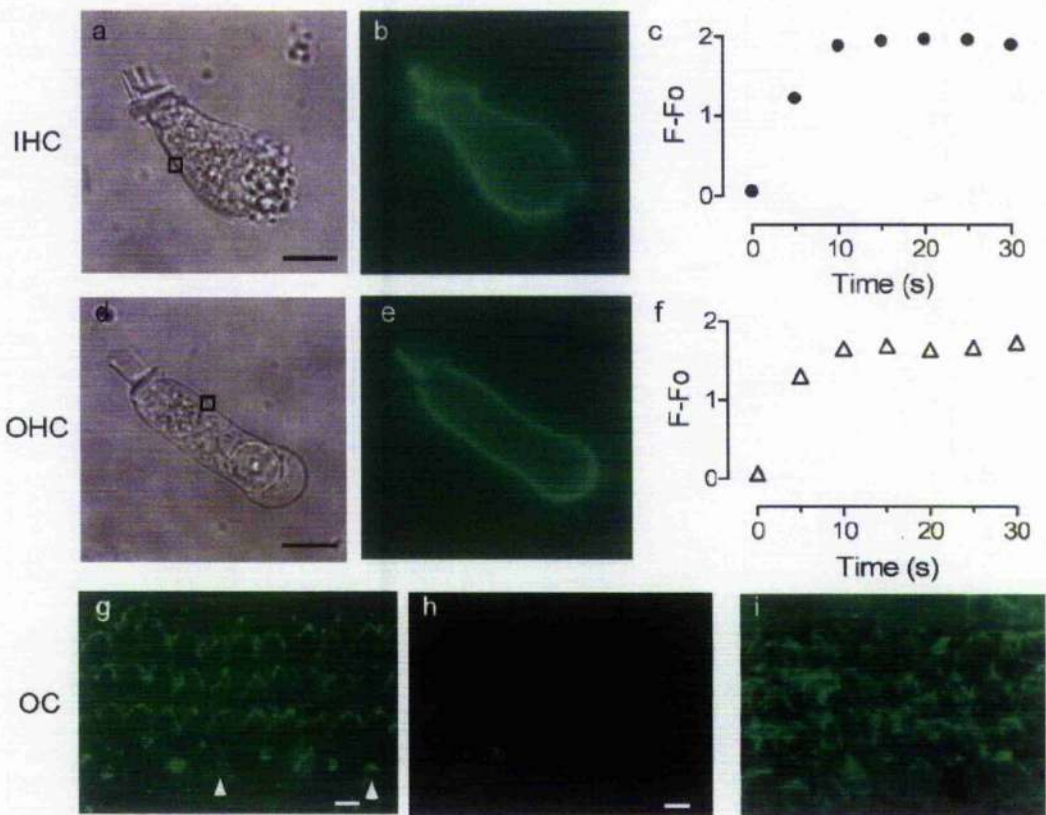


Figure 3.7: Binding of PLY in cochlear HC cultures

The eGFPPPLY ($5 \text{ ng } \mu\text{l}^{-1}$) was pressure puffed for 2 s on isolated rat HCs. An example of an IHC (A) and OHC (D) is shown in brightfield. Fluorescent images (B,E) were obtained 10 s after the puff of PLY on the same cell (A,D). The eGFPPPLY labelling was localized in the plasma membrane of IHCs and OHCs. Graphs (C,F) show the time course of the incorporation of eGFPPPLY in the HC plasma membrane. The fluorescence intensity was quantified by integration of a small zone shown by the rectangular box shown on the brightfield images. Fluorescence ($F - F_0$) is corrected from background fluorescence (F_0). G, binding of eGFPPPLY in OC cultures (representative of four explants) treated 24 h with $1 \text{ ng } \mu\text{l}^{-1}$ of the conjugated-toxin. A more sustained labelling in OHCs' hair bundles compared to IHCs' (arrowhead) could be observed. Note a high disorganization of the IHC stereocilia when remaining. H,I, immunolocalisation of PLY in control (H) and PLY (I) ($1 \text{ ng } \mu\text{l}^{-1}$, 24 h) - treated OC cultures (representative of three explants). Surface preparation of the OC showed a staining of stereocilia and plasma membrane of IHCs and OHCs, while no labelling was observed in control cultures. Scale bars $10 \mu\text{m}$. Figure taken from Beurg et al, 2005.

eGFPPPLY was distributed homogenously in the plasma membrane of freshly dissociated inner hair cells (IHCs) and outer hair cells (OHCs) and was restricted to the membrane surface with no fluorescence detected in the cell cytosol (Figure 3.7). No significant difference in the fluorescence intensity of eGFPPPLY-treated

IHCs and OHCs was observed. Epifluorescence microscopy of eGFPPLY-treated OC explants revealed that eGFPPLY labelled the hair bundles of both IHCs and OHCs with the staining being more pronounced in the OHCs (Figure 3.7).

Raised extracellular calcium was found to reduce the binding of eGFPPLY to IHCs and OHCs (Figure 3.8). eGFPPLY was pressure puffed for 5 seconds on isolated rat IHCs or OHCs in the presence of 0mM, 1mM or 10mM calcium and epifluorescence micrographs were recorded. Fluorescence of a membrane portion was plotted on a histogram from a number of repeat samples for each condition. The amount of eGFPPLY bound with external 10mM CaCl_2 was drastically reduced from that bound at 0mM and 1mM CaCl_2 (Figure 3.8). To eliminate the possibility that the observed effect was due to a reduction of the fluorescence of eGFPPLY with increased calcium concentration, these results were confirmed by examining the binding of PLY in cultures OC in the presence of 1.8mM or 10mM calcium using PLY-specific antibody (Beurg *et al.*, 2005).

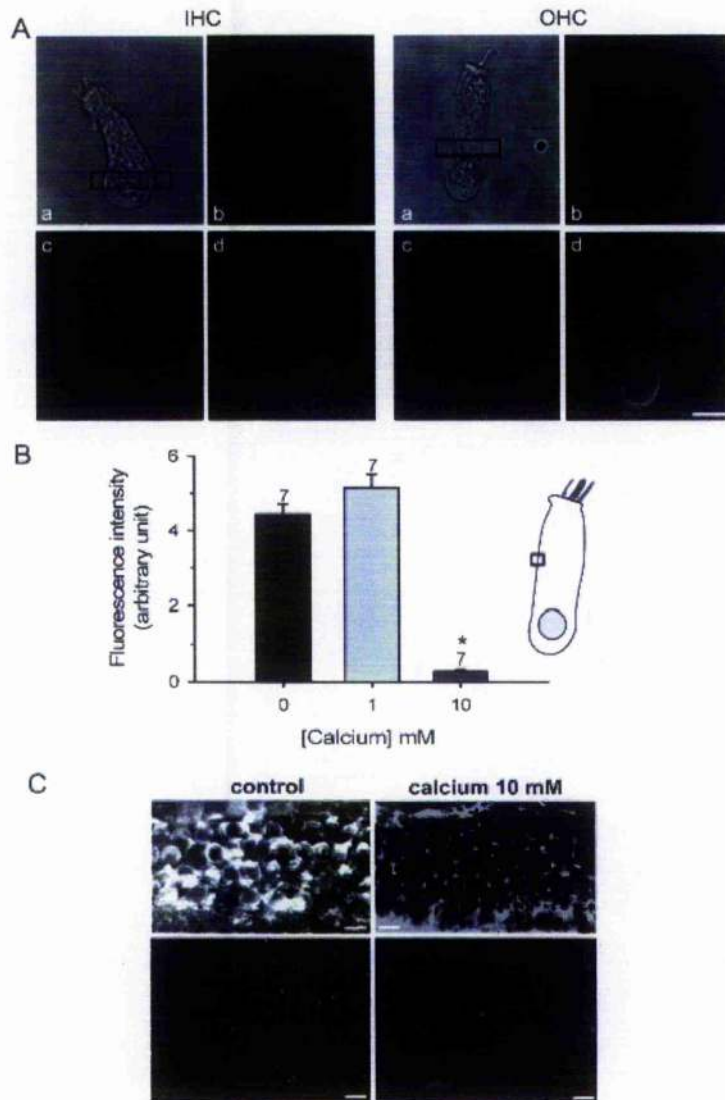


Figure 3.8: Elevation of extracellular calcium prevents binding of eGFPPLY to HCs

A, the eGFPPLY ($5 \text{ ng } \mu\text{l}^{-1}$) was pressure puffed for 5 s on isolated rat IHC and OHC shown in (*a*). Fluorescent images before (*b*) and after the puff of PLY in 10 mM (*c*) or 1mM (control) CaCl_2 (*d*) in the same IHC and OHC. In the presence of 10 mM CaCl_2 , eGFPPLY is not seen in the HC membrane while a strong signal is present in control conditions. **B**, histogram represents the intensity of eGFPPLY fluorescence bound to the HC plasma membrane as a function of external calcium concentration. eGFPPLY ($5 \text{ ng } \mu\text{l}^{-1}$) was pressure puffed for 5 s on isolated rat HC. Fluorescence intensity was measured in a fixed-size area of the plasma membrane, illustrated by the box in the HC scheme. Fluorescence intensity corresponds to $F - F_0$. The asterisk indicates a significant different data (unpaired t test, $P < 0.001$). Results are obtained over the number of indicated cells. **C**, top images show the immunolocalisation of PLY in PLY ($1 \text{ ng } \mu\text{l}^{-1}$, 24 h)-treated OC cultures ($n = 4$) in the presence of control (left panel) (DMEM $1.8 \text{ mM } \text{CaCl}_2$) or high external calcium concentration (right panel) (10 mM). Bottom images show binding of eGFPPLY in OC cultures treated 24 h with $1 \text{ ng } \mu\text{l}^{-1}$ in the presence of control or high external calcium concentration (representative of four explants for each condition). Surface preparation of the OC showed a staining of stereocilia and plasma membrane of IHCs and OHCs in control condition, while no labelling was observed in high calcium. Error bars show standard error. Scale bars $10 \mu\text{m}$. Figure taken from Beurg et al 2005.

Visualisation of eGFPPLY and $\Delta 6$ eGFPPLY binding by confocal fluorescence microscopy

The binding and localisation of eGFPPLY and $\Delta 6$ eGFPPLY on Detroit 562 human nasopharyngeal cells was visualised by laser scanning confocal fluorescence microscopy. Cells were also treated with an equimolar concentration of eGFP as a negative control to ensure that binding localisation was due to the toxin component of the fusion proteins. Micrographs of cells treated with 700nM eGFPPLY, 700nM $\Delta 6$ eGFPPLY or 700nM eGFP are shown in

Figure 3.9, Figure 3.10 and

Figure 3.11 respectively. eGFP localisation was visible on the green channel, actin localisation was indicated with rhodamine-phalloidin staining on the red channel and cell nuclei were visualised on the blue channel by DAPI staining.

eGFPPLY and $\Delta 6$ eGFPPLY could both be observed bound to Detroit 562 cells but no fluorescence was observed on cells treated with eGFP. Both eGFPPLY and $\Delta 6$ eGFPPLY localised to the plasma membrane of the treated cells and no internalisation of the toxins was visualised, however the morphology of the treated cells was vastly different. Cells treated with $\Delta 6$ eGFPPLY remained spread out on the slide surface and the overall cell or actin cytoskeletal morphology did not differ from that of untreated cells or those treated with eGFP. The actin in these cells covered the entire area within the cell. However, cells treated with eGFPPLY were rounded up from the slide surface with a marked change in the actin cytoskeleton, whereby the actin was found to be condensed around the nuclei.

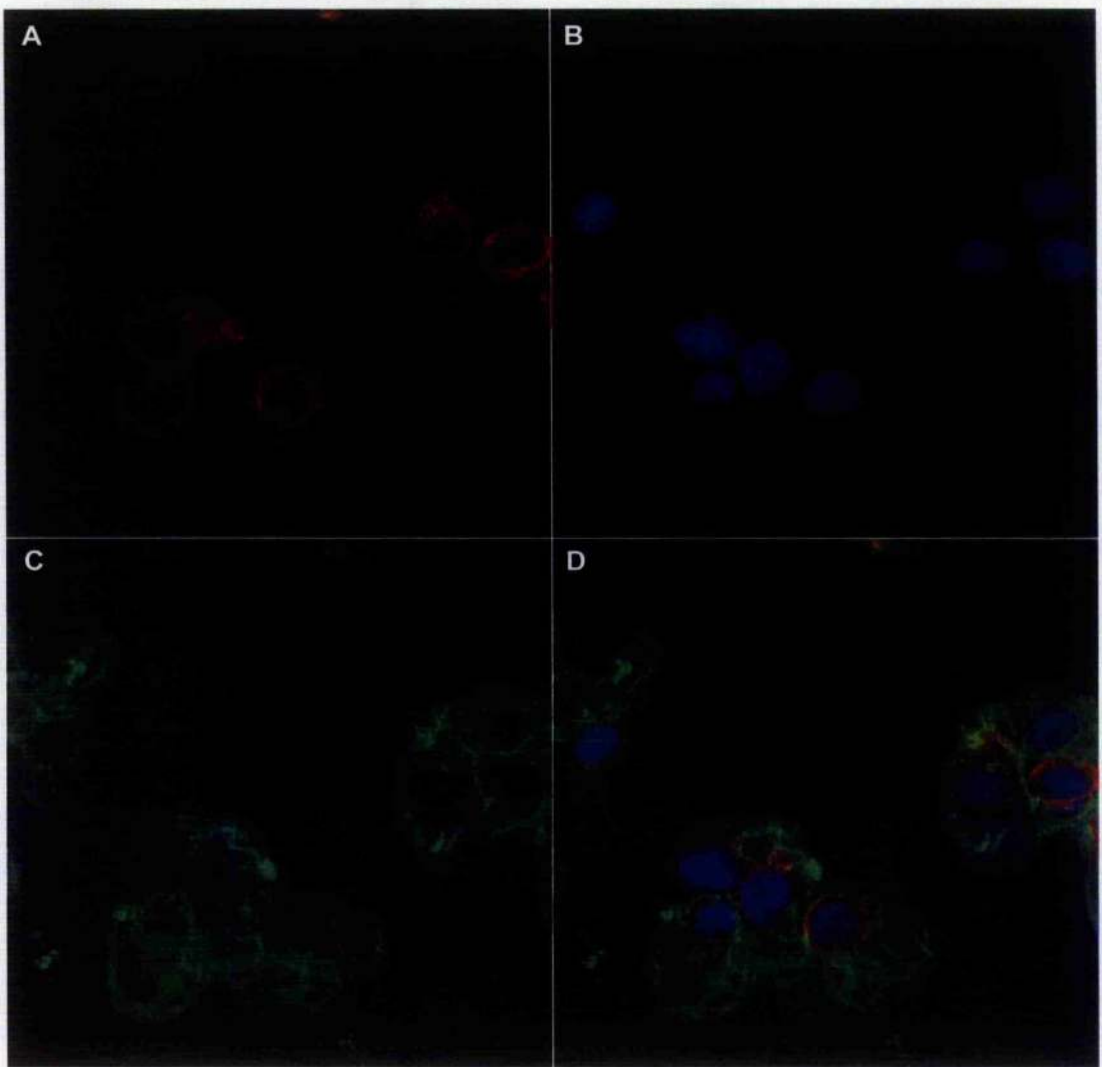


Figure 3.9: Laser Scanning Confocal Microscopy of Detroit 562 cells treated with 700nM eGFPPLY. All images captured with 63x objective lens under oil immersion.

A) Red Channel (Ex. 543nm Em. BP 561-625nm) shows localisation of rhodamine-phalloidin stain for actin.

B) Blue Channel (Ex. 405nm Em. BP 420-480nm) shows localisation of DAPI nuclear DNA stain.

C) Green channel (Ex. 488nm Em. BP 505-530nm) shows localisation of eGFPPLY.

D) Combined image of all three channels.

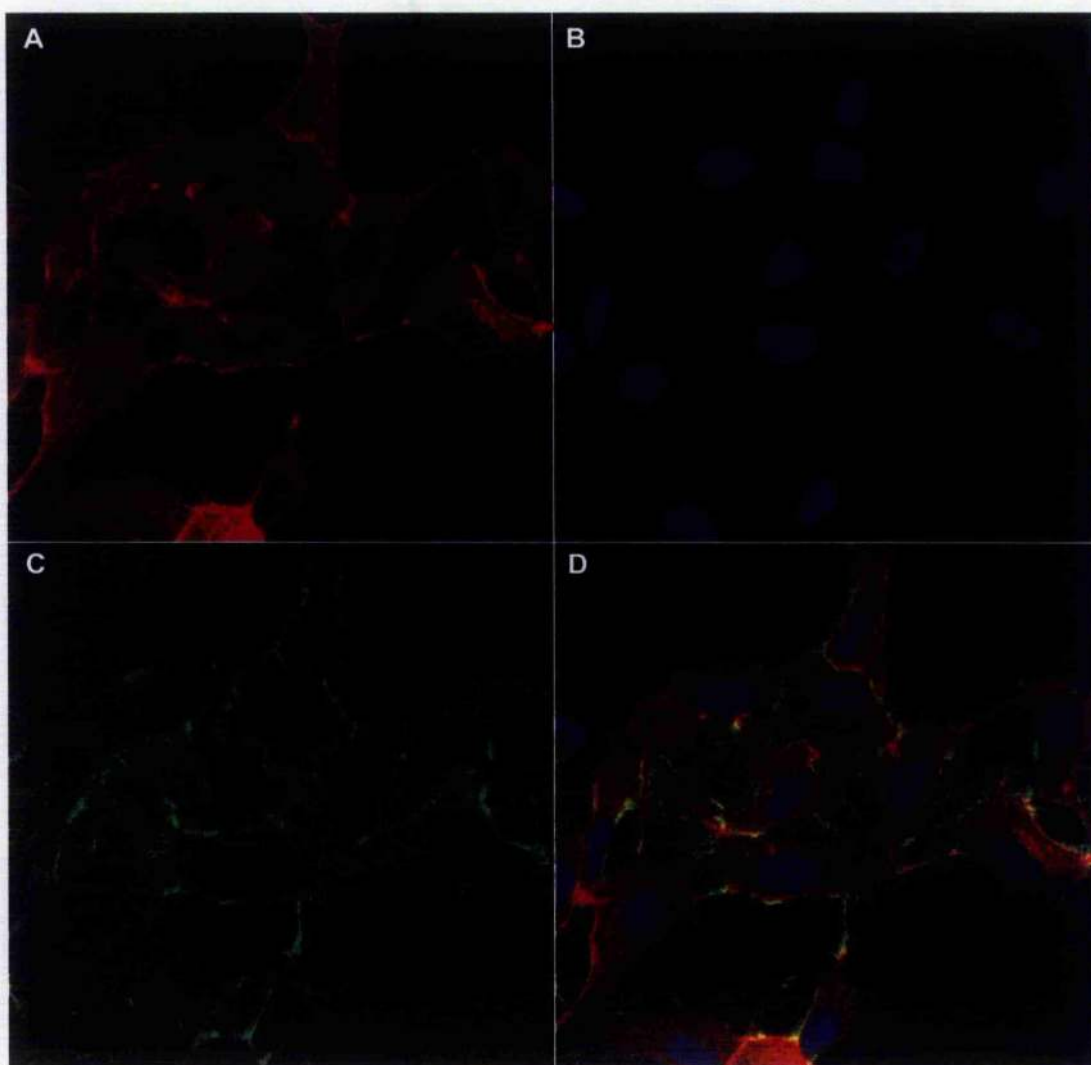


Figure 3.10: Laser Scanning Confocal Microscopy of Detroit 562 cells treated with 700nM $\Delta 6eGFPPLY$. All images captured with 63x objective lens under oil immersion.

A) Red Channel (Ex. 543nm Em. BP 561-625nm) shows localisation of rhodamine-phalloidin stain for actin.

B) Blue Channel (Ex. 405nm Em. BP 420-480nm) shows localisation of DAPI nuclear DNA stain.

C) Green channel (Ex. 488nm Em. BP 505-530nm) shows localisation of $\Delta 6eGFPPLY$.

D) Combined image of all three channels.

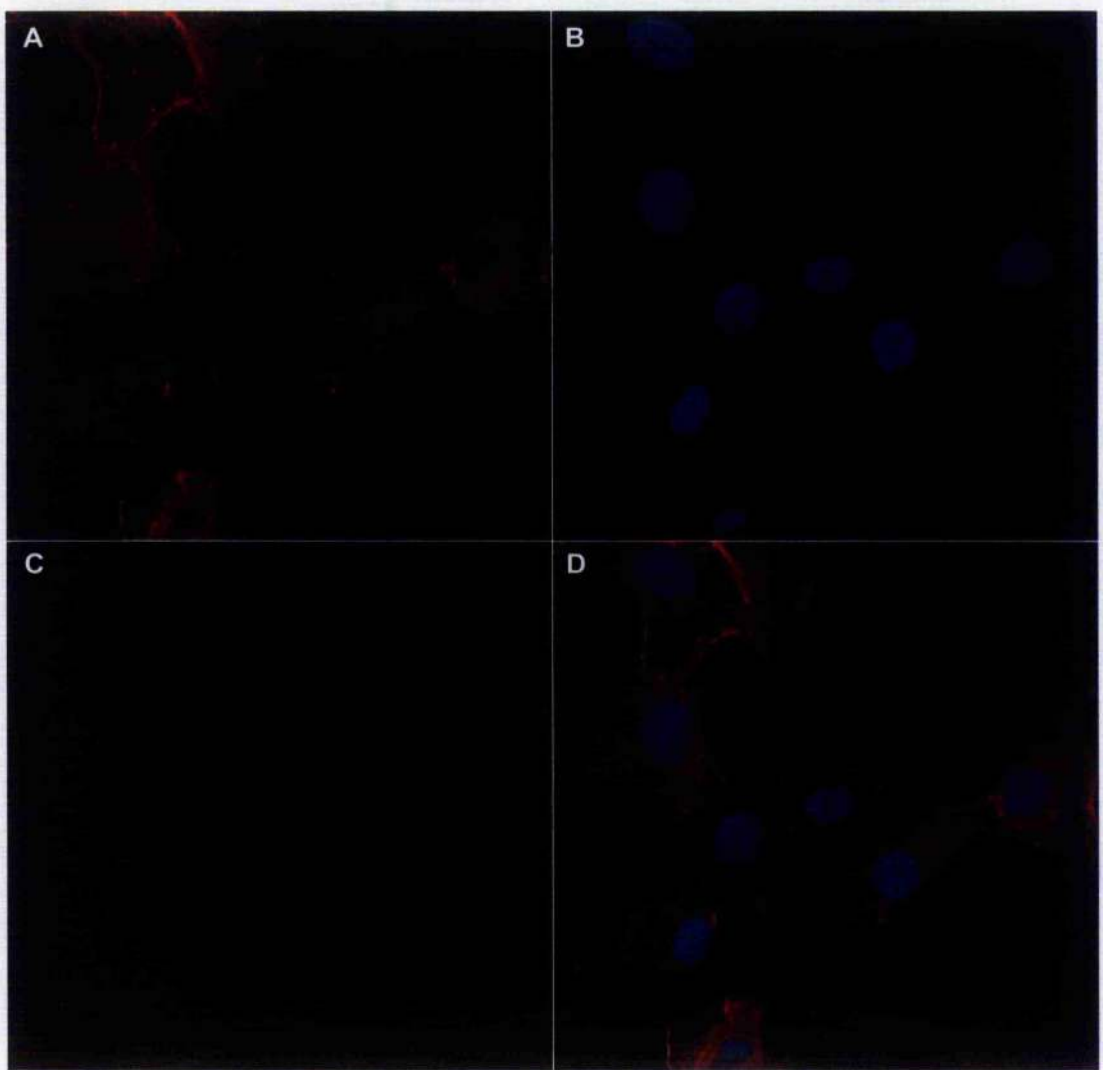


Figure 3.11: Laser Scanning Confocal Microscopy of Detroit 562 cells treated with 700nM eGFP. All images captured with 63x objective lens under oil immersion.

A) Red Channel (Ex. 543nm Em. BP 561-625nm) shows localisation of rhodamine-phalloidin stain for actin.

B) Blue Channel (Ex. 405nm Em. BP 420-480nm) shows localisation of DAPI nuclear DNA stain.

C) Green channel (Ex. 488nm Em. BP 505-530nm) shows localisation of eGFP.

D) Combined image of all three channels.

Scanning Electron Microscopy of eGFPPLY and $\Delta 6$ eGFPPLY

Rod-like structures were previously observed on erythrocytes treated with $\Delta 6$ eGFPPLY under examination by fluorescence microscopy. From the fluorescence microscopy work, it was not possible to ascertain whether the structures were a characteristic of the $\Delta 6$ mutant of PLY or whether this was due to the addition of the eGFP domain. In order to determine this and to visualise the structures in more detail, human erythrocytes treated with PLY, $\Delta 6$ PLY, eGFPPLY and $\Delta 6$ eGFPPLY were examined by scanning electron microscopy (Figure 3.12).

Untreated erythrocytes had a bi-concave appearance with smooth membranes. Rod-like structures were observed on the surface of cells treated with $\Delta 6$ PLY or $\Delta 6$ eGFPPLY. Examination of micrographs revealed that some of the strands spanned between adjacent erythrocytes. The bi-concave shape of the erythrocytes appear to have been distorted but the overall size of the cells was similar to untreated erythrocytes. No such structures were observed on erythrocytes treated with PLY or eGFPPLY, although these 'ghost erythrocyte' cells differed from the untreated cell by losing their smooth bi-concave shape, having many folds in their membranes and being of larger size.

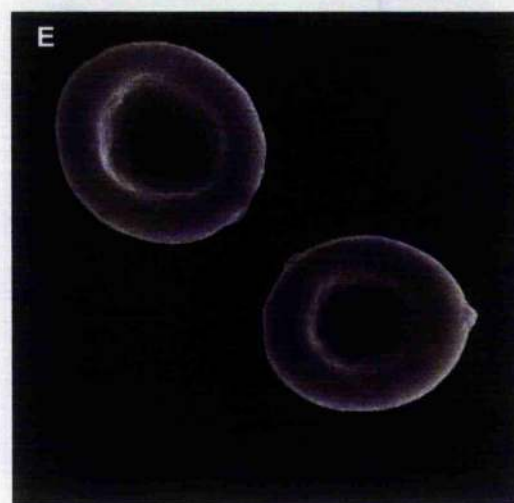
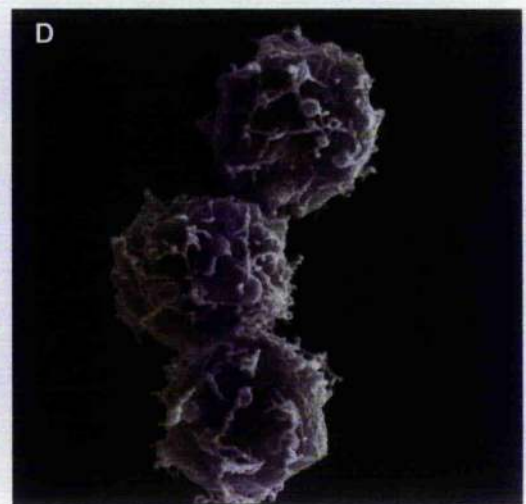
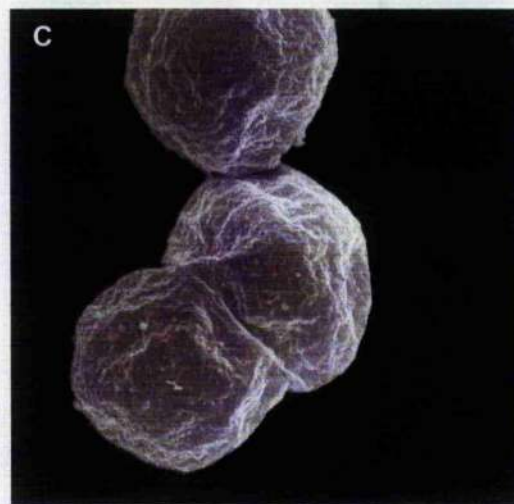
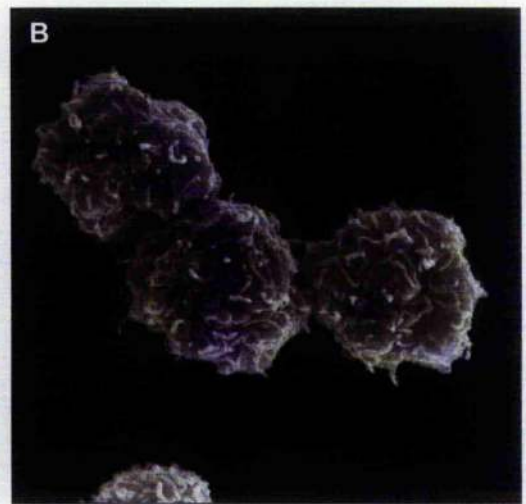
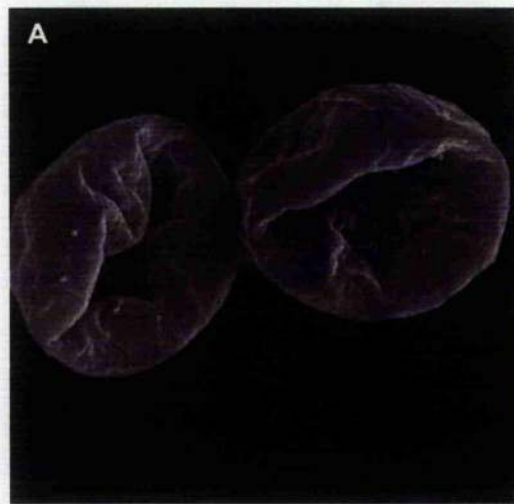


Figure 3.12: Scanning electron micrographs of erythrocytes treated with:

- A) 700nM eGFPPLY
- B) 700nM $\Delta 6$ eGFPPLY
- C) 700nM PLY
- D) 700nM $\Delta 6$ PLY
- E) No toxin.

Magnification x 8000.

Detection of eGFPPLY and $\Delta 6$ eGFPPLY binding to erythrocytes by flow cytometry

The potential use of eGFPPLY and $\Delta 6$ eGFPPLY in a flow-cytometry based binding assay was investigated. Suspensions of human erythrocytes in PBS were treated with a range of concentrations of eGFPPLY, $\Delta 6$ eGFPPLY or eGFP between 0.7nM and 70nM and incubated for 10 minutes at 37°C. Cell fluorescence was measured by flow-cytometry using the FL-1 fluorescence channel (Ex 488nM, Em 530nM).

Erythrocytes treated with eGFPPLY and $\Delta 6$ eGFPPLY showed a concentration-dependent increase in fluorescence (Figure 3.13) indicating that both eGFPPLY and $\Delta 6$ eGFPPLY bound to erythrocytes in a dose-dependent manner.

No increase in fluorescence of erythrocytes treated with equimolar concentrations of eGFP was observed, confirming that the binding was due to the toxin component of the fusion proteins and not a non-specific binding by the eGFP component.

The range of fluorescence intensities per detection event was greater for eGFPPLY than $\Delta 6$ eGFPPLY, with the result that tighter peaks were obtained for each of the concentrations of $\Delta 6$ eGFPPLY used than for eGFPPLY. The mean fluorescence at each concentration of toxin was greater for eGFPPLY than

$\Delta 6$ eGFPPLY, possibly as a result of absorption of part of the fluorescence signal by the haemoglobin within the unlysed cells.

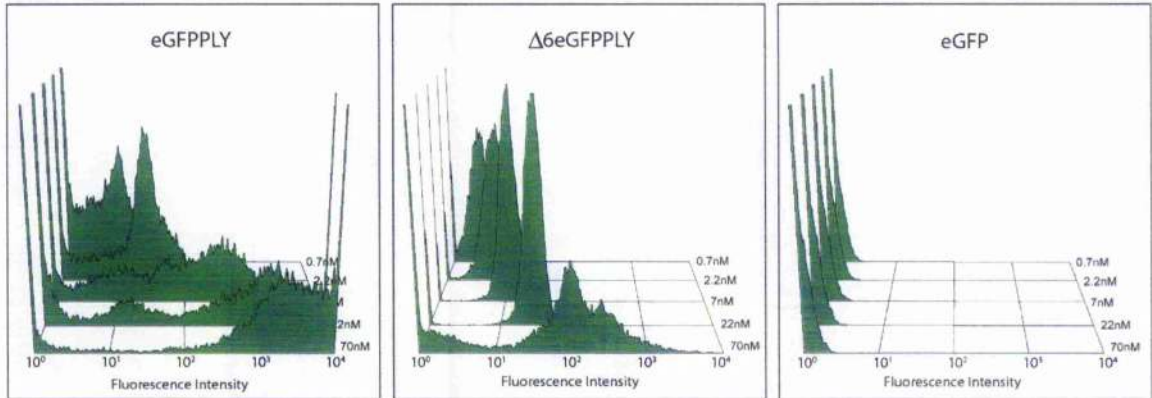


Figure 3.13: Histograms of fluorescence (Ex 488nm, Em 530nm) of cells treated with eGFPPLY (left), $\Delta 6$ eGFPPLY (centre) and eGFP (right). Flow cytometry data was plotted using WinMDI (<http://facs.scripps.edu>).

Application of the eGFPPLY binding assay

The eGFPPLY flow cytometry binding assay was used to study the antagonistic effects of docosahexaenoic acid (DHA) on binding of eGFPPLY to neutrophils, an omega-3 poly-unsaturated fatty acid (Fickl *et al.*, 2005). This work was done in collaboration with Dr. R. Anderson's group at the University of Pretoria, South Africa. The results showed that the addition of 5 or 10 $\mu\text{g}/\text{mL}$ DHA reduced binding of eGFPPLY to the neutrophils by 18% ($\pm 5\%$) and 45% ($\pm 7\%$) respectively (Figure 3.14). It is likely that this is, at least in part, responsible for the antagonism of PLY-induced IL-8 release, influx of extracellular calcium and activation of NF κ B that was also observed in this work (Fickl *et al.*, 2005).

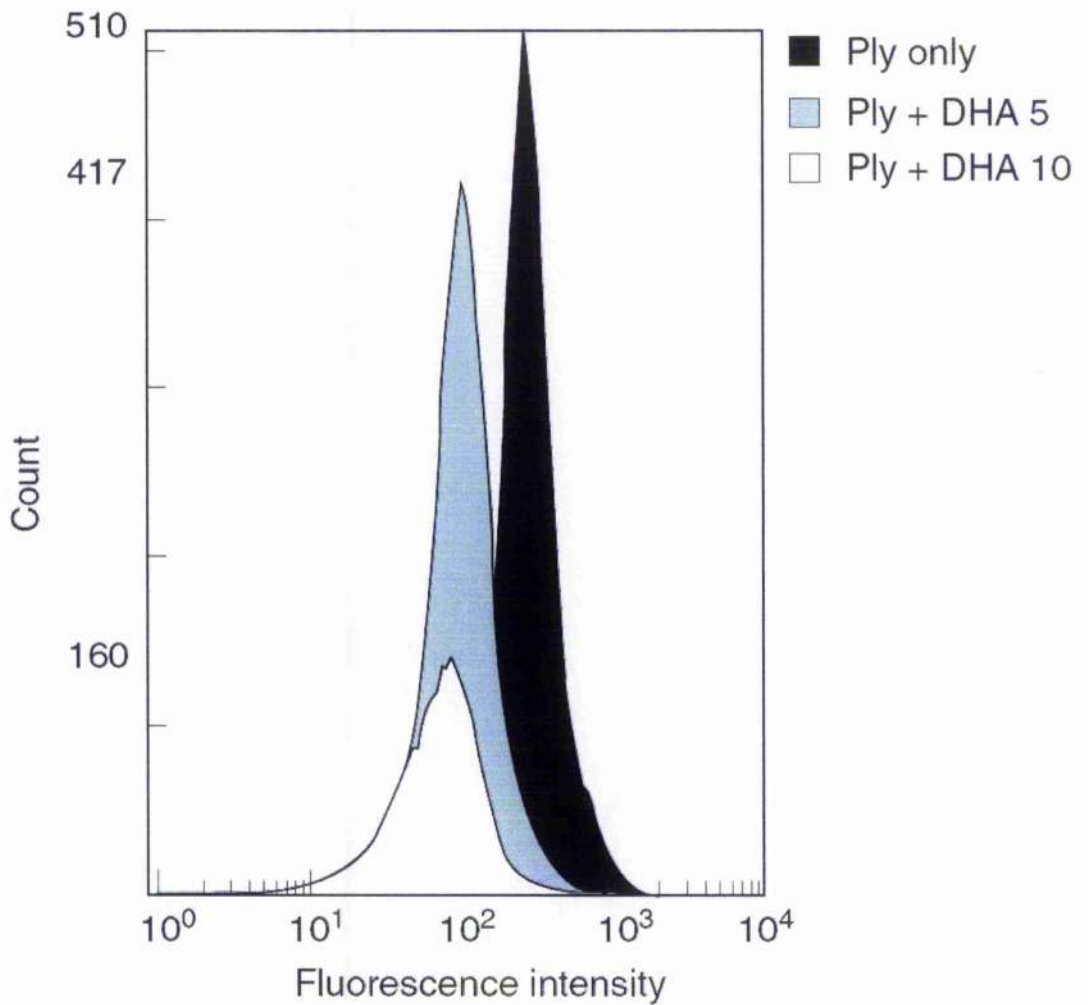


Figure 3.14: Effects of docosahexaenoic acid (DHA, 5 and 10 mg/ml) on the binding of the eGFPPPLY protein (500 ng/ml) to neutrophils. The cells were treated with DHA for 5 min at 37°C followed by addition of the construct and flow cytometric analysis of cell-associated toxin. The results shown are those of a single representative experiment with three in the series. Figure taken from Fickl et al, 2005.

Discussion

Rationale for using eGFP as a fusion partner

Green fluorescent protein is a protein produced by *Aequorea aequoria*, a bioluminescent jellyfish with a wide geographical distribution. During the course of studies of aequorin, the light-emitting protein of *A. aequoria*, Dr. Osamu Shimomura discovered that purified aequorin produced blue light, not the green-light produced by live specimens, and discovered a protein which exhibited green fluorescence under UV light (Chalfie & Kain, 1998; Shimomura *et al.*, 1962). This protein, later to be named green fluorescent protein (GFP), is excited by the blue luminescence of aequorin and emits the green light observed in specimens of *A. aequoria* (Morise *et al.*, 1974).

Following cloning and expression of GFP (Chalfie *et al.*, 1994; Prasher *et al.*, 1992), interest in GFP increased enormously and a number of modifications have subsequently been made to alter its excitation and emission spectra, stability and solubility. One such variant, enhanced green fluorescent protein (eGFP), is a widely used fusion partner for studies of protein expression and localisation.

A number of different versions of eGFP exist – the variant used in this study is GFPmut1 discovered by Cormack and Valdivia (Cormack *et al.*, 1996) and is a mutant of GFP containing two mutations - F64L and S65T. These mutations increase the excitation at 488nm enabling compatibility with flow cytometers and microscopes that utilise argon lasers or FITC filter sets (Cormack *et al.*, 1996). This version of eGFP was picked in preference to the variant of eGFP marketed by

Clontech as this produces the same amino acid sequence but has been 'humanised' by alteration of codon usage in the eGFP cds and this can lead to reduced expression in bacterial systems (Dr. Georgina Donovan, Clontech Laboratories Inc, personal communication). In fact the S65T mutant has been shown to fold as well as wild-type GFP in bacterial systems and 10-fold less in mammalian cells (Sacchetti *et al.*, 2001).

Since eGFP is a protein, it offers the advantage that it can be linked to PLY by expression as a genetic fusion and does not require chemical conjugation as would be required for chemical fluorophores. This may allow the toxin to be expressed within *S. pneumoniae*, allowing study of toxin production and localisation within model infection systems.

eGFP is fluorescent without the addition of exogenous substrates or co-factors (Inouye & Tsuji, 1994) and therefore it facilitates easier experimental design than some other tracking systems where external substrates are required such as fluorescein arsenical hairpin (FIAsH) tags (Adams *et al.*, 2002; Griffin *et al.*, 1998), which may also have problems of penetration of the substrate to the site of toxin localisation. Such systems would indicate toxin localisation only where that region is also accessible to the substrate.

Yet another alternative approach to tagging of pneumolysin would be to use immunohistochemistry (IHC) whereby the toxin is recognised by specific anti-toxin antibodies and detected with a secondary fluorophore-labelled antibody. This technique requires fixation of the specimen which prevents real-time visualisation

and raises the possibility that artefacts may be produced by fixation. It also requires that antibodies are able to penetrate to the site of localisation and this can be a limiting factor with this technique. However, anti-eGFP antibodies are widely available and very specific, so this technique could be used to confirm localisation findings. This may be especially useful in tissue samples where levels of auto-fluorescence are often high and the use of a fluorophore with a different emission wavelength may be useful to demonstrate that the localisation pattern is a specific event.

One of the major disadvantages of eGFP is that it is a 27kDa β -barrel protein and so is much larger than most chemically-conjugated fluorophores or FIASH tagging systems.

In design of fusion constructs, eGFP may be located as an N-terminal or C-terminal fusion, or fused between domains of the protein. From previous work, we know that the C-terminus is critical to toxin activity as modification of C-terminal residues drastically reduces the binding activity of the toxin (Baba *et al.*, 2001; Owen *et al.*, 1994). Domain 4 of the protein is thought to be the only contiguous domain, and it is likely that addition of eGFP at this site would radically alter the activity of the protein. Based on the homology model for the structure of PLY (Rossjohn *et al.*, 1998) and the model for the mode of action of the toxin as discussed in the introduction to this thesis, it is likely that addition of eGFP to the C-terminus or between domains 123 and domain 4 would hinder the binding of the protein to the cells or the conformational change required for pore formation. The N-terminus is thought to be much less critical for activity, although deletion of 21

residues from the N-terminus of PLY has been shown to drastically reduce the activity of the toxin (Baba *et al.*, 2001). It was therefore considered that tagging of the N-terminus represented the best chance for production of the fully active protein.

Comparison of the haemolytic and cytolytic properties of eGFP-tagged PLY to wild-type toxins

In order to be confident that the eGFP-labelled toxin was a suitable substitute for the wild-type toxin in tracking experiments, it was necessary to demonstrate that the properties of the toxin were not affected by the addition of the eGFP-tag.

Comparison of the haemolytic activity of eGFPPLY to recombinant PLY revealed that it has a specific activity identical to pneumolysin when expressed in molar terms. This indicates that the addition of the 27 kDa eGFP moiety to the N-terminus of pneumolysin did not inhibit the haemolytic activity of the toxin.

The $\Delta 6$ mutant of eGFPPLY, $\Delta 6$ eGFPPLY was not haemolytic, even at concentrations 100,000 times greater than that required for 100% erythrocyte lysis with PLY or eGFPPLY. This $\Delta 6$ mutation of PLY has previously been shown to be non-lytic (Kirkham *et al.*, 2006b) therefore as expected the $\Delta 6$ eGFPPLY molecule has inherited this property from the parent toxin.

In addition to the haemolytic activity of pneumolysin, the molecule has been shown to cause cell toxicity to a number of nucleated cell types at sub-lytic concentrations (Braun *et al.*, 2002; Hirst *et al.*, 2002). Although the haemolytic activity of the

eGFPPPLY was identical to that of PLY, we were interested to determine whether the proteins shared the same cytotoxic potential. Cytotoxicity of the toxins to L929 mouse fibroblasts was measured by MTT uptake assay. Both eGFPPPLY and PLY were cytotoxic to L929 fibroblasts and both had similar cytotoxicity within the resolution provided by variability within the assay.

$\Delta 6$ eGFPPPLY, $\Delta 6$ PLY and eGFP were not cytotoxic to L929 cells even at high concentrations. This confirms that $\Delta 6$ eGFPPPLY had the detoxified properties of $\Delta 6$ PLY as described by Kirkham *et al* (Kirkham *et al.*, 2006b).

Comparison of pore formation by tagged and untagged toxins by TEM

Transmission electron microscopy was used to compare the pores produced by eGFPPPLY to those produced by PLY to determine whether there were any morphological differences. Pores produced by eGFPPPLY were similar in appearance to those formed by PLY. There was no apparent difference in the size of complete pores, and arcs and double arcs were formed by both eGFPPPLY and PLY. No pores were formed by $\Delta 6$ eGFPPPLY and this correlates with the lack of haemolytic activity previously measured.

No difference in the appearance of the pore structures, either in width of the ring or diameter of the pores was observed and the presence of the eGFP moiety was therefore not detected. It is possible that the eGFP domain of the fusion protein sits vertically above domain 1 in the pore structure, preventing an increase in width of the oligomeric ring. This could be further investigated using immunogold labelling to identify the position of eGFP, although the required length of the

antibody chain would distance the gold particle from the eGFP domain so that it would not be possible to determine exactly where the domain was situated. Exact localisation of the eGFP moiety could be determined by cryo-electron microscopy as previously used to visualise the pore structure of pneumolysin (Gilbert *et al.*, 1999; Tilley *et al.*, 2005).

Visualisation of toxin binding by epifluorescence microscopy

Part of the aim of this project was to produce a tagged form of PLY that could be used to visualise the localisation of the toxin. Human erythrocytes treated with eGFPPLY and $\Delta 6$ eGFPPLY were examined by fluorescence microscopy. Addition of the toxin highlighted the plasma membrane of the erythrocytes in green, indicating that both eGFPPLY and $\Delta 6$ eGFPPLY bound to erythrocyte membranes. As expected from the haemolytic assay results previously discussed, eGFPPLY lysed human erythrocytes whereas $\Delta 6$ eGFPPLY was non-lytic. Lysis was evident by the retention of the erythrocyte's bi-concave shape and the leakage of haemoglobin upon cell lysis observed by brightfield microscopy (not shown).

The concentration of eGFPPLY used in this microscopy work was 700nM since this gave a clear and high intensity signal, although binding of the toxin to cells could be visualised at concentrations down to 700pM in preliminary microscopy experiments. For wild-type pneumolysin, 700nM is equivalent to 37.1 μ g/mL. It is difficult to estimate whether this concentration is physiologically relevant since the total amount of PLY that is released by *S. pneumoniae in vivo* is not known. Studies of cerebral spinal fluid CSF from patients with pneumococcal meningitis showed that pneumolysin was present in the supernatant of CSF at concentrations

ranging from 0.85ng/ml to 180ng/ml (Stringaris *et al.*, 2002). However, since it is possible that much of the pneumolysin produced may have bound to host cells, this does not give an accurate figure for the amount of PLY produced, and therefore the amount of pneumolysin that should be added to cells in vitro to simulate physiological events.

A punctuate appearance was observed on erythrocytes treated with $\Delta\delta$ eGFPPLY and further examination revealed these to be fluorescent linear structures associated with the surface of the erythrocyte. Although it appeared that these structures occurred on and slightly protruded from the plasma membrane, the resolution of the fluorescence micrographs limited the amount of information that could be obtained about the nature and attachment of these structures.

Ohno-Iwashita *et al* have used GFP-tagged domain 4 of perfringolysin as a probe for lipid rafts (Ohno-Iwashita *et al.*, 2004). Based on their previous work which demonstrated that a proteolytically-derived fragment of PFO selectively bound to lipid rafts, the group hope to use the probe to monitor lipid rafts in real-time and to study lipid raft dynamics (Ohno-Iwashita *et al.*, 2004).

Binding of eGFPPLY to cochlear hair cells of the rat

Epifluorescence microscopy of eGFPPLY was successfully used in collaboration with Dr. D. Dulon's group at the University of Bordeaux to study the binding of eGFPPLY to rat cochlear hair cells (Beurg *et al.*, 2005).

This study provided further verification of the similarity between the properties of eGFPPLY and PLY as the toxicity of eGFPPLY in an organ of corti (OC) explant culture model and was found to be similar to that of PLY (Beurg *et al.*, 2005).

eGFPPLY binding to IHCs and OHCs could be visualised and a homogenous distribution on the plasma membrane was observed. The use of eGFPPLY allowed a comparison of the amount of toxin bound to cells and no difference was observed between the amount of eGFPPLY bound to freshly dissociated inner hair cells (IHCs) and outer hair cells (OHCs). However, in OC explant cultures, eGFPPLY appeared to preferentially label the hair bundles of both IHCs and OHCs with the staining being more pronounced in the OHCs.

Measurement of the fluorescence of cells recorded by epifluorescence microscopy showed that raised extracellular calcium reduced the binding of eGFPPLY to IHCs and OHCs (Figure 3.8). This was not a result of reduction of the fluorescence of eGFPPLY due to increased calcium concentration since these results were confirmed by examination of PLY binding in OC explant in the presence of 1.8mM or 10mM calcium using PLY-specific antibody (Beurg *et al.*, 2005). The mechanism is unknown and it is also not known whether this is an effect restricted to rat cochlear hair cells. This effect appears to be different from that observed in studies on the effect of calcium on PLY-induced channel conductance (Korchev *et al.*, 1992; Korchev *et al.*, 1998), since CDC-induced conductance channels were inhibited by di-valent cations in cells pre-treated with toxin (Menestrina *et al.*, 1990; Olofsson *et al.*, 1993).

Examination of toxin-treated erythrocytes by scanning electron microscopy

To gain a more detailed view of the structures that occurred on $\Delta 6$ eGFPPLY-treated cells and to investigate whether they were also present in cells treated with $\Delta 6$ PLY, toxin-treated erythrocytes were examined by scanning electron microscopy. In addition to eGFPPLY and $\Delta 6$ eGFPPLY treated samples, PLY and $\Delta 6$ PLY treated samples were included to determine whether the effect was related to the presence of the eGFP tag or if it was a property inherent to the $\Delta 6$ mutant of PLY.

Linear structures have previously been observed by TEM to be present on the surface of rat adipocytes treated with $\Delta 6$ PLY (L. Kirkham, University of Glasgow, unpublished results). The SEM examination of erythrocytes treated with $\Delta 6$ PLY and $\Delta 6$ eGFPPLY confirmed that formation of these structures is a property of $\Delta 6$ PLY, and is not an artefact from the addition of the eGFP moiety. The structures were very large and roughly circular in cross-section. It was not possible to determine their dimensions accurately by the SEM approach used. They appeared to be attached to the cell in a number of places along their length and were able to span between cells, and this may be involved in aggregation of erythrocytes when treated with $\Delta 6$ PLY (Kirkham *et al.*, 2006b).

No structures were observed on the surface of erythrocytes treated with PLY and eGFPPLY but these cells lost the bi-concave shape of untreated cells and appeared to be slightly larger with crumpled membranes, most likely as a result of lysis of the cells.

An assumption is being made that the structures are composed of oligomerised toxin and not composed of target cell materials re-arranged as a result of toxin activity. The fluorescent nature of the structures suggests that toxin must be present but this could also be verified using immuno-gold labelling for the toxin.

Further study of how these structures form and the arrangement of the toxin monomers on these large oligomeric structures may assist with studies of monomeric interactions of pneumolysin.

Confocal fluorescence microscopy of Detroit D562 cells treated with eGFP-tagged toxin

Laser scanning confocal electron microscopy was used to study the localisation of eGFPPLY and $\Delta 6$ eGFPPLY on Detroit 562 cells, a human pharyngeal cell line (Peterson *et al.*, 1971). eGFPPLY caused a marked rounding-up of cells and was largely bound to the plasma membrane of the host cell. $\Delta 6$ eGFPPLY also bound to the plasma membrane but did not cause cells to round up – the actin-cytoskeleton of these cells appeared identical to those of untreated or eGFP-treated cells.

The experiments discussed here have shown that eGFPPLY is a useful tool for monitoring the localisation of PLY by conventional fluorescence of laser scanning confocal fluorescence microscopy. It is likely that the same approach could be used to study other members of the CDC family or to compare any differences that may occur between the localisation of different members of the CDCs.

It is possible that the toxin could also be used in more complex cell systems – through direct addition to tissues or application *in vivo*, followed by sectioning and study by fluorescence microscopy. Developing technologies such as two-photon microscopy and live imaging systems may allow real-time tracking of toxin localisation *in vivo*, and this could give new insights into how and where the toxin acts.

Expression of the eGFPPLY fusion protein in the host organism

It may be also possible to express the eGFPPLY fusion protein in *S. pneumoniae* to allow tracking of the toxin expressed in its host organism during a model infection. Comparison of the virulence of this new construct to wild type *S. pneumoniae* would give a clear indication whether any important properties of the toxin had been altered by the addition of the eGFP tag. Such a construct could be used in combination with the live imaging systems mentioned above or with sectioning and fluorescent microscopic examination of tissues.

As part of this project, we attempted to replace the PLY allele in *S. pneumoniae* D39 with eGFPPLY using Janus mutagenesis (Sung *et al.*, 2001). The D39-Janus construct was successfully generated by Dr. Gavin Paterson but introduction of eGFPPLY failed on repeated attempts, and sequencing and PCR analysis of resulting clones indicated that unexpected truncation events appeared to be occurring in the eGFPPLY gene upon incorporation into the *S. pneumoniae* genome.

Another potential application of the eGFPPLY is use in determining whether PLY demonstrates cell tropism in complex cell systems. Fluorescence intensities of cells from complex mixtures of cells could be compared using fluorescence microscopy or FACS to compare the binding preference of PLY in heterogeneous cell systems. It is already recognised that different eukaryotic cell types can have different susceptibilities to pneumolysin (Hirst *et al.*, 2002). The FACS based binding assay or microscopic techniques described here could be used to investigate whether cell tropism occurs, perhaps as a result of different binding affinities or greater access to particular cell types.

Development of a fluorescence-based quantitative binding assay for PLY

A possible application of eGFPPLY and $\Delta 6$ eGFPPLY is use in a FACS-based binding assay. Potential applications of this assay would include use as a quantitative PLY binding assay for cellular receptor studies, discovery of small molecule inhibitors and other inhibitors of PLY binding, or investigations of the cellular tropism of PLY. A FACS-based binding assay using eGFPPLY and $\Delta 6$ eGFPPLY was therefore developed to demonstrate the level of sensitivity and dynamic range of detection of toxin binding by this method.

The fluorescence of eGFPPLY-treated or $\Delta 6$ eGFPPLY-treated erythrocyte membranes increased with the concentration of the toxin. Application of the same molar concentrations of eGFP did not lead to an increase in fluorescence of erythrocytes, confirming that the effect was not due to non-specific incorporation of eGFP.

The dynamic range of sensitivity was very good – and binding of eGFPPLY could be quantified above background fluorescence over a range of at least 100-fold variation in toxin concentration from 0.7nM to 70nM.

The concentration of eGFPPLY used in this flow cytometry work ranged from 0.7nM to 70nM. For wild-type pneumolysin, this range is equivalent to 37.11ng/mL to 3.71 μ g/mL. As mentioned previously, pneumolysin has previously been found to be present in CSF from patients at concentrations ranging from 0.85ng/mL to 180ng/mL (Stringaris *et al.*, 2002), but due to the likelihood that much of the pneumolysin present would bind to host cells, it does not give guidance on how much pneumolysin is produced *in vivo*. Although the flow cytometry assay was not tested at the lower concentrations in this range, it was capable of detecting eGFPPLY binding to erythrocytes at concentrations equivalent to the higher PLY concentrations present in CSF. As shown in the haemolytic assays earlier in this section, PLY and eGFPPLY cause 100% lysis at 0.7nM concentration, therefore it is unknown whether this technique can detect binding at sub-lytic concentrations.

A broader range of fluorescence intensity values was obtained for each concentration of eGFPPLY than Δ 6eGFPPLY resulting in different profiles on the flow cytometry histograms. The cause of this is unknown but it may result from the lytic effect of eGFPPLY. The mean fluorescence at each concentration of toxin was greater for eGFPPLY than Δ 6eGFPPLY. It is possible that this could also reflect cell lysis by eGFPPLY. A portion of the fluorescence may be absorbed by the haemoglobin remaining in the Δ 6eGFPPLY-treated erythrocytes, or the

fluorescence of the membrane at the side distal to the fluorescence detector may not be read, resulting in lower fluorescence readings.

It was therefore demonstrated that toxin binding can be easily quantified using eGFPPLY and $\Delta 6$ eGFPPLY in a flow cytometry-based assay. It is hoped that this will be useful in further research and characterisation of toxin mutants where it offers an alternative to dot-blot or western blot techniques that are currently commonly used to monitor CDC binding to target cells (Nato *et al.*, 1991; Owen *et al.*, 1994). A different flow cytometry-based binding assay based on cross-linking a chemical fluorophore to the toxin has been developed (Giddings *et al.*, 2003). The flow cytometry based technique offers good sensitivity and it is more rapid than immunoblotting, and it could therefore allow binding determination where a large number of samples are required to be measured, such as in high throughput screening.

The flow cytometry technique is also able to determine the quantity of toxin bound to single cells rather than a population as a whole. The quantity of PLY per cell can be plotted against specific cell markers to ascertain whether there is a greater affinity for particular cells in a mixture of cell types. Fluorescence-activated cell sorting (FACS) could be used to select cells within a population that have been successfully transformed or altered to affect toxin binding activity.

The eGFPPLY binding assay was used successfully by our collaborators at the University of Pretoria, South Africa to measure the antagonistic effect of docosahexaenoic acid (DHA) on binding of PLY to human neutrophils (Fickl *et al.*,

2005). The presence of DHA at concentrations of 5 or 10 μ g/ml reduced the binding of eGFPPLY, and this effect was also observed where neutrophils were pre-incubated with DHA and then subsequently washed. It was therefore suggested that this is a cell-directed mechanism of action rather than a direct inactivation of the toxin (Fickl *et al.*, 2005). It is likely that the interference to PLY binding by DHA is in part responsible for the reduction on PLY-mediated calcium influx, but there may be other factors involved since Ca-influx was reduced by 86% but binding and haemolysis were reduced by only 18% and 21.8% respectively upon addition of 5 μ g/mL DHA.

Further work

Although eGFPPLY has been shown to be very similar to PLY in terms of haemolytic activity and pore formation, it has not been tested to determine whether it is capable of all of the same biological activities of the unlabelled toxin, such as induction of cytokine production, complement activation or activation of the p38 signalling pathway. It would be useful and interesting to determine whether the addition of the eGFP tag has altered the activity of pneumolysin in any way by running as many such assays as possible.

Similarly, although it has been determined that eGFPPLY can be visualised when bound to cells, no experiments have been performed to ensure that the localisation of the tagged toxin is the same as the unlabelled toxin. This would require the use of immunohistochemistry but would be another useful step in validating eGFPPLY as a tool.

Conclusions

- The eGFP-tagged toxins produced, eGFPPLY and $\Delta 6$ eGFPPLY, are not altered in haemolytic and cytotoxic activities relative to their untagged parent toxins.
- There are no visible differences in the pores produced by eGFPPLY from those produced by PLY.
- eGFPPLY can be used in a sensitive and quantitative binding assay using flow-cytometry.
- eGFPPLY and $\Delta 6$ eGFPPLY binding and localisation on target cells can be monitored by fluorescence and laser scanning confocal fluorescence microscopy.
- $\Delta 6$ PLY and $\Delta 6$ eGFPPLY produce large rod-like structures on erythrocyte membranes that are capable of spanning between cells.

Chapter 4: Intermedilysin – a rogue member of the CDC family

Summary

Intermedilysin (ILY) is a member of the CDCs produced by *S. intermedius*. It is unique within the group in that it exhibits human-specific haemolysis, with 1% of activity remaining on erythrocytes of chimpanzees and cynomolgus monkeys but no activity on erythrocytes from all other species tested (Nagamune *et al.*, 1996). Initial studies suggested that this is due to binding of a different cellular receptor to other toxins of the family and that this receptor was a protein (Nagamune *et al.*, 1996).

As a prelude to experiments to determine the cellular receptor for ILY, eGFP-tagged forms of ILY and $\Delta 6$ ILY - eGFPsILY, and $\Delta 6$ eGFPsILY - were produced to allow tracking of the localisation of ILY and for use in development of a quantitative binding assay. It was confirmed that these proteins could be easily visualised by fluorescence microscopy and that binding could be detected by flow cytometry.

This FACS-based binding assay was intended for use to screen mouse tissue-culture cells transformed with a human-cDNA library to identify the human cell-specific receptor for intermedilysin. With the same aim, a two-hybrid screen was also used to identify proteins from a human brain cDNA library that were capable of interaction with ILY. No likely receptor candidates were identified. During the course of this work, the cellular receptor for ILY was identified as CD59, therefore the FACS based screen was not attempted and candidate protein:protein interactions were not further investigated.

In order to determine which region is responsible for the human specificity of intermedilysin, a bank of chimeras between ILY and PLY was created. The chimeric toxins were expressed and purified and the specificity of the mutants was determined by haemolytic assay on human and rabbit erythrocytes. It was found that the specificity of the chimeric toxin was determined by the origin of the C-terminal 53/56 residues, indicating that this region of domain 4 is responsible for the human specificity of intermedilysin.

To further resolve the region involved in human specificity or cholesterol-binding, a series of small substitution mutants was created. These revealed that promiscuous cell binding activity of the other CDCs was conferred by residues in the undecapeptide loop as this property could be transferred to ILY by introduction of the typical undecapeptide sequence.

Surface-plasmon resonance analysis of substitutions of ILY and PLY was used to detect any mutants possessing altered binding affinity. However, problems with aggregation of purified proteins prevented a valid comparison from being made.

Results

Construction of pET33bmILY

A plasmid containing the coding sequence for mature intermedilysin (mILY) was constructed in pET33b to allow high level expression with the addition of a six-histidine tag to facilitate protein purification. mILY is composed of residues E34-D532 of ILY such that the putative signal sequence is removed. The pET33bmILY plasmid was transformed into BL21(DE3) *E. coli* for protein expression.

Initial cloning was confirmed by PCR using gene specific primers and primers that anneal to the T7 promoter and T7 terminator sequences flanking the multiple cloning site of pET33b.

The construction of all plasmids was checked by DNA sequencing. The sequence was confirmed to be as expected with no mutations present. Plasmid maps of pET33bEGFPPLY and pET33bDel6EGFPPLY plasmids are shown in Figure 3.1.

Constructs were transformed into BL21(DE3) *E. coli* for protein expression.

Construction of vectors for expression of chimeric toxins between PLY and ILY

Plasmids were constructed containing the coding sequences of eight chimeric toxins between PLY and ILY. The individual components were first amplified using specific primers as described in the materials and methods section then these

were joined in an overlap PCR reaction to produce full-length toxin chimeras. These DNA fragments were cloned into pET33b(+) and the sequence of the resulting clones was confirmed by DNA sequencing. All plasmids were transformed into BL21(DE3) *E. coli* for protein expression.

Table 4.1: Crossover positions of PLY/ILY chimeric toxins

Site	DNA sequence position		Amino acid sequence position	
	PLY	Mature ILY	PLY	Mature ILY
1	441	516	147	172
2	759	834	253	276
3	993	1068	331	356
4	1251	1326	417	442

NB Residues are the last residue before the crossover position.

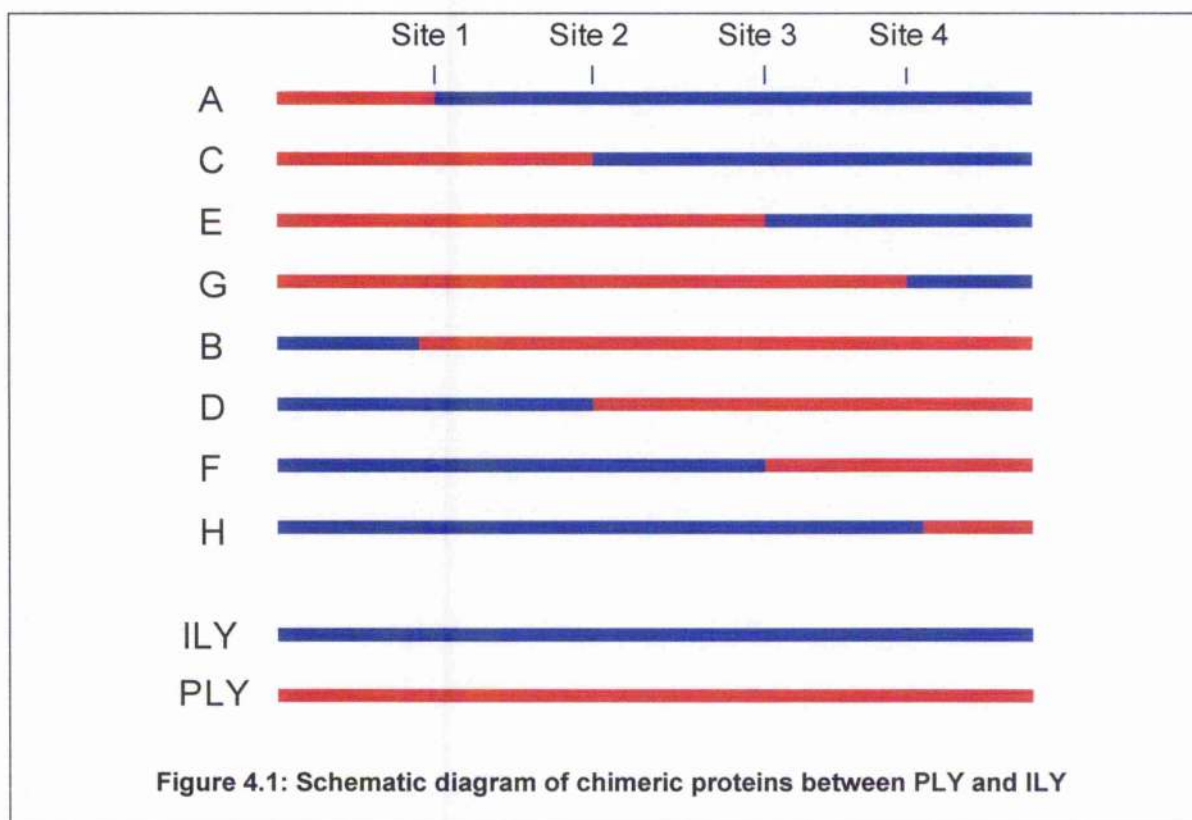


Figure 4.1: Schematic diagram of chimeric proteins between PLY and ILY

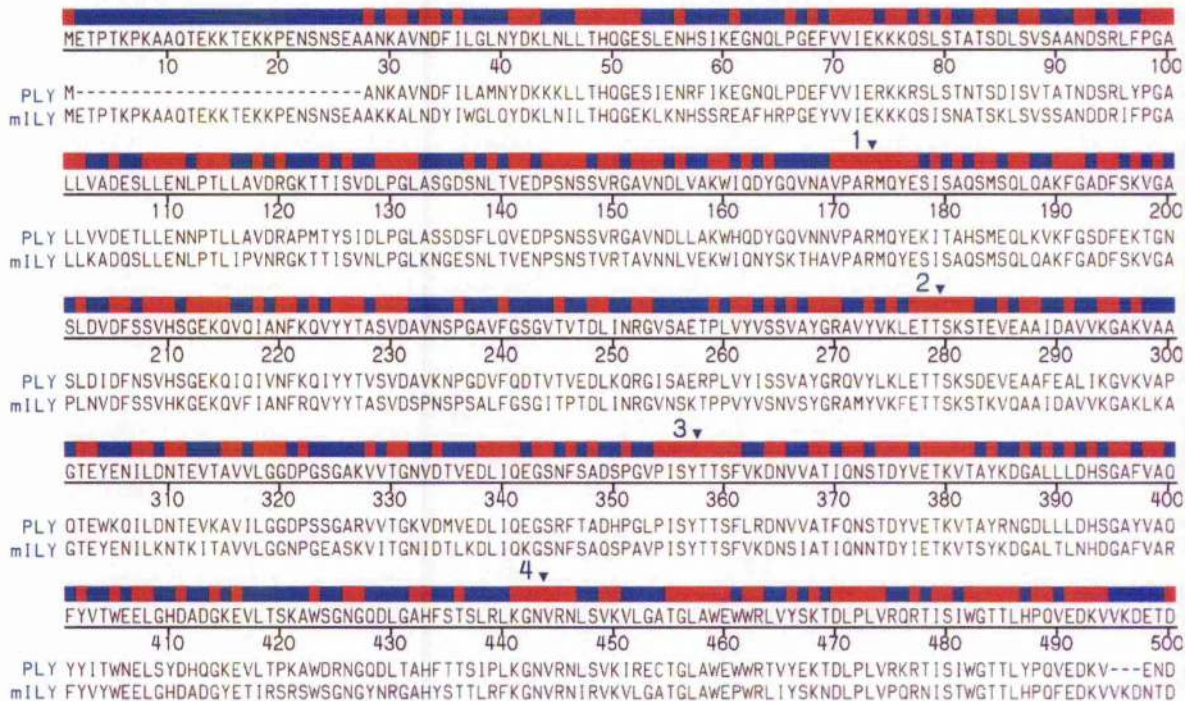


Figure 4.2: Alignment of PLY and mILY amino acid sequences indicating conserved regions selected as cross-over junctions in ILY/PLY chimeras (labelled 1, 2, 3 & 4). Sequence alignment generated using DNASTAR software.

Expression and purification of pneumolysin, intermedilysin and chimeric toxins

Recombinant pneumolysin, intermedilysin and chimeric toxins were initially expressed and purified by nickel-affinity chromatography using the Swell-Gel tab system. Purified protein preparations were assessed by SDS-PAGE to be of greater than 90% purity.

Haemolytic activities of chimeric toxins

The haemolytic activities of chimeras A-H and PLY and mILY were determined by semi-quantitative haemolysis assay (Table 4.2). Pneumolysin, chimera D, chimera F and chimera H were lytic to both horse and human erythrocytes whereas ILY, chimera C, chimera E and chimera G were lytic to human but not horse erythrocytes. Chimeras A and B were not lytic on either human or horse erythrocytes, and chimera B caused aggregation of both human and horse erythrocytes.

Table 4.2: Haemolytic activity of PLY, ILY and chimeric toxins A-H by semi-quantitative haemolysis assay.

	Human	Horse
PLY	+	+
ILY	+	-
A	-	-
B	- (Aggregation)	- (Aggregation)
C	+	-
D	+	+
E	+	-
F	+	+
G	+	-
H	+	+

Haemolytic activities of chimeric toxins G and H

In order to allow full characterisation and comparison of their haemolytic activities, PLY, mILY, chimera G and chimera H were purified by Nickel-affinity chromatography. Protein preparations were estimated by Coomassie-blue stained SDS-PAGE to be of greater than 98% purity.

Haemolysis assays were performed using ILY, PLY, chimera G and chimera H on human and rabbit erythrocytes. Specific activities of the toxins were calculated and are shown in Table 4.3. All toxins were haemolytic on human erythrocytes, although the haemolytic activity of chimera G was very low at 1.785×10^3 HU mg^{-1} . The activity of chimera H was also lower than the activities of either of the two parent toxins, PLY and ILY. PLY and chimera H were both haemolytic to rabbit erythrocytes whereas ILY and chimera G were non-lytic (Figure 4.3).

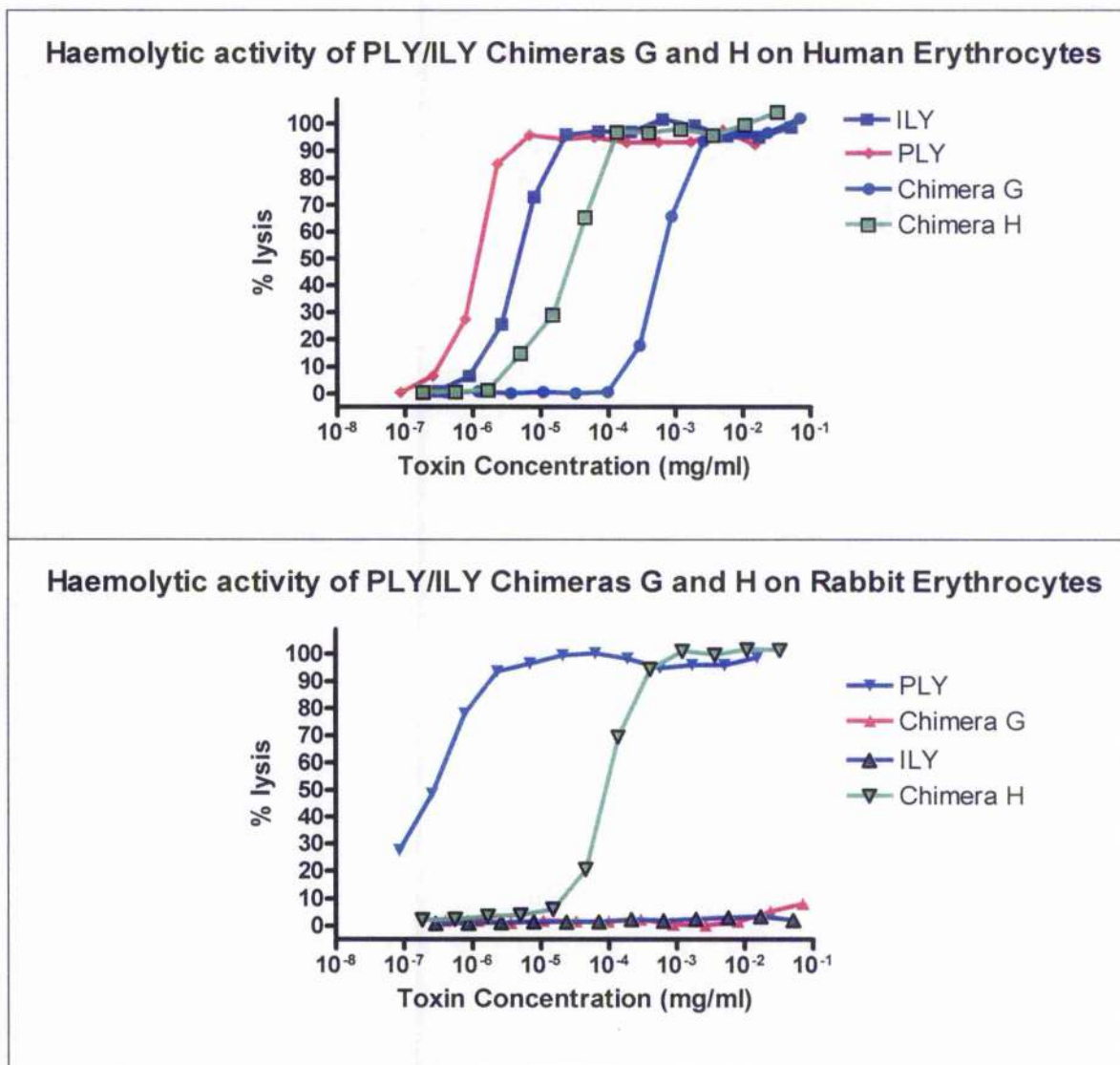


Figure 4.3: Haemolysis assays of PLY, ILY, chimera G and chimera H on A) Human erythrocytes and B) Rabbit Erythrocytes.

Table 4.3: Specific activities of PLY, ILY, chimera G and chimera H on human or horse erythrocytes

	Human	Horse
PLY	9.09×10^5 HU mg ⁻¹	3.87×10^6 HU mg ⁻¹
ILY	2.02×10^5 HU mg ⁻¹	Non-lytic
Chimera G	1.785×10^3 HU mg ⁻¹	Non-lytic
Chimera H	3.616×10^4 HU mg ⁻¹	1.051×10^4 HU mg ⁻¹

Inhibition of action of chimeras G and H by ghost erythrocytes

In order to determine whether the species-specific haemolytic activities of chimeras G and H were due to binding specificities, the inhibition of the action of these toxins on human erythrocytes by human or rabbit erythrocyte ghosts was determined (Figure 4.4).

Inhibition of Activity of Chimeras G and H by Erythrocyte Ghosts

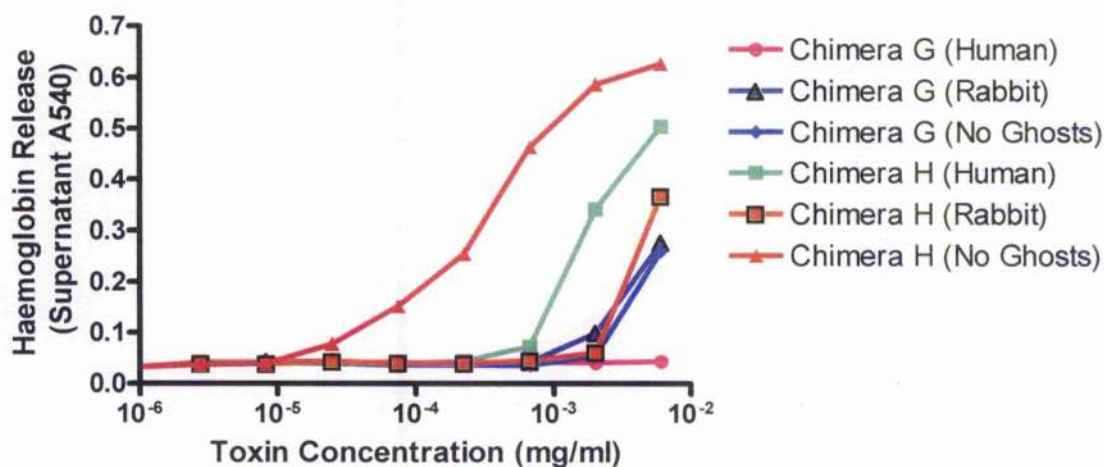


Figure 4.4: Inhibition of the haemolytic activity of chimeras G and H by human or rabbit erythrocyte ghosts

Chimera H was absorbed by both human and rabbit erythrocyte ghosts indicating that it was capable of binding to either of the erythrocyte species. Chimera G was

absorbed by human but not rabbit ghost erythrocytes and therefore demonstrated a human-specific binding activity.

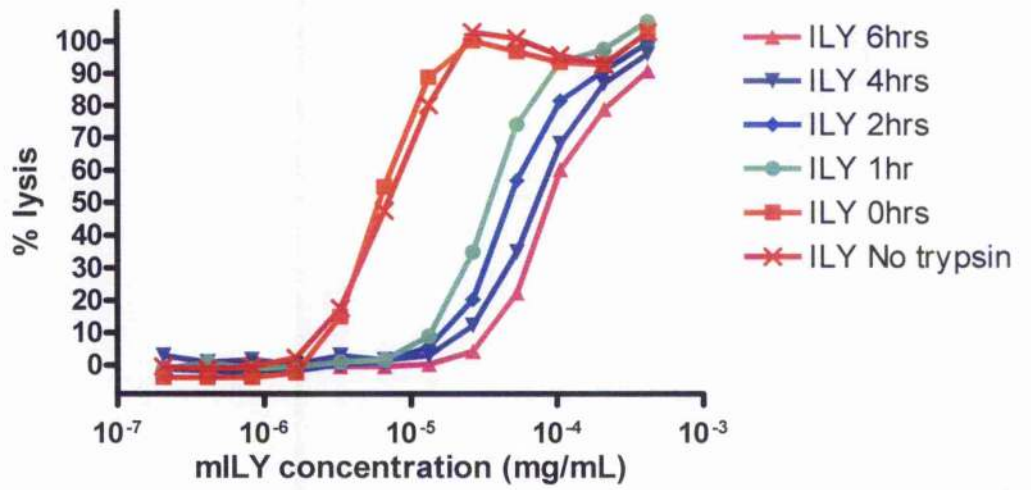
Effect of trypsinisation of erythrocytes on susceptibility to PLY and ILY mediated lysis.

Nagamune et al, 1996 showed that treatment of erythrocytes with trypsin reduced their susceptibility to lysis by intermedilysin. This effect was confirmed and further investigated by determining the effect of the trypsin treatment time on lysis by intermedilysin. The effect on lysis by pneumolysin was also investigated.

Trypsin treatment of human erythrocytes was found to reduce their susceptibility to lysis by ILY (Figure 4.5). The effect of ILY was progressively reduced as trypsin treatment time was increased.

The effect of trypsin treatment on susceptibility of human erythrocytes to pneumolysin showed the opposite effect (Figure 4.5) - trypsinisation of erythrocytes decreased the concentration of PLY required for haemolysis. The maximum effect was reached within 1 hour of trypsin treatment.

Effect of trypsinisation of erythrocytes on lysis by mILY



Effect of trypsinisation of erythrocytes on lysis by PLY

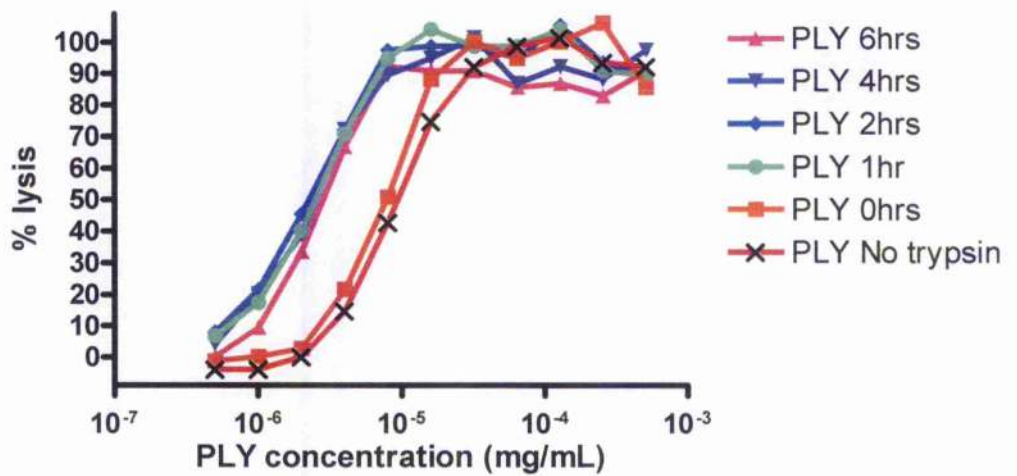


Figure 4.5: The effect of trypsinisation of human erythrocytes on lysis by mILY and PLY

Construction of pDest32-D4ILY Yeast-2-hybrid bait vector

A yeast-2-hybrid assay was performed to screen for proteins that are able to interact with ILY and therefore may be candidate receptors for ILY. Since this assay requires the expression of the toxin ligand in the yeast cytoplasm, domain 4 of ILY was chosen as the 'bait' fusion partner to the Gal4-DNA-binding domain as this is capable of specific binding to human cells (Nagamune *et al.*, 2004a) but is much smaller than the whole toxin molecule. A human brain cDNA library was selected for the 'prey' as it has previously been shown that brain and liver cells are highly sensitive to ILY (Nagamune *et al.*, 1996).

The D4ILY coding sequence was amplified from pQE9mILY using primers that added Gateway Att-B1 and Att-B2 sites to the ends of the coding sequence. A one-tube gateway cloning reaction was used to insert the D4ILY PCR product into pDEST32 (the DNA binding domain fusion vector) via pDONR221.

One clone was selected and the full sequence between the gateway flanking sequences was confirmed to be correct by DNA sequencing.

Yeast-2-hybrid screen with pDest32-D4ILY against human brain cDNA library

A yeast-2-hybrid screen was performed using a bait plasmid (pDest32-D4ILY) containing D4ILY fused to the DNA binding domain of Gal4 against a human foetal brain cDNA library.

A sequential transformation method was used as this is reported to give greater library coverage than combined transformation. Firstly, the pDest32-D4ILY plasmid was transformed into MAV203 yeast and presence of the plasmid was confirmed by PCR. The resulting MAV203 yeast clone containing the pDest32-D4ILY bait vector was then transformed with a human brain cDNA Gal4-AD-fusion library. Cells were plated onto SC-leu-trp-his+25mM 3AT and SC-leu-trp plates and incubated at 28°C for 3 days.

To ensure full coverage of the cDNA library where all cDNAs present in the library have been screened, it is necessary to ensure that the number of transformants is several fold greater than the likely maximum number of cDNAs present. Invitrogen suggest that greater than 1×10^6 transformants must be screened to ensure adequate library coverage. pDest32 codes for leucine biosynthesis and pEXP-AD502 codes for tryptophan biosynthesis.

Since MAV203 yeast are auxotrophic for both of these amino acids, colonies will only grow if both plasmids are present. The colonies on the SC-leu-trp plates were counted and multiplied by the dilution factor to give the total number of transformants screened in the assay. However, since uracil and histidine are provided in the medium, no protein:protein interaction is required. In this screen, it was calculated that greater than 2.4×10^6 transformants were screened.

29 colonies were obtained from the primary screen and these were further tested for activation of the remaining two reporter genes. Confirmatory assays were performed for all of the positive colonies from the D4ILY screen (1-29) and

controls A-E on YPAD (with membrane for B-gal assay), SC-leu-trp-ura, SC-leu-trp-his(+25mM 3AT), and SC-leu-trp+2mM 5FOA. Five control strains of known protein:protein interaction strength were also included to act as reference strains for interpretation and ensure that the replica cleaning step was sufficiently thorough to eliminate false positives. Plates were replica cleaned as described in the protocol (Invitrogen Proquest Manual).

After 24 hours, the membrane was removed from the YPAD plates and an X-gal assay performed. Results were monitored after 1 hour and after 24 hours.

The results of the confirmatory assays are shown in Table 4.4.

The inserts from clones 1-29 were amplified by PCR using primers 43L and 43M which flank the MCS of pDest32. PCR products were run on an agarose gel, gel purified and DNA sequenced using primer 43L. For those clones where a product was not obtained by PCR, plasmids were purified using the Qia-prep plasmid miniprep kit and transformed into *E. coli*. Plasmids were then minipreped from each *E. coli* clone and the insert was DNA sequenced using primer 43L which primes upstream of the insert in the flanking region of the MCS of pDest32.

Returned DNA sequences were compared against the human genome sequence using stand-alone NCBI blast v 2.2.5 (Altschul *et al.*, 1990) to determine their identity. The top hits for each clone for which sequence data was obtained are shown in Table 4.5. A number of the clones contained only very short coding sequences in the multiple cloning site of the prey plasmid. These results could not

give reliable results in the BLAST search due to their short length, therefore these results are not shown in Table 4.5.

Table 4.4: Confirmatory assays of yeast-2-hybrid clones

D4iLY Y2H clone #	-URA	-His	β -gal	+5FOA
1	+	++	++	++
2	++	++	++	-
3	++	++	++	++
4	+	++	+	++
5	++	++	++	++
6	-	+	+	++
7	++	++	++	-
8	-	++	+	++
9	++	+	++	-
10	-	++	+	++
11	weak (+)	++	++	++
12	-	+	+	+
13	++	++	++	++
14	++	++	++	++
15	++	++	++	++
16	-	+	++	++
17	++	++	++	++
18	++	++	++	++
19	++	++	++	-
20	-	++	++	++
21	++	++	++	+(weak)
22	-	+	++	++
23	++	++	++	++
24	++	++	++	++
25	++	++	++	weak
26	-(very weak)	++	++	++
27	-(very weak)	++	+	++
28	-(very weak)	++	++	++
29	-(very weak)	++	+	++
Control A	-	-	-	+/- inconsistent
Control B	-	+	-	-/weak
Control C	++	++	+	-
Control D	++	++	++	-
Control E	++	++	++	-

A number of clones yielded two PCR products, despite the clones previously being streaked to single colonies. It is likely that these clones took up two plasmids during the transformation process. As a result, where two plasmids were present

in a strain, only one may have interacted with the bait protein. For each of the positive clones, the interaction must be re-confirmed by purification of the plasmids and repeat of the yeast-2-hybrid assay.

Table 4.5: Top blast hits of proteins interacting with D4ILY in a yeast-2-hybrid screen

Clone	Blast Hits
1	Homo sapiens BCL2/adenovirus E1B interacting protein 3 gl45709255
2	Homo sapiens myosin X (MYO10), mRNA 211/216
3	Homo sapiens kinesin family member 17, mRNA 183/191
3	Homo sapiens glucosidase, beta (bile acid) 1 (GBA2), mRNA 153/153 & Homo sapiens mitochondrial RNA-processing endoribonuclease RNA (RMRP) 153/153
4	Homo sapiens LYST-interacting protein LIP8, mRNA 332/339
5	Homo sapiens heterogeneous nuclear riboprotein G mRNA 348/350 & Homo sapiens RNA binding motif protein, X-linked, mRNA 348/350 & Homo sapiens kynurenine aminotransferase III, mRNA 338/350
6	Homo sapiens EGF-containing fibulin-like extracellular matrix 444/450
6	Homo sapiens EGF-containing fibulin-like extracellular matrix 305/319 & Human extracellular protein (S1-5) mRNA 249/260
6	Homo sapiens regulatory element binding transcription factor 333/344
7	Homo sapiens kinesin family member 17 (KIF17) 497/508
9	Homo sapiens pleckstrin homology-like domain, family B, member 1 511/532 & Homo sapiens DLNB07 mRNA, complete cds 511/532
9	Homo sapiens kinesin family member 17, mRNA 453/463
10	Homo sapiens transcription factor CP2 454/470
11	PREDICTED: Homosapiens Zinc finger protein 592 459/471 & Homo sapiens mRNA for KIAA0211 gene 459/471
13	Homo sapiens glutathione S-transferase A4 (GSTA4), mRNA 453/458
14	Homo sapiens kinesin family member 17 (KIF17) 252/255
15	Homo sapiens kinesin family member 17 (KIF17) 334/342
23	H. sapiens actinin, alpha 1 mRNA 180/191
28	Homo sapiens kinesin family member 17, mRNA 320/322

Construction of eGFPmILY, eGFPsILY and Δ 6eGFPsILY expression vectors

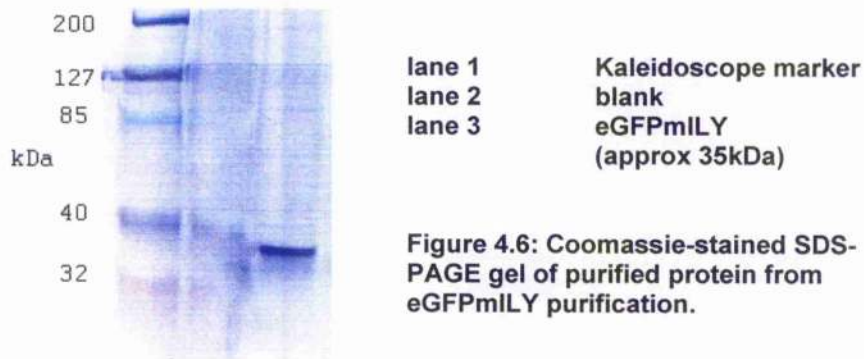
pET33bEGFPmILY

An expression construct containing the eGFP coding sequence fused to the N-terminus of mature ILY was constructed. The eGFP and mILY coding sequences were amplified by PCR and joined by overlap PCR. The resulting PCR product was cloned into pET33b. The ligation mixture was transformed into TOP10 *E. coli*

and the plasmid was purified and checked by DNA sequencing. The sequence was confirmed to be correct over the complete coding sequence for eGFPmILY.

Expression and purification of eGFPmILY

eGFPmILY was expressed and purified by nickel-affinity chromatography. The purified protein was run on an SDS-PAGE gel and stained with Coomassie blue stain. A single protein band corresponding to approximately 35kDa was observed (Figure 4.6).



It was therefore likely that either premature transcriptional termination or proteolytic cleavage of the whole protein had occurred. A qualitative haemolytic assay was performed using the crude lysate on human and horse blood and the lysate was found to cause lysis only on human erythrocytes. Since a sufficient quantity of the mILY component was present to cause human-specific lysis, the truncated protein that was purified is most likely a result of proteolysis of eGFPmILY. From the size of the remaining fragment and the production of a fluorescent green protein and active mILY toxin, cleavage is most likely to have occurred at or around the junction between eGFP and mILY.

Construction of pET33bEGFPsILY

Owing to difficulties experienced with cleavage or instability of the eGFPmILY fusion protein, another fusion construct was made with a shortening of mILY at the N-terminus. Whereas mILY codes for residues E34-D532 of full-length ILY, short intermedilysin (sILY) codes for residues A60-D532 of ILY.

The eGFP cds was amplified from pET33bEGFPPLY by PCR and the sILY fragment was amplified from pET33bILY. PCR products were gel purified and an overlap PCR reaction was performed to join the two products. The resulting PCR product was digested with SpeI and SacI, ligated into NheI/SacI cut pET33b and the ligation reaction was transformed into TOP10 *E. coli*. The sequence of the insert was checked by DNA sequencing and no errors were found.

Construction of pET33bDel6EGFPsILY

A deletion mutation, termed $\Delta 6$ mILY (deletion of residues equivalent to A204 and R205 of ILY precursor) which is based on the $\Delta 6$ PLY deletion mutation previously described (Kirkham *et al.*, 2006b), was introduced to pET33bEGFPsILY by SDM (Stratagene Quikchange XL SDM kit). Construction of was checked by DNA sequencing.

Plasmid maps of pET33bEGFPsILY and pET33bDel6EGFPsILY are shown in Figure 4.7.

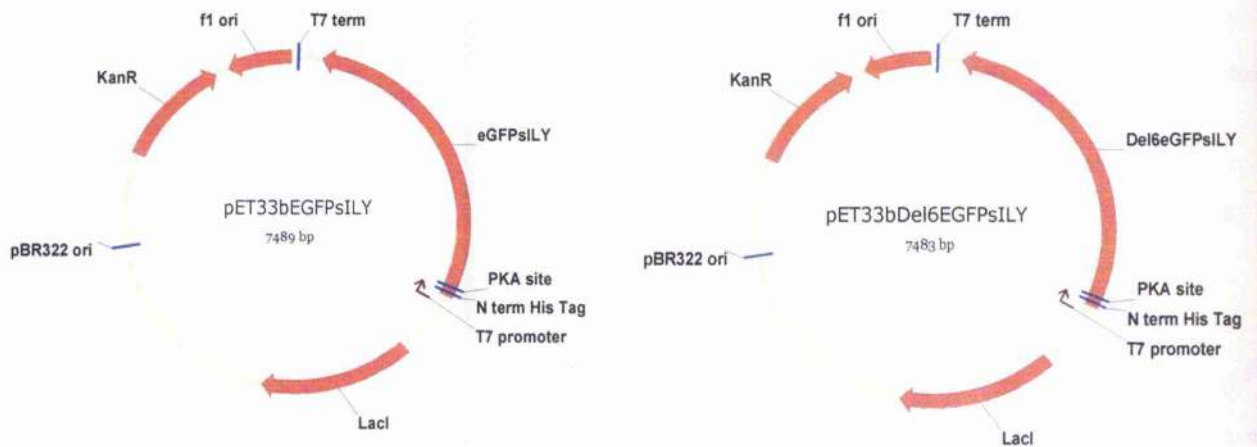


Figure 4.7: Plasmid maps of pET33bEGFPsILY and pET33bDel6EGFPsILY

Expression of eGFPsILY and Δ 6eGFPsILY

Recombinant eGFPsILY and Δ 6eGFPsILY were expressed and purified by nickel-affinity chromatography followed by anion exchange chromatography. Purified proteins were dialysed into PBS and Tris buffer as Tris-buffered eGFPsILY was required for collaborative work with UWCM Cardiff. Proteins were estimated by Coomassie-blue stained SDS-PAGE to be greater than 98% pure (Figure 4.8).

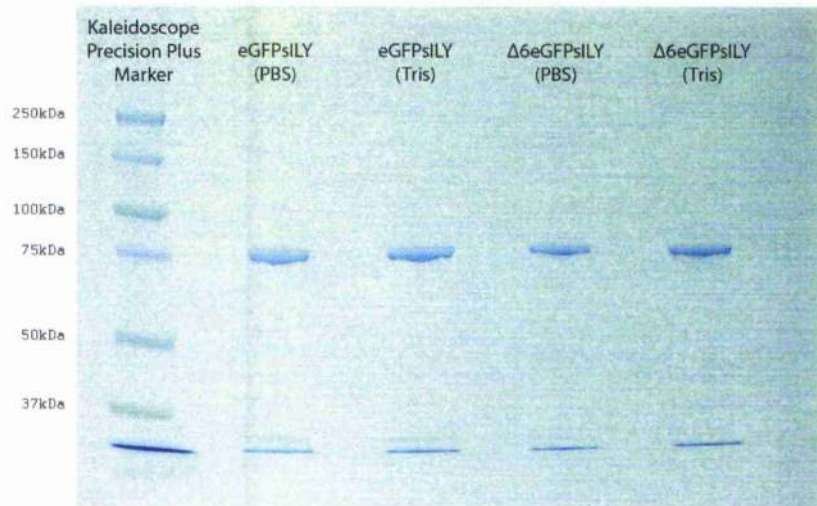


Figure 4.8: Coomassie-stained SDS-PAGE gel of eGFPsILY and $\Delta 6$ eGFPsILY in PBS or Tris buffer.

The haemolytic activities of mILY, eGFPsILY and $\Delta 6$ eGFPsILY were determined to investigate the effect of the addition of the eGFP tag (Figure 4.9). The specific activity of eGFPsILY (2.85×10^7 HU/M) in this assay was calculated to be slightly greater than that of the wild-type toxin, mILY (1.53×10^7 HU/M). $\Delta 6$ eGFPsILY was not haemolytic at concentrations up to 0.75mM.

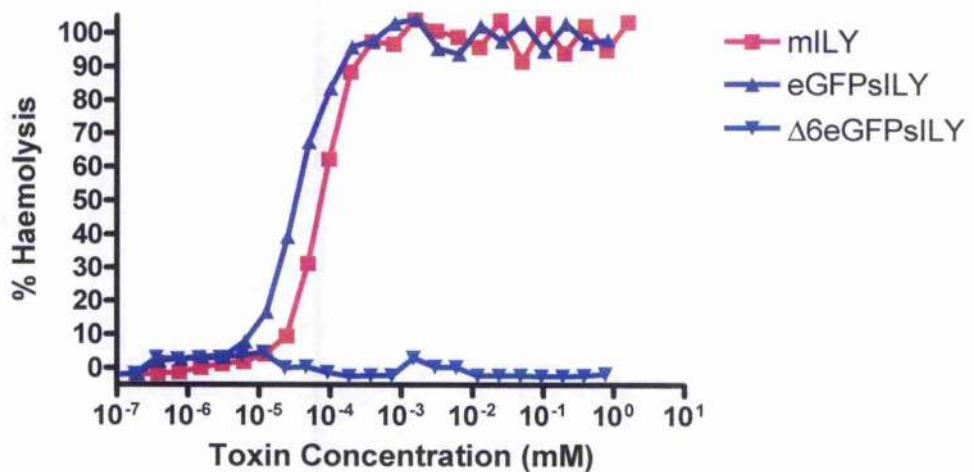


Figure 4.9: Haemolytic activities of mILY, eGFPsILY and $\Delta 6$ eGFPsILY

Laser scanning confocal fluorescence microscopy of eGFPsILY and Δ 6eGFPsILY binding to human and horse erythrocytes

Laser scanning confocal fluorescence microscopy was used to visualise the binding of eGFPsILY and Δ 6eGFPsILY to erythrocytes. Human or horse erythrocytes were treated with 700nM eGFPsILY, Δ 6eGFPsILY or eGFP and viewed by confocal fluorescence microscopy to determine whether the tagged toxins retained human cell binding specificities and could be used to detect cell binding by fluorescence microscopy.

eGFPsILY and Δ 6eGFPPLY both bound to the plasma membranes of human erythrocytes but neither bound to horse erythrocytes. eGFP alone did not bind to the plasma membrane of either human or horse erythrocytes.

eGFPsILY-treated human erythrocytes appeared very crumpled and folded. Membranes treated with Δ 6eGFPsILY retained a smoother membrane shape and overall rounded appearance, although they appeared to be distorted from the usual bi-concave shape of erythrocytes.

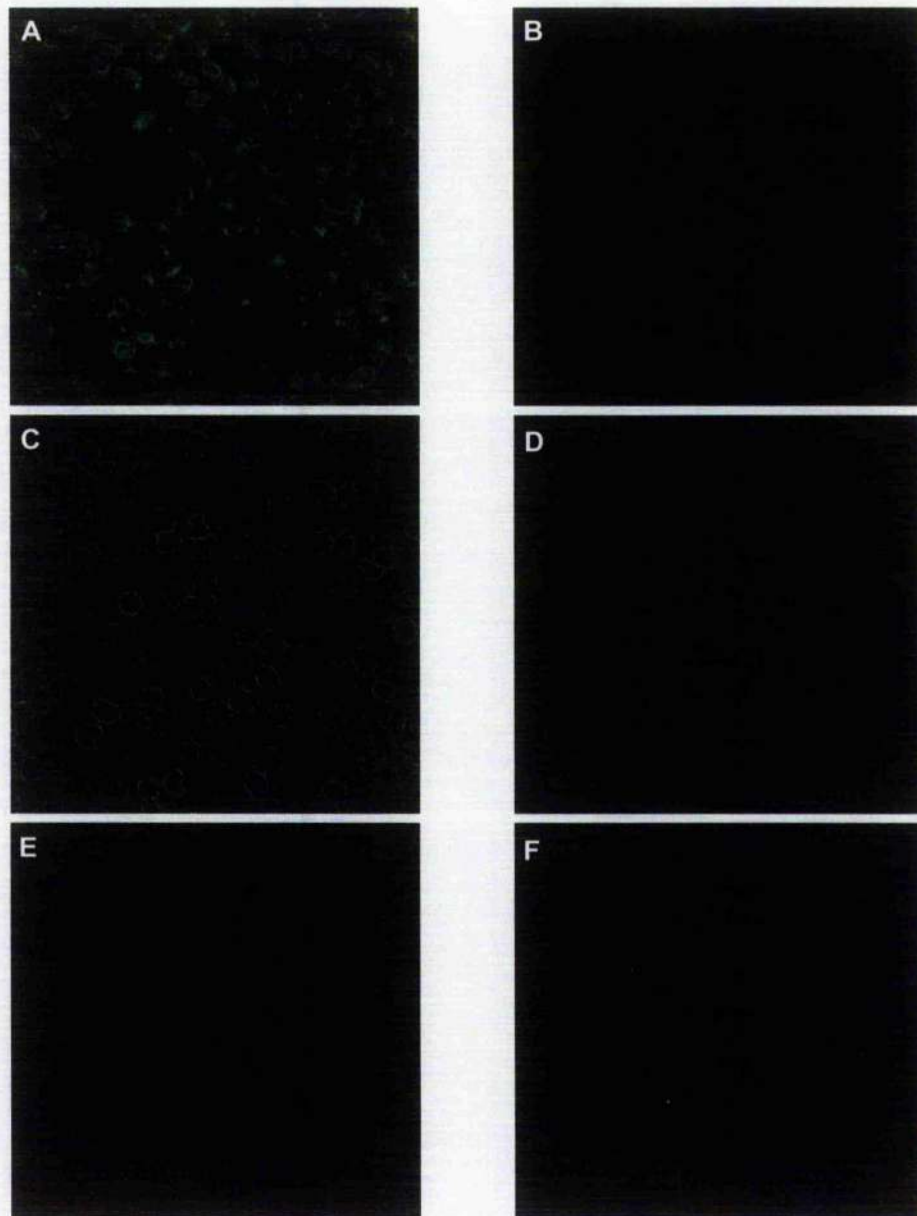


Figure 4.10: Laser scanning confocal microscopy of human and horse erythrocytes treated with eGFPsILY, $\Delta 6$ eGFPsILY or eGFP. Magnification x63 under oil immersion. Green channel (Ex. 488nm Em. BP 505-530nm) shows localisation of eGFP. Laser intensity and amplifier gain settings were the same for all images captured.

- A) Human erythrocytes + 700nM eGFPsILY
- B) Horse erythrocytes + 700nM eGFPsILY
- C) Human erythrocytes + 700nM $\Delta 6$ eGFPsILY
- D) Horse erythrocytes + 700nM $\Delta 6$ eGFPsILY
- E) Human erythrocytes + 700nM eGFP
- F) Horse erythrocytes + 700nM eGFP

Detection of eGFPsILY and $\Delta 6$ eGFPsILY binding to erythrocytes and U937 cells by flow cytometry

As a prelude to experiments to determine the cellular receptor of mILY, as alluded to further in the discussion section, a FACS-based cell binding assay was developed.

Human or horse erythrocytes were treated with eGFPsILY, $\Delta 6$ eGFPsILY, eGFP or mILY at concentrations of 0.7nM, 7nM and 70nM. Following incubation, the fluorescence of the erythrocytes was measured by flow cytometry using a FACScalibur flow cytometer on the FL-1 channel (Ex 488nM, Em 530nM) (Figure 4.11).

Human erythrocytes treated with eGFPsILY and $\Delta 6$ eGFPsILY showed an increase in fluorescence. The fluorescence increased with the concentration of toxin used in the assay. eGFPsILY and $\Delta 6$ eGFPsILY did not bind to horse erythrocytes as no increase in fluorescence was observed upon addition of the toxins to horse erythrocytes.

The range of fluorescence values for erythrocytes treated with eGFPsILY was greater than those for $\Delta 6$ eGFPsILY, resulting in a broader histogram profile. A similar profile was previously observed for eGFPPLY and $\Delta 6$ eGFPPLY (chapter 3) and this effect may be a result of lysis of the erythrocytes by eGFPsILY.

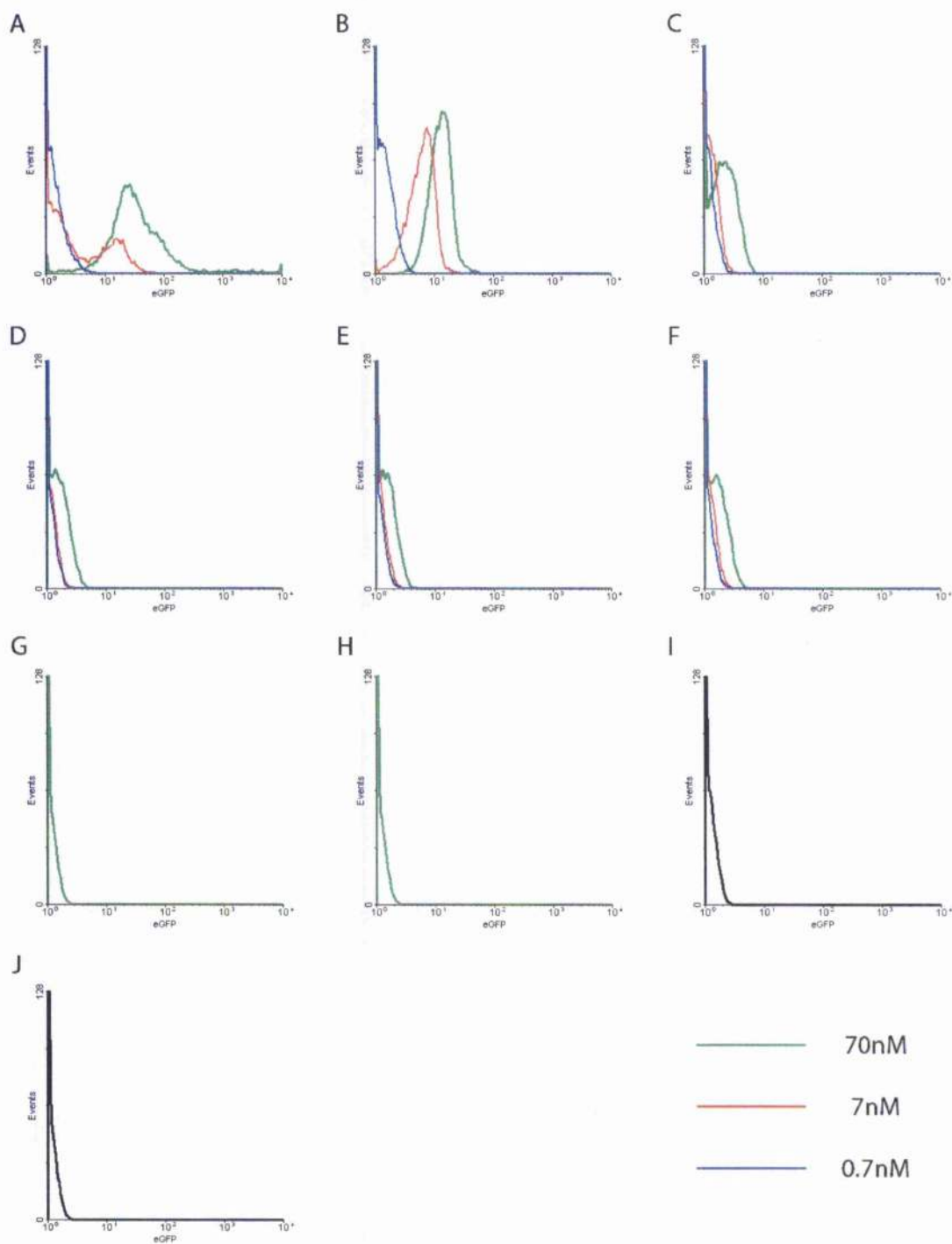


Figure 4.11: Flow cytometry analysis of eGFPsILY binding to human and horse erythrocytes. Histograms show fluorescence of human and horse erythrocyte membranes detected by flow cytometry FL-1 channel, (Excitation 488nm, Emission 530nm). A: eGFPsILY on human erythrocytes, B: $\Delta 6$ eGFPsILY on human erythrocytes, C: eGFP on human erythrocytes, D: eGFPsILY on horse erythrocytes. E: $\Delta 6$ eGFPsILY on horse erythrocytes F: eGFP on horse erythrocytes, G: mILY on human erythrocytes, H: mILY on horse erythrocytes, I: Untreated human erythrocytes, J: Untreated horse erythrocytes. Toxin/protein concentration is denoted by the colour of the histogram line; Green – 70nM, Red – 7nM, Blue - 0.7nM, Black - No toxin.

Construction of vectors for expression of mutants with small substitutions within domain 4 of PLY and ILY

To further resolve the region of the CDC responsible for determining promiscuity or human-specificity, a series of mutants of domain 4 within PLY or ILY were constructed. These mutations were designed to swap small regions of sequence between PLY and ILY. Mutations were introduced either by SDM or PCR-based mutagenesis according to the mutagenesis strategy indicated in Table 4.6. A diagram indicating the location of the mutations relative to the primary sequences of ILY and PLY is shown in Figure 4.12. Primers used are also indicated in Table 4.6.

Table 4.6: Design and creation of small substitution mutants of PLY and ILY

	Mutation	Primers	Mutagenesis strategy	Plasmid backbone
ILY Sub 1	mILY T481I	35K + 35S	SDM	pQE9mILY
ILY Sub 2	mILY L464T, I465V	35L + 35O	SDM	pQE9mILY
ILY Sub 3	mILY I447L, R448S	35M + 35N	SDM	pQE9mILY
ILY Sub 4	mILY S467E, N469T	35P + 35Q	SDM	pQE9mILY
ILY Sub 5	mILY P475R, Q476K, N478T	35R + 35T	SDM	pQE9mILY
ILY Sub 6	mILY H487Y	35U + 35V	SDM	pQE9mILY
ILY Sub 7	mILY F490V	35W + 35X	SDM	pQE9mILY
ILY Sub 8	mILY V451I, L452R, G453E, A454C	33C + 33D	SDM	pET33bmILY
ILY Sub 9	mILY P461W	32Y + 32Z	SDM	pET33bmILY
ILY Sub 10	mILY V495E, K496N, ΔN498, ΔT499, ΔD500	28W + 32U	PCR mutagenesis	pET33bmILY
ILY Sub 11	mILY R400Q	46Q + 46R	SDM	pQE9mILY
ILY Sub 12	mILY Y404T	46S + 46T	SDM	pQE9mILY
ILY Sub 13	mILY I418L R419T S420P R421K	46U + 46V	SDM	pQE9mILY
ILY Sub 14	mILY N429D R430L	46W + 46X	SDM	pQE9mILY
ILY Sub 15	mILY F440L	46Y + 46Z	SDM	pQE9mILY
PLY Sub 8	PLY I425V, R626L, E427G, C428A	33A + 33B	SDM	pET33bPLY
PLY Sub 9	PLY W433P	32W + 32X	SDM	pET33bPLY
PLY Sub 10	PLY E469V, N470K, (ins)472N, (ins)473T, (ins)474D	9Y + 32V	PCR mutagenesis	pET33bPLY

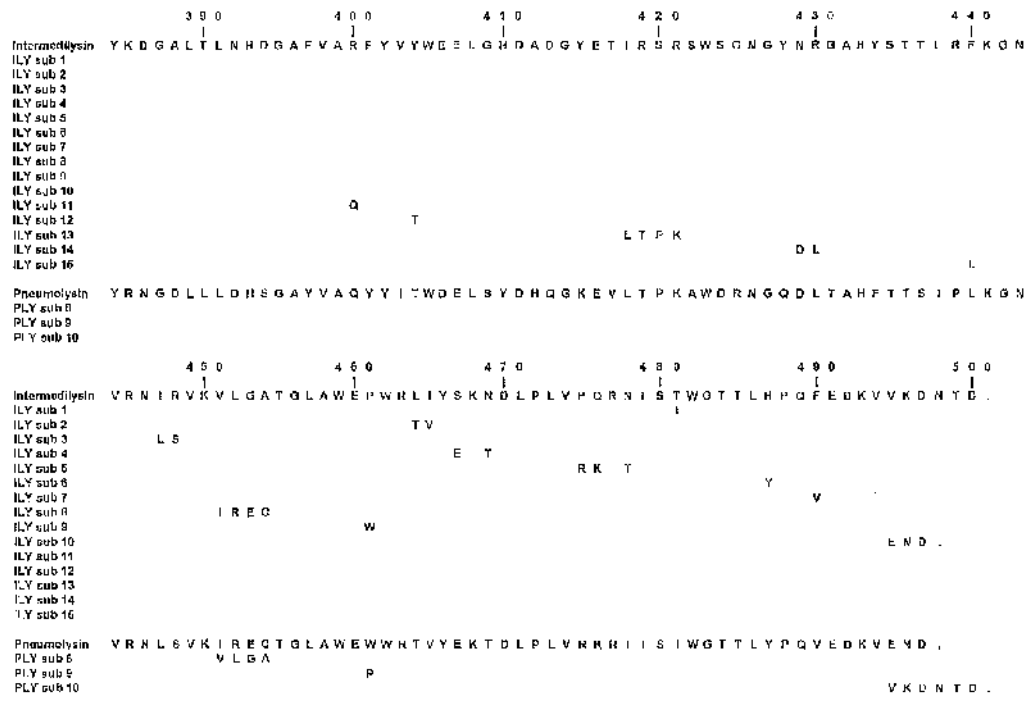


Figure 4.12: Diagram showing location of mutations of ILY and PLY present in ILY and PLY substitution mutants

Expression of toxin mutants with small substitutions within domain 4 of PLY and ILY

All small substitution mutants, in addition to ILY and PLY were purified by nickel-affinity chromatography. All proteins were run on an SDS-PAGE gel, Coomassie-stained and protein purities estimated to be greater than 95%.

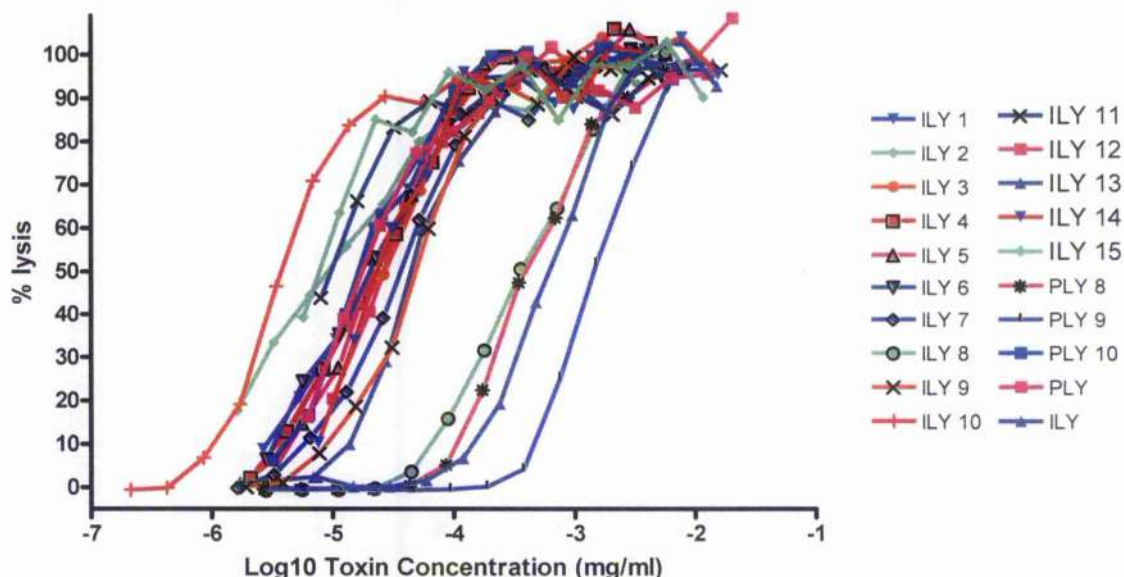
Haemolytic activity of toxin mutants with small substitutions within domain 4 of PLY and ILY

Haemolysis assays of all small substitution mutants, in addition to ILY and PLY, were performed on human erythrocytes to determine whether any of the mutants had reduced haemolytic activity (Figure 4.13). Most of the toxin mutants had similar activities to ILY and PLY, although ILY substitution 10 had the highest

recorded activity. Much reduced specific haemolytic activities were obtained for ILY sub 8, ILY sub 13, PLY sub 8 and PLY sub 9 (Figure 4.13).

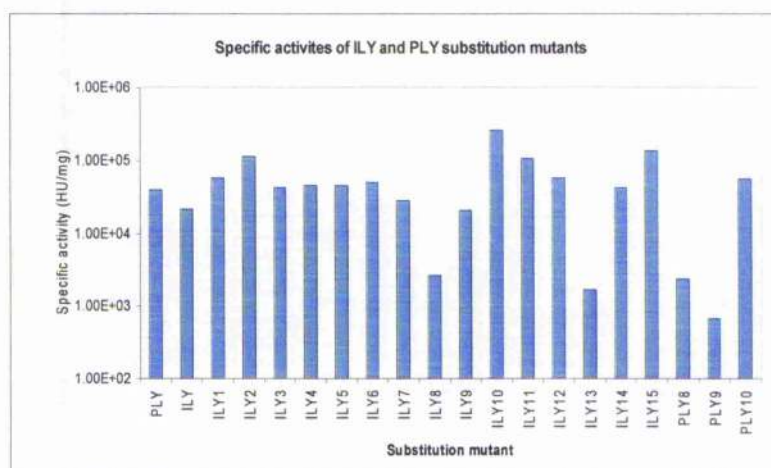
Figure 4.13: Haemolytic activity and calculates specific activities of ILY substitutions 1-15 and PLY substitutions 8-10 on human erythrocytes

Haemolytic activities of ILY substitutions 1-15 and PLY 8-10



Specific haemolytic activities of ILY and PLY substitution mutants

Toxin	Specific activity (HU/mg)
PLY	3.94 x 10 ⁴
ILY	2.13 x 10 ⁴
ILY1	5.82 x 10 ⁴
ILY2	1.13 x 10 ⁵
ILY3	4.17 x 10 ⁴
ILY4	4.56 x 10 ⁴
ILY5	4.60 x 10 ⁴
ILY6	5.06 x 10 ⁴
ILY7	2.79 x 10 ⁴
ILY8	2.62 x 10 ³
ILY9	2.11 x 10 ⁴
ILY10	2.60 x 10 ⁵
PLY8	2.39 x 10 ³
PLY9	6.74 x 10 ²
PLY10	5.63 x 10 ⁴
ILY11	1.05 x 10 ⁵
ILY12	5.77 x 10 ⁴
ILY13	1.66 x 10 ³
ILY14	4.23 x 10 ⁴
ILY15	1.36 x 10 ⁵



Measurement of CD59 binding activity by Surface Plasmon Resonance

Measurement of binding of the ILY and PLY substitution mutants was examined by surface plasmon resonance (SPR) to determine whether any of the mutants showed altered binding capability which might indicate that the mutated residues are important in binding to its cellular receptor, human CD59 (Giddings et al, 2004). This work was a collaboration with Prof Paul Morgan and Dr Tim Hughes from UWCM, Cardiff and the binding assay was performed by Dr Tim Hughes.

The binding of each of the ILY substitution mutants to thiol-coupled CD59 was assessed by surface plasmon resonance using a Biacore 3000. 40 μ l of each of the substitution mutants, as well as ILY and PLY were passed through the CM-5 thiol coupled CD59 sensor chip at 25 μ g/mL and the response difference was monitored over 5 minutes. The sensor chip was washed twice with two 10 μ l injections of 50mM NaOH prior to the injection of the next sample.

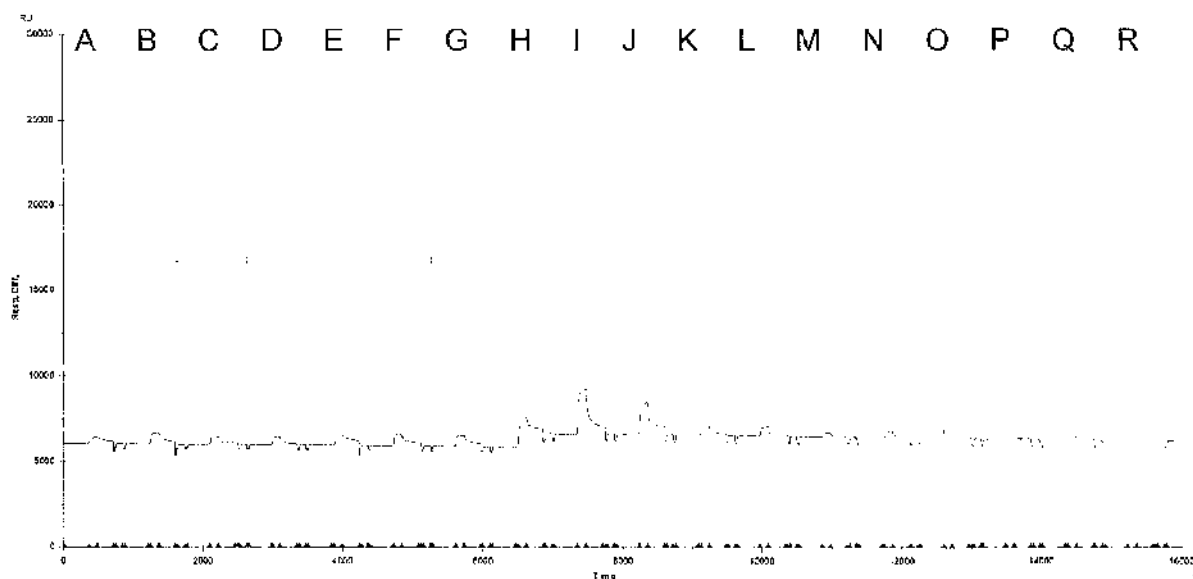


Figure 4.14: Biacore sensorgram for analysis of ILY and PLY substitution mutant binding to CD59. 40 μ l of each toxin was passed over a CD59-coated CM5 sensor chip at a concentration of 25 μ g/mL in the following sequence: A) ILY Sub 1, B) ILY Sub 2, C) ILY Sub 3, D) ILY Sub 4, E) ILY Sub 5, F) ILY Sub 6, G) ILY Sub 7, H) ILY Sub 8, I) ILY Sub 9 J) ILY Sub 10, K) ILY Sub 11, L) ILY Sub 12, M) ILY Sub 13, N) ILY Sub 14, O) ILY Sub 15, P) PLY Sub 8, Q) PLY Sub 9 and R) PLY Sub 10. Sensor gram shows response measurement for test flow cell with CD59-coupling (violet line), control flow cell without CD59-coupling (blue line) and subtraction of control from test flow cell values (black line).

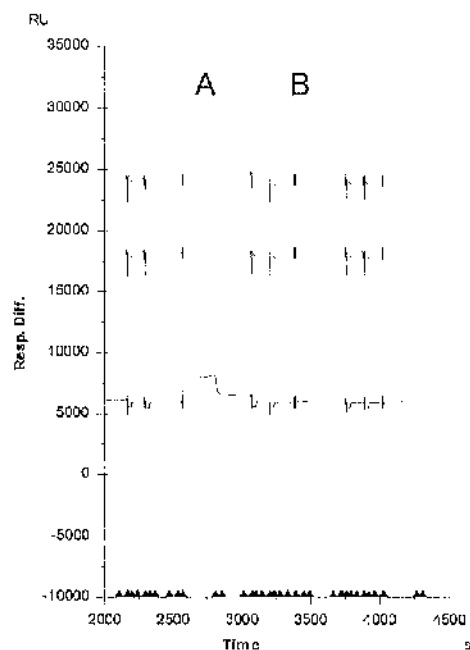


Figure 4.15: Biacore sensorgram analysis of ILY and PLY binding to CD59. 40 μ l of each toxin was passed over a CD59-coated CM5 sensor chip at a concentration of 25 μ g/mL in the following sequence: A) mILY, B) PLY Sensor gram shows response measurement for test flow cell with CD59-coupling (violet line), control flow cell without CD59-coupling (blue line) and subtraction of control from test flow cell values (black line).

Figure 4.14 and Figure 4.15 show that binding to CD59 was observed for ILY and all of the ILY substitution mutants, but was not observed for PLY or any of the PLY substitution mutants. The response obtained for the ILY and the mutants varied from 300 response units for ILY sub 13 up to 3000 response units for ILY sub 9. ILY yielded a response difference of 2100 response units. However, a number of the protein preparations appeared cloudy prior to assay and were centrifuged to remove any large protein aggregates present. It is highly likely that this would affect the binding response therefore these data cannot be used quantitatively. A number of the mutant proteins also bound very tightly to the chip and were not completely removed by the two sodium hydroxide washes between samples. If this was a specific binding event, this could affect the number of available sites for binding.

Discussion

Unlike the other CDCs described to date, the haemolytic activity of ILY is human-specific (Nagamune *et al.*, 1996). The initial study by Nagamune and colleagues did not identify which part of the intermedilysin molecule was involved in species restriction. In order to determine which region of ILY was responsible for human specificity, a bank of chimeric toxins were produced between ILY, which is human-specific and PLY, which has broad specificity. Crossover regions were selected to be at regions containing runs of amino acids identically conserved between PLY and ILY, as indicated in Figure 4.2.

Initially, chimeric toxins were purified using swell-gel Ni-NTA tablets. These tablets allowed rapid purification of small quantities of the toxins for characterisation of their species specificities.

All of the chimeric toxins that shared the C-terminal 56 residues of ILY were active on human erythrocytes, with the exception of chimera A, which has no haemolytic activity on human or horse erythrocytes. Similarly, all of the toxins carrying the C-terminal 53 residues of PLY had broad specificity, with the exception of chimera B which aggregated both human and horse erythrocytes. It can therefore be concluded that it is the 56 C-terminal residues of ILY that are responsible for human specificity and the 53 C-terminal residues of PLY are responsible for its promiscuity.

Chimera A and B were reciprocal swaps that crossed over within the conserved VPARMQYE motif. Interestingly, the aggregation of erythrocytes observed for chimera B is also a characteristic of a deletion mutant of this region - $\Delta 6$ PLY (Lea-ann Kirkham, PhD thesis) and this may signify that like the $\Delta 6$ mutant, chimera B can bind to cell but fails to form pore structures. It is possible that crossovers at this position suffer from steric clashes, folding problems or similar incompatibilities between the two sections of the toxins such that the considerable conformational change required (Tilley *et al.*, 2005) is restricted. However further work would be required to determine the reason for the lack of activity of these chimeras.

Chimeras G and H were purified by nickel-affinity purification using FPLC in order to yield larger quantities and more pure preparations for further study. The species specificities of chimeras G and H were the same as determined with the swell-gel purified chimeras – i.e. chimera G was human specific and chimera H had broad specificity. Both toxins had reduced activity on human erythrocytes when compared to ILY or PLY – chimeras G and H had 110-fold and 5-fold reduced activity compared to ILY. The specific activity of ILY was 5-fold lower than PLY, and this appears to be a result of an intrinsic lower activity of the toxin.

It is difficult to determine the reason for the greatly reduced activity of chimera G. It may indicate that only part of the receptor-binding site was transferred to the PLY backbone. Alternatively, if the entire site was transferred, perhaps the binding site is not folded in the optimal conformation due to incompatibilities between the two halves of domain four. There may be differences in the angle that domain 4 of ILY sits relative to the rest of the molecule (Polekhina *et al.*, 2005) and perhaps this is

incorrect in chimera G to allow optimal binding. The overall folding and shape of the molecule may simply be disrupted leading to inhibited binding or pore formation.

Erythrocyte ghost absorption assays were performed to determine whether the chimera cross-overs were species specific in their binding actions or whether specificity was determined at a later stage of the mode of action. Chimera G was inhibited by human erythrocyte ghosts but not rabbit erythrocyte ghosts, whereas chimera H was inhibited by both human and rabbit erythrocyte ghosts. This indicates that the human-specific action was a result of human-specific binding rather than a downstream process.

Nagamune et al showed that trypsin-treated erythrocytes were less susceptible to lysis by intermedilysin (Nagamune *et al.*, 1996). This effect was confirmed and further investigated here and it was found that susceptibility to intermedilysin reduced as trypsin treatment time increased. The control without trypsin was equally susceptible to ILY lysis as trypsinised erythrocytes to which trypsin inhibitor was added immediately. This confirmed that the inhibition was a result of the action of the enzyme on the erythrocytes and neither the presence of the trypsin nor trypsin inhibitor.

This study also investigated the effect of trypsinisation of PLY-mediated haemolysis and found that trypsinised cells were more susceptible to PLY. This may be due to greater access of the toxin to the cell membrane when surface proteins are cleaved, or possibly a reduction in stability of the membrane. The

maximum effect was reached within one hour suggesting that the proteins involved were cleaved quickly by trypsin.

Following this work and the suggestion that there was a protein receptor for ILY, a yeast-2-hybrid system was developed and used to screen for proteins capable of interacting with ILY. The screen used domain 4 of ILY fused to the DNA-binding domain of GAL-4 as the bait protein and a human brain cDNA library was the prey library. Greater than 2.4×10^8 transformants were screened and this was more than twice the recommended number to give full library coverage.

23 putative interacting proteins were identified, although only one was surface-expressed. As with all yeast-2-hybrid screens, the interactions need to be confirmed by other means and the biological-relevance examined before an interaction can be positively identified. During the course of this experiment, the receptor for ILY was identified as CD59 (Giddings *et al.*, 2003) and therefore further work was not carried out on these putative interacting proteins.

Production of eGFP-tagged intermedilysin

Another method of identification of the receptor for ILY was proposed and this required the production of a non-lytic and fluorescent-tagged form of ILY. The experiment involved transfecting a mouse tissue culture cell line with a human cDNA library and addition of the non-lytic, fluorescent ILY toxin. This would be expected to bind to transfected cells expressing the human cellular receptor for ILY and these cells could be selected using a FACS machine and the selected

clonal lines grown up. Plasmid recovery and DNA sequencing would then allow identification of the cellular receptor ILY.

Previously, eGFP-tagged forms of PLY and $\Delta 6$ PLY were produced (this thesis) and these were found to be easily detected by flow cytometry. The $\Delta 6$ PLY mutant was found to be a binding, non-lytic mutant of PLY (Kirkham *et al.*, 2006b) and eGFP tagged toxins were shown to be detectable by fluorescence microscopy and flow cytometry, therefore a similar strategy was employed for ILY.

An initial attempt to produce eGFP-tagged mature ILY (mILY) produced a purified protein of approximately 35kDa. This protein was fluorescent and was capable of binding to the His column to allow purification, and this suggests that the protein was susceptible to proteolytic cleavage. Cleavage between the eGFP and mILY portions would produce a protein of this approximate molecular weight. Another possible explanation was that premature transcriptional termination was occurring, however since human-specific haemolytic activity of a crude lysate was observed, this is unlikely. It was therefore concluded that proteolytic cleavage was likely to be occurring within the N-terminal region of ILY and therefore a shorter construct, eGFPsILY, was produced.

The N-terminal shortened form of ILY, sILY (short intermedilysin), is composed of residues A60-D532 of ILY. sILY contains the whole portion of ILY that corresponds to PLY in an amino acid alignment but the N terminal region which has no corresponding equivalent in PLY is removed.

eGFPsILY was found to have slightly higher specific haemolytic activity compared to ILY confirming that eGFP-tagging did not significantly alter the haemolytic activity of the toxin. The difference between the activities of the toxins is not any greater than that which can be observed between batches from the same toxin but it is not possible to determine whether there is any true difference in specific activity as a result of addition of the eGFP tag.

$\Delta 6$ eGFPsILY, a mutant form of eGFPsILY with a deletion of A204 R205 of ILY corresponding to those deleted in $\Delta 6$ PLY, was non-lytic. This confirmed that the mutation of these residues eliminated haemolytic activity as described for $\Delta 6$ PLY (Kirkham *et al.*, 2006b).

The degree of binding of eGFPsILY and $\Delta 6$ eGFPsILY to human and horse erythrocytes was measured by fluorescence microscopy and flow cytometry.

Laser scanning confocal microscopy revealed that both toxins could be visualised bound to the membranes of human erythrocytes but no binding was observed to horse erythrocytes. eGFP alone did not bind to human or horse erythrocyte membranes, indicating that no non-specific binding events were taking place and that the fluorescence of the human erythrocyte membranes was not a result of intrinsic autofluorescence. Human erythrocyte membranes treated with eGFPsILY appeared crumpled and folded, probably as a result of lysis of the cells. $\Delta 6$ eGFPsILY-treated human erythrocytes remained more smooth but their morphology appeared to have been slightly altered from the bi-concave shape typical of erythrocytes. This may be a result of the suspension buffer not being

isotonic for erythrocytes, physical pressure on slide preparation, or an action of the toxin.

Flow cytometry also confirmed that eGFPsILY and $\Delta 6$ eGFPsILY bound to human but not horse erythrocytes. Human erythrocyte fluorescence increased with the concentration of toxin added. The fluorescence increase upon addition of eGFPsILY and $\Delta 6$ eGFPsILY was less than that previously observed upon addition of eGFPPLY and $\Delta 6$ eGFPPLY. This could suggest that a lesser quantity of ILY is able to bind to erythrocytes than PLY, perhaps due to a lower availability of CD59 than for the receptor for PLY. However, we also cannot exclude the possibility that eGFPsILY may have a lower fluorescence per molar quantity as this would lead to the same result.

Since $\Delta 6$ eGFPsILY was confirmed to be a human-specific binding, non-lytic mutant of ILY, it is therefore a suitable reagent for use in a FACs-based assay to identify the receptor for ILY. As eluded to earlier, during the course of this experiment the cellular receptor for ILY was identified by another group (Giddings *et al.*, 2004) therefore the FACS-based screen was not completed.

A number of mutants with small substitutions in domain 4 of PLY and ILY were developed. These mutants were designed to mutate regions of difference between ILY and PLY to the sequence found in the other toxin. An abolition or reduction in activity of the substitutions made in ILY might indicate that the receptor binding site has been disrupted.

The haemolytic activities of all of the toxins on human erythrocytes was therefore measured. Most of the substitution mutants had similar specific activities compared with wild-type ILY and PLY. ILY sub 8, ILY sub 13, PLY sub 8 and PLY sub 9 were found to have drastically reduced activities compared with the other toxins.

The activities of the toxins having 'similar' activities to the wild-type were spread over an approximately 10-fold range of toxin concentrations. The activity of PLY was greater than ILY in this assay and may be true differences between the activities of the toxins. However, the accuracy of this assay is likely to be influenced by the purity of the toxins and the proportion of fully active/non-denatured toxin in the preparation. In addition to this, variation may occur as a result of aggregation of these proteins in solution. The samples used for haemolytic assay were centrifuged prior to use to check for aggregation, however it is possible that this was insufficient to eliminate micro-aggregation that may have occurred prior to more noticeable aggregation and this could have an effect on haemolytic activity. All preparations were purified twice and the same pattern of haemolysis was observed with the same pattern of specific activities but with a similar spread of data.

It is not possible to state from the results whether the reduced haemolytic activities observed for ILY sub 8, ILY sub 13, PLY sub 8 and PLY sub 9 were a result of alteration of residues important in cell binding or pore formation, or a result of differences in the structure / stability of the overall toxin molecule. It is also not clear whether differences in binding affinity would lead to variation of the endpoint

of a haemolytic assay, or if any affinity of binding would be sufficient to allow subsequent steps in pore formation to take place.

In order to investigate whether the binding affinities of any of the mutants were altered from the wild-type toxin, CD59 binding was measured by surface plasmon resonance (SPR) using sensor chip coated with CD59. SPR revealed that ILY and all of the ILY mutants bound to CD59 but PLY and the PLY-based substitution mutants did not bind CD59. It is therefore likely that CD59-binding ability has not been introduced to the PLY mutants or entirely abolished from any of the ILY substitution mutants. It is interesting that the lowest binding activity measures was for ILY sub 13, which had the lowest specific activity. However, due to problems with protein aggregation, quantitative results can not be obtained from this assay.

This assay should be repeated using newly purified protein preparations, and better stability may be obtained using an alternative buffer. Proteins should be checked for aggregation using techniques such as dynamic light scattering or analytical ultracentrifugation prior to repeat of the binding assay. If aggregation remains a problem, it may be beneficial to pass the preparation through a gel filtration column immediately prior to assay.

Chapter 5: Immunisation studies with Anthrolysin O, the CDC from *Bacillus anthracis*

Summary

Anthrolysin O (ALO) is a toxin produced by *Bacillus anthracis*, the causative agent of anthrax. It is a member of the cholesterol-dependent cytolysin (CDC) group of toxins, many of which are potential vaccine candidates that protect against their producing organisms. Pore formation by ALO was studied by transmission electron microscopy and pores were found to be consistent with those formed by other members of this toxin family. We constructed and characterised a novel genetic toxoid of anthrolysin O, $\Delta 6mALO$, which was able to bind to cells but was incapable of pore-formation or haemolysis. The capacity of the haemolytic and non-haemolytic forms of ALO to protect against challenge with the toxin or *B. anthracis* was determined. Immunisation with both active and non-haemolytic forms of ALO elicited protection against lethal i.v. challenge with ALO but neither was protective against *B. anthracis* in a murine i.p. challenge model. Immunisation with another CDC, pneumolysin, did not confer cross-protection against challenge with ALO. Histopathological investigation following lethal i.v. challenge with ALO revealed acute pathology in the lungs with occlusion of alveolar vessels by fibrin deposits.

Introduction

Bacillus anthracis is a Gram-positive spore-forming bacillus that is the causative agent of anthrax. Primarily a disease endemic to herbivores, anthrax can also affect humans, most often through contact with infected animals or their products. The disease is classified as cutaneous, gastrointestinal or inhalational anthrax according to the route of infection. While fatality rates from cutaneous anthrax are less than 1% with antibiotic treatment, they are extremely high for gastrointestinal and inhalational forms of the disease as infections have often progressed too far for treatments to be effective (Oncu *et al.*, 2003).

Two major virulence determinants of *B. anthracis* have been well characterised; an anti-phagocytic poly-D-glutamic acid capsule that is encoded on plasmid pX02 and two toxins, lethal factor (LF) and edema factor (EF), encoded on plasmid pX01. These enzymatic toxins are translocated across the cell membrane by a third bacterial protein, protective antigen (PA), and interfere with host cell signalling pathways (Duesbery *et al.*, 1998; Leppla, 1982). The toxins are responsible for much of the acute pathology of anthrax and LF and EF, in combination with PA, are capable of causing many of the clinical signs associated with the disease (Fish *et al.*, 1968; Klein *et al.*, 1962).

During inhalation anthrax, *B. anthracis* spores are phagocytosed by alveolar macrophages which transport the bacterium across the alveolar barrier upon migration to the lymph nodes (Guidi-Rontani *et al.*, 1999). The spores then germinate within the phagolysosome of the macrophage, and escape from the

macrophage allowing the bacterium to proliferate within the bloodstream. The role of the LF and EF in release from the macrophage is unclear and contradictory results have been obtained as to whether expression of these toxins is linked to loss of macrophage viability and survival of the germinated bacterium (Dixon *et al.*, 2000; Guidi-Rontani *et al.*, 2001).

There is also evidence for the presence of chromosomally-located virulence factors since strains of *B. anthracis* cured of both plasmids (pXO1, pXO2) retain some virulence in mice (Fouet *et al.*, 1995). A gene encoding Anthrolysin O (ALO), a member of the family of cholesterol-dependent cytolysins (CDCs), was recently discovered in the genome sequence of *B. anthracis* Ames (Read *et al.*, 2003). Many other members of this toxin family have been shown to be virulence factors of their producing organisms (Awad *et al.*, 2001; Cossart *et al.*, 1989; Jost *et al.*, 1999; Rubins *et al.*, 1995) and it has been proposed that ALO may have a role in the virulence of *B. anthracis* (Shannon *et al.*, 2003; Wei *et al.*, 2005). ALO is secreted in an active form by *B. anthracis* Sterne and was shown to be inhibited by cholesterol, a characteristic of many members of the CDC family (Shannon *et al.*, 2003). ALO has been shown to activate Toll-like receptor 4 leading to induction of macrophage apoptosis in combination with LF (Park *et al.*, 2004).

Another Gram-positive pathogen which is capable of phagosomal escape within the macrophage is *Listeria monocytogenes*. This activity is a result of the combined effects of listeriolysin O (LLO), phosphatidylinositol-specific phospholipase C (PI-PLC) and phosphatidylcholine phospholipase C (PC-PLC) (Camilli *et al.*, 1993; Gedde *et al.*, 2000; Portnoy *et al.*, 1992). In addition to a

homolog of LLO, homologs of the PI-PLC and PC-PLC genes of *L. monocytogenes* are also present in *B. anthracis* (Read *et al.*, 2003). Given the similar requirement of *B. anthracis* for escape from the phagosome of macrophages, it is possible that ALO plays a role in the disruption of the phagosomal and/or plasma membranes. Recombinant strains of *L. monocytogenes* expressing anthrolysin O were capable of escape from the phagocytic vacuole but unlike LLO also damaged the plasma membrane of the cell (Wei *et al.*, 2005).

Immunisation with liposome-encapsulated LLO has been shown to induce protective immunity against *L. monocytogenes* (Tanabe *et al.*, 1999), and a number of other members of the CDC family, or peptides and genetic toxoids derived from them, have been shown to protect against infection with their producing organisms (Jacobs *et al.*, 1994; Jost *et al.*, 2003; Kirkham *et al.*, 2006b; Paton *et al.*, 1983).

Based upon these previous studies and the potential for the involvement of ALO in the pathogenicity of *B. anthracis* we have investigated the capacity of immunisation with mature ALO (mALO) or a novel genetic toxoid, $\Delta 6mALO$, to protect against challenge with mALO or *B. anthracis* in a murine model. Another member of the CDC family, pneumolysin (PLY), was included in the study to investigate whether other members of the CDCs could induce cross-protection against ALO.

Results

Construction of plasmid vectors

A 2433bp DNA fragment containing the coding sequence for anthrolysin O and upstream and downstream regions was amplified by PCR from *B. anthracis* Ames genomic DNA and transformed into pCR2.1-TOPO. This initial cloning step was done by Prof. R. Titball, DSTL. The coding sequence for mature anthrolysin O (mALO), which is composed of residues E35-H512 of ALO such that the putative signal sequence has been removed, was amplified by PCR and cloned into pET33b. The resulting plasmid is referred to as pET33b-mALO. Primers were designed so that the fragment would in frame with the N-terminal His-tag and the C-terminal His-tag in the vector is not expressed.

A deletion mutation of ALO named $\Delta 6$ mALO was then produced. This mutant is based on the $\Delta 6$ PLY mutation described by Kirkham and colleagues (Kirkham *et al.*, 2006b). Residues A156 and R157 of mALO (corresponding to A190 R191 of ALO) were deleted in pET33b-mALO at by site directed mutagenesis to form pET33b- $\Delta 6$ mALO.

All pET33b-based plasmids were transformed into BL21(DE3) *E. coli* for protein expression.

The construction of all plasmids was confirmed by DNA sequencing. A silent mutation, T>C at position 1227 of mALO was found to be present.

$\Delta 6$ mALO is non-haemolytic but retains binding activity

A mutant of mALO with a deletion of amino acid residues A156 and R157 was constructed. This mutant, named $\Delta 6$ mALO, was based on $\Delta 6$ PLY where the deletion of two corresponding amino acid residues of PLY abolished the haemolytic activity of the protein (Kirkham *et al.*, 2006b). $\Delta 6$ mALO was characterised to determine whether this mutant possessed similar toxoided properties to those of $\Delta 6$ PLY.

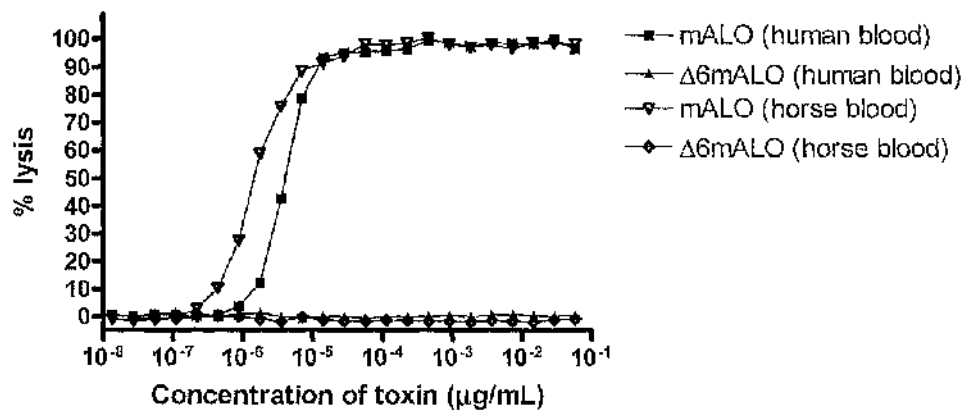


Figure 5.1: Haemolysis assay of purified mALO and $\Delta 6$ mALO toxins on human and horse erythrocytes.

The specific activities of recombinant mALO and $\Delta 6$ mALO proteins on human and horse erythrocytes were measured by haemolysis assay (Figure 5.1). mALO was lytic to both human and horse erythrocytes, with specific activities of 6×10^5 and 3.3×10^5 HU mg^{-1} , respectively. No lysis was detected on human or horse erythrocytes treated with $\Delta 6$ mALO at concentrations up to 0.1mg/ml.

The ability of mALO and $\Delta 6$ mALO to bind to human erythrocyte membranes was determined by erythrocyte binding assay (Figure 5.2). Both toxins bound to human

erythrocyte membranes. For mALO, most of the recovered toxin was in a very high molecular weight state consistent with oligomers produced upon pore formation, with a small proportion of a lower molecular weight corresponding to the size of the toxin in the monomeric state. For $\Delta 6$ mALO, no high molecular weight species was present and all of the recovered toxin corresponded to the molecular weight of monomeric toxin.

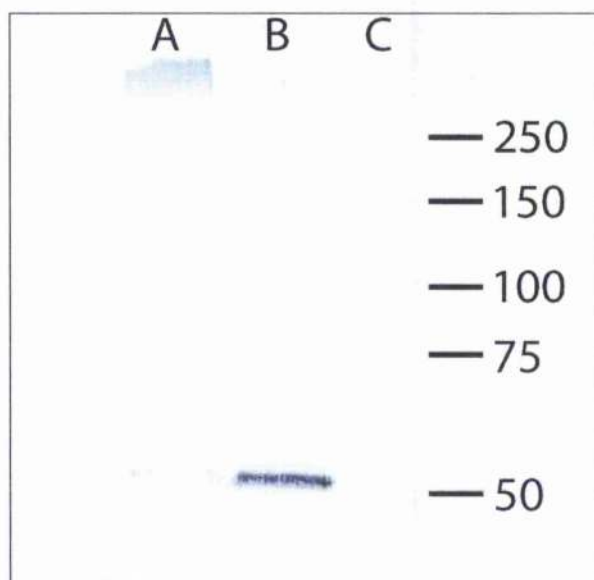


Figure 5.2: Binding assay of mALO and $\Delta 6$ mALO to human erythrocytes. Erythrocyte membranes were treated with A) 4 μ g/mL mALO B) 4 μ g/mL $\Delta 6$ mALO C) PBS and incubated for 10 minutes at 37°C. Membranes were washed in PBS, the pellet was resuspended in SDS-PAGE sample buffer and samples were run on an SDS-PAGE gel. Proteins were transferred to a nitrocellulose membrane and an immunoblot was performed using anti-mALO antiserum from mice as the primary antibody (1:1000 dilution) and anti-mouse IgG HRP-linked secondary antibody (1:2000 dilution).

Electron microscopy of erythrocyte membranes treated with mALO and $\Delta 6$ mALO

Human erythrocyte membranes treated with mALO and $\Delta 6$ mALO were negative stained and examined by transmission electron microscopy (Figure 5.3). Pores were visualised on membranes treated with mALO but no pores were visible on membranes treated with $\Delta 6$ mALO. For mALO pores, the mean inner pore

diameter was measured to be $26.1\text{nm} \pm 0.8\text{nm}$ with a ring width of $6.4 \pm 0.4\text{nm}$ ($n=20$, mean $\pm 95\%$ confidence interval).

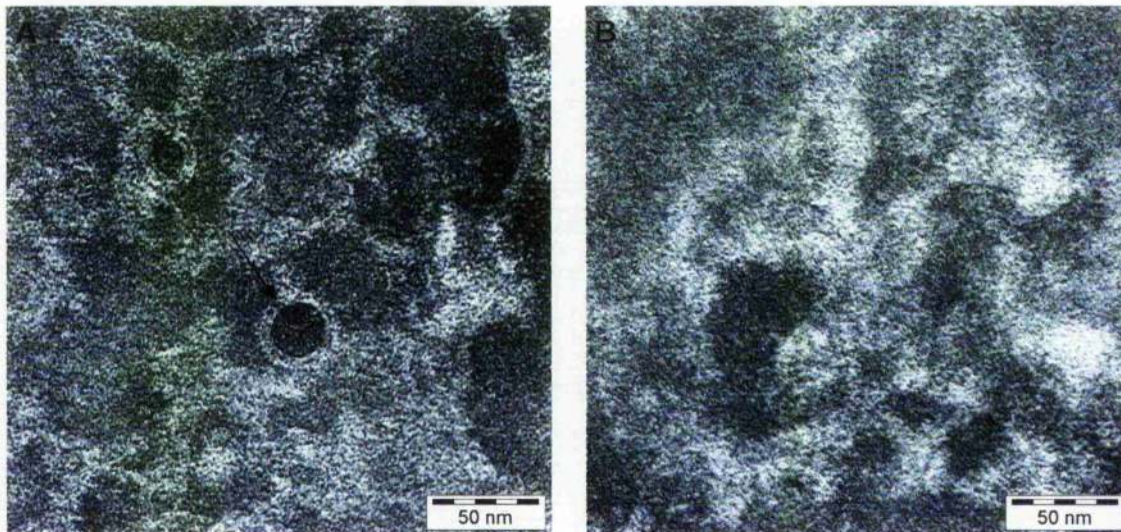


Figure 5.3: Transmission electron micrographs of human erythrocyte ghost membranes treated with A) mALO and B) $\Delta 6\text{mALO}$ visualised by negative staining with uranyl formate. Pores were observed on mALO treated membranes (arrow).

Determination of the toxicity of mALO to A/J mice

In order to determine the toxicity of anthrolysin O *in vivo*, groups of female A/J mice were challenged i.v. with doses of between $0.1\text{-}5\mu\text{g}$ mALO. All mice in the group treated with $0.1\mu\text{g}$ mALO survived, whereas no mice survived in the group treated with $5\mu\text{g}$ mALO (Figure 5.4). The experimental LD_{50} was calculated by interpolation to be 0.7 mg , equivalent to 35mg kg^{-1} . In most cases where treatment was terminal, fatality occurred within minutes of injection.

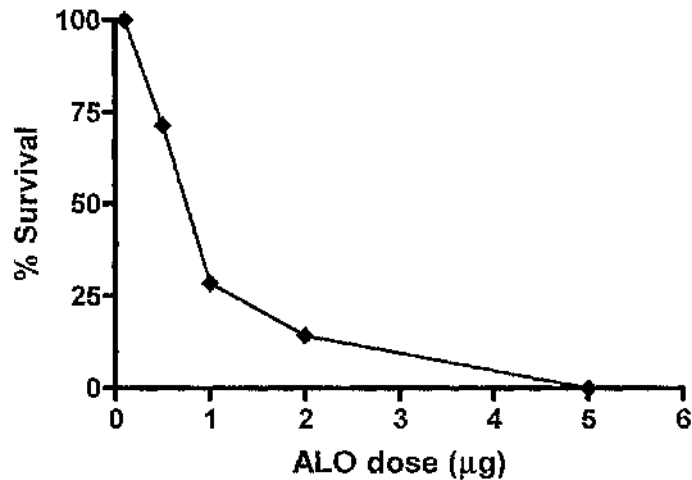


Figure 5.4: Survival of A/J mice after i.v. challenge with different concentrations of mALO toxin.

Histopathological investigation of mice lethally challenged with Anthrolysin

O

Spleen, heart, kidney, liver and lung tissues from 2 mice that died immediately from i.v. challenge with 1µg mALO, and a naïve control mouse, were examined histologically. Examination of the lung sections from the mice challenged with mALO revealed multifocal intravascular fibrin deposition with alveolar congestion and oedema (Figure 5.5). Many small to medium sized pulmonary vessels were fully occluded by thrombi. Vessels of an untreated mouse lacked fibrin thrombi. Examination of the other tissues of the mALO challenged mice revealed minimal pathology in these cases of peracute mortality.

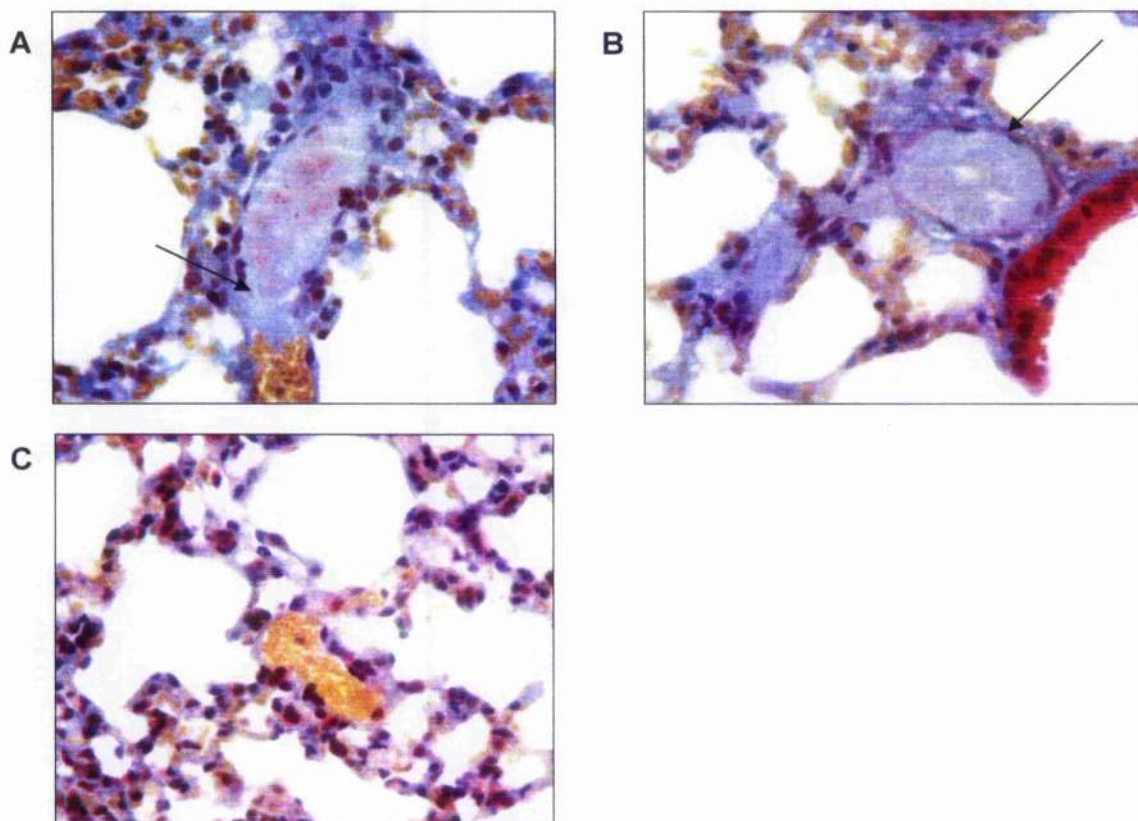


Figure 5.5: Light microscopy of histological sections of lungs taken from mice lethally challenged with mALO or a naïve control mouse. Sections were stained with Martius Yellow-Brilliant Crystal Scarlet-Soluble Blue (MSB) stain. RBCs are yellow, new fibrin is orange/red and older fibrin is blue, muscle is paler red, collagen is blue, and epithelial cells stain with a bright red appearance. Magnification 400x.

A) Mouse 1: Fibrin-occluded vessel (arrow) at the junction with patent vasculature containing red blood cells.

B) Mouse 2: Occlusion of vascular lumen by an acellular thrombus (arrow).

C) Control Mouse: Normal lung with patent vessel containing (yellow) red blood cells.

Determination of the effect of immunisation with mALO, $\Delta 6$ mALO and PLY against challenge with the mALO toxin

Groups of A/J mice were immunised with the mALO, $\Delta 6$ mALO, or PLY antigens with adjuvant, and control groups were administered adjuvant alone or left untreated. Anti-mALO and anti-PLY IgG levels were determined by ELISA from sample bleeds taken from all mice 9 days prior to challenge with mALO (Figure 5.6). High anti-mALO IgG titres were present in the sera from groups immunised with mALO and $\Delta 6$ mALO but 100-fold lower levels were detected in the group immunised with PLY. Anti-PLY titres were high in groups immunised with mALO and PLY but were 100 fold lower in groups immunised with $\Delta 6$ mALO.

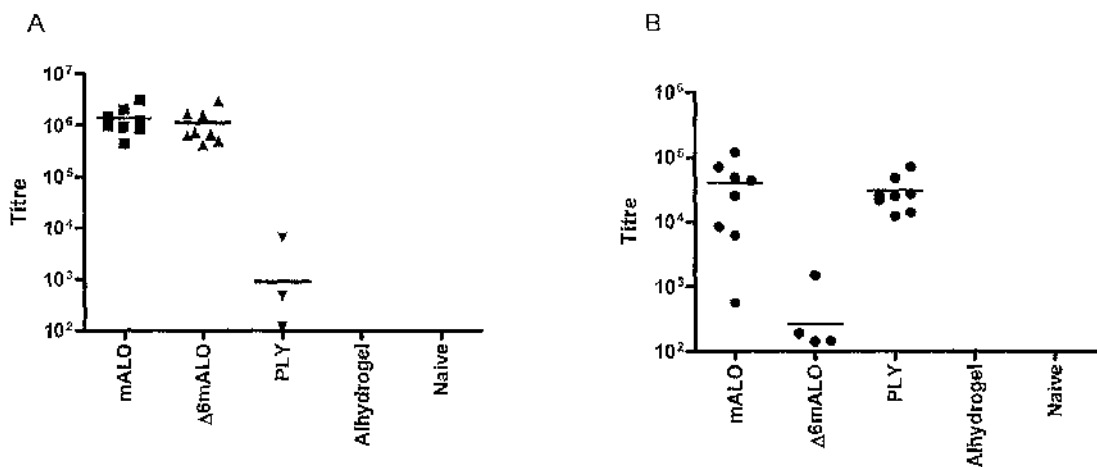


Figure 5.6: Anti-mALO (A) and anti-PLY (B) ELISAs showing titres (1/dilution of serum giving A_{540} of 0.3) of anti-mALO IgG antibody detected for each immunised group of animals subsequently challenged with mALO (n=8 for each group). Horizontal bar denotes mean titre.

Toxin neutralising activity was measured using serum neutralisation assays of mALO and PLY activity with pooled serum from each of the immunisation groups (Figure 5.7). Serum from groups immunised with mALO and $\Delta 6$ mALO had 10-fold greater capacity for neutralisation of mALO activity than PLY immunised serum or the control groups.

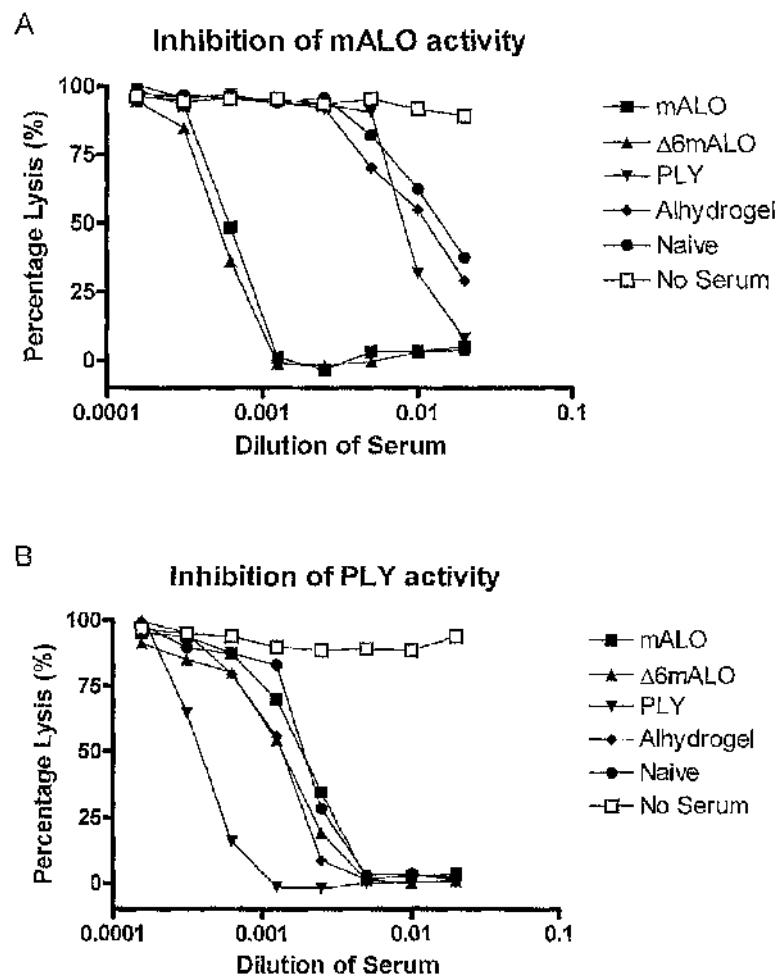


Figure 5.7: Neutralisation of A) mALO or B) PLY activity by pooled sera from each immunised group.

Serum from the PLY immunised group neutralised the activity of PLY to the greatest extent and this was similar to the extent of neutralisation of mALO by the mALO immunised group serum. The background level of neutralisation by naïve serum in the PLY neutralising assay was greater than for the mALO neutralising activity. Levels of PLY neutralisation by the serum from ALO and $\Delta 6$ mALO vaccinated groups were similar to that of the naïve control group.

In order to determine the level of protection afforded by immunisation with mALO, $\Delta 6$ mALO and PLY to lethal challenge with the mALO toxin, the immunised mice were challenged i.v. with 5 μ g mALO.

All of the mice immunised with mALO or $\Delta 6$ mALO survived whereas none of the mice in the groups immunised with PLY, adjuvant alone or in the naïve group survived (Figure 5.8).

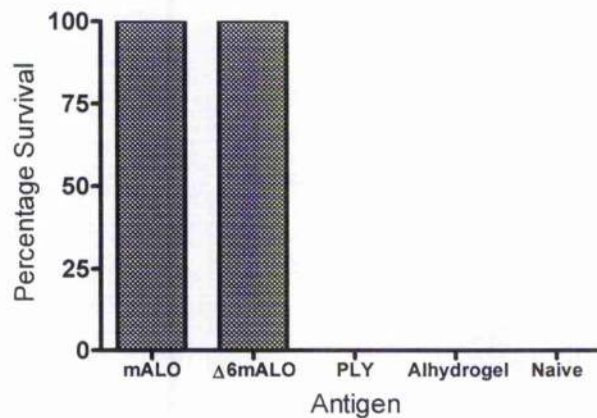


Figure 5.8: Survival of mice immunised with mALO, $\Delta 6$ mALO, PLY or adjuvant alone after challenge with mALO. Survival expressed as percentage of mice surviving 14 days after challenge (n=8 for each group).

Evaluation of the protection afforded by immunisation with mALO, Δ 6mALO and PLY against challenge with *B. anthracis* spores

To investigate whether immunisation with mALO protected against challenge with *B. anthracis* spores, groups of female A/J mice were immunised i.p. with mALO, Δ 6mALO, PLY or rPA, then infected with *B. anthracis* STI spores. Adjuvant-only and naïve groups were also included. Complete protection was afforded to all mice immunised with rPA but no protection was afforded to the mice immunised with ALO, Δ 6mALO, PLY, or the control groups (Figure 5.9).

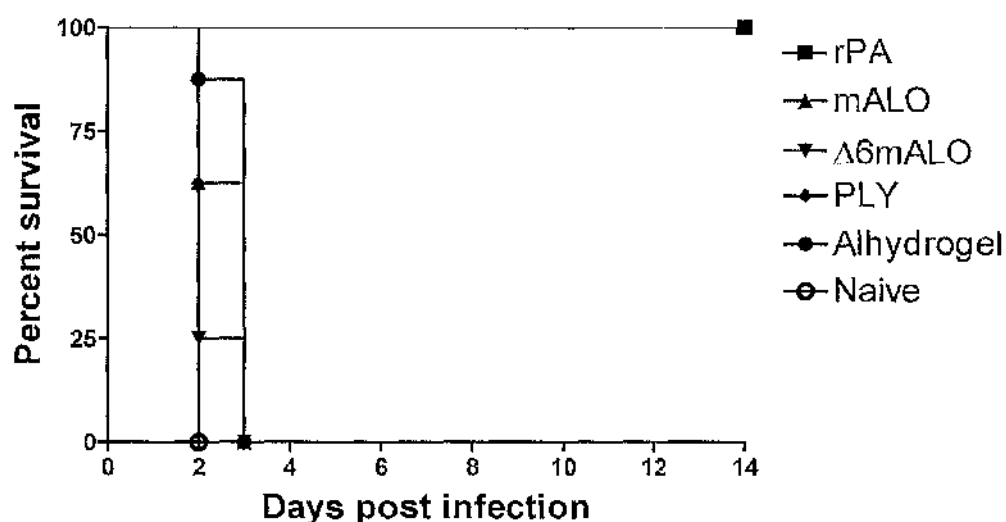


Figure 5.9: Survival of immunised A/J mice following i.p. challenge with 10^5 *B. anthracis* strain STI spores.

Sample bleeds were obtained from all mice 8 days prior to challenge to confirm that a response to the antigens was produced. The levels of anti-mALO IgG were determined by ELISA and very high titres of anti-mALO IgG were detected in the sera from groups immunised with mALO and Δ 6mALO (Figure 5.10). The level of anti-mALO IgG detected for the group immunised with PLY was greater than three

orders of magnitude lower although this was still higher than that of adjuvant-only or naïve groups.

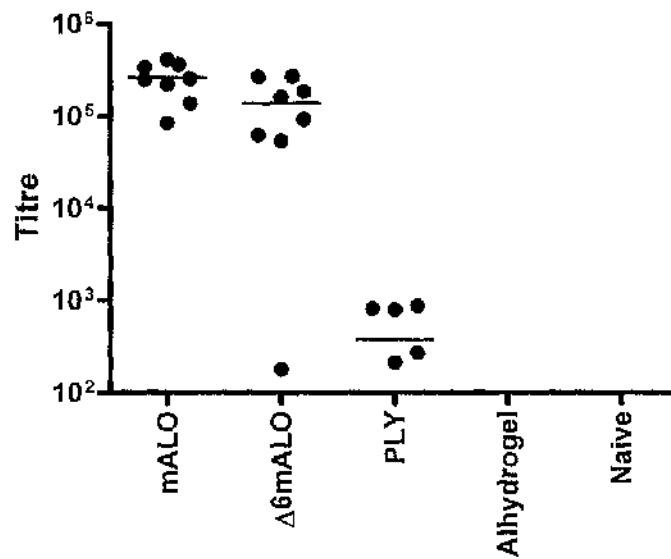


Figure 5.10: Determination of levels of anti-mALO IgG in sera from groups of mice immunised with mALO, Δ6mALO, PLY and adjuvant, prior to challenge with *B. anthracis*. Horizontal bar denotes mean titre.

Discussion

In this study, a mutant version of mALO was created with a double amino acid deletion at the predicted domain 1 / domain 3 interface. This mutant protein was termed $\Delta 6$ mALO after $\Delta 6$ PLY, a non-haemolytic mutant with a double deletion of the corresponding residues of PLY (Kirkham *et al.*, 2006b). The haemolytic activities of mALO and $\Delta 6$ mALO were measured to determine whether $\Delta 6$ mALO was similarly non-haemolytic. mALO was lytic to human erythrocytes but no haemolytic activity was detected for the $\Delta 6$ mALO mutant on either human or horse erythrocytes, even at greater than 10000 fold higher concentration than that required to produce pores with mALO.

Members of the cholesterol-dependent cytolysin group typically produce pores on erythrocyte membranes that can be visualised by transmission electron microscopy (Sekiya *et al.*, 1993; Sekiya *et al.*, 1998). Human erythrocyte membranes treated with the wild-type and mutant toxins were examined by TEM to ascertain whether pores produced by ALO were typical of those of other members of the family of cholesterol-dependent cytolysins, and whether the $\Delta 6$ mALO mutant protein was capable of forming pore structures. Pores were observed on human erythrocytes treated with mALO and these were similar in appearance to those produced on membranes treated with PLY and those produced by other CDCs. The mean inner pore diameter was estimated to be 26.1nm, which lies within the range of pore sizes described for other CDCs (Bhakdi *et al.*, 1985; Mitsui *et al.*, 1979; Morgan *et al.*, 1995; Sekiya *et al.*, 1993; Sekiya *et al.*, 1998). Pores were not observed on membranes treated with the

$\Delta 6\text{mALO}$ mutant toxin and this agrees with work previously performed using a mutant of PLY carrying the same mutation, $\Delta 6\text{PLY}$ (Kirkham *et al.*, 2006b).

Since $\Delta 6\text{mALO}$ had been shown to be non-haemolytic and non-pore-forming, a binding assay was used to determine whether it was capable of binding to erythrocytes. mALO was shown to bind to erythrocytes with two band sizes; one of very high molecular weight and one of a lower molecular weight of approximately 56 kDa, corresponding to the size of monomeric mALO .

It has previously been shown for PFO that pores can maintain their oligomeric state after treatment with SDS (Shepard *et al.*, 2000) and the larger species may therefore be mALO pores. In work by Bhakdi and colleagues (Bhakdi *et al.*, 1985), SLO binding to membranes was detected by SDS-PAGE but the protein ran at the size corresponding to the monomeric molecular weight. It is likely that SDS-PAGE techniques differed from this work as here samples were only heated to 70°C rather than a more typical 95°C to help prevent precipitation of erythrocyte membrane proteins, or alternatively this may suggest that the toxin oligomers were less stable than those formed by PFO or ALO.

A 56kDa band was obtained for $\Delta 6\text{mALO}$ indicating that this mutant is capable of binding to the cell membrane. No larger molecules were present in the $\Delta 6\text{mALO}$ sample, and this concurs with the electron microscopy in suggesting that $\Delta 6\text{mALO}$ does not form pores.

Examination of the lungs of mice lethally challenged with anthrolysin O revealed multifocal occlusion of pulmonary vessels by fibrin thrombi in both mice examined. Fibrin deposits were not present in pulmonary vessels of a control mouse.

The family of CDCs are produced by an array of Gram-positive pathogenic organisms that can cause a wide range of diseases. Vaccination with CDCs or their derivatives, including pneumolysin (Paton *et al.*, 1983), pyolysin (Jost *et al.*, 2003), suilyisin (Jacobs *et al.*, 1994) and listeriolysin O (Harty & Bevan, 1992), have been shown to protect against diseases caused by the producing organisms.

Anthrolysin O is one of the most recently discovered cholesterol-dependent cytolysins and its production by *B. anthracis* (Shannon *et al.*, 2003) gives rise to the possibility that it may play a role in the pathogenesis of anthrax, possibly as a mechanism of escape from the phagosomes of macrophages (Wei *et al.*, 2005). We were therefore interested to determine whether vaccination with anthrolysin O conferred protection against anthrax. On the basis of this hypothesis, we studied the capacity of immunisation with mALO, $\Delta 6$ mALO and PLY to protect against challenge with the mALO toxin and with *B. anthracis* spores.

As a prelude to vaccination experiments, the toxicity of mALO *in vivo* was determined. A dose of 5 μ g mALO i.v. was immediately lethal to all of the animals in the group. This dose was therefore used in experiments to detect protection against challenge with the mALO toxin. The LD₅₀ for listeriolysin O and streptolysin O have previously been calculated as 3-12 μ g/kg and 8 μ g/kg i.v. respectively (Gill, 1982), indicating that these toxins were found to be approximately five-fold more

potent than mALO. A recent study examined the lethal effect of LLO, ILO, SLO and PLY and found that the toxicity of these varied by up to 2.5 fold (Watanabe *et al.*, 2006). Since Watanabe *et al.* used survival time rather than percentage survival it is difficult to relate the results to those shown here or to those of Park *et al.* Comparison between studies is also hindered as variation may be a result of differences in toxin purity or differing susceptibilities of mouse strains.

The first step was to determine whether a toxin-neutralising response could be raised *in vivo* by immunisation with mALO, $\Delta 6$ mALO and PLY. Complete protection against lethal i.v. challenge with mALO was afforded equally to the groups immunised with mALO and $\Delta 6$ mALO but not the group immunised with PLY. This indicated that despite good homology across the group of cholesterol-dependent cytolysins, which typically show 40-97% identity between members, neutralising cross-reactivity is not necessarily afforded between members of this family.

A previous study on the cross-reactivity of the CDCs used Ouchterlony immunodiffusion to study cross-reactivity between horse antisera to tetanolysin, streptolysin O and perfringolysin O with cereolysin O, tetanolysin, streptolysin O and perfringolysin O (Cowell *et al.*, 1978). In this study, CDCs were found to be antigenically identical or similar depending on the particular combination of CDCs tested, however some unexpected results were observed, e.g. anti-tetanolysin antisera did not appear to precipitate tetanolysin but did precipitate the other CDC. Cross-reaction of sera appears to require the use of high-titre anti-sera, as can be obtained from immunisation of horses, (Cowell *et al.*, 1978). Cowell and

Bernheimer also remark that they have observed that rabbit anti-serum raised against cereolysin O neutralises and precipitates cereolysin O itself but not any of the other CDCs they tested, although this data is not presented in the paper (Cowell *et al.*, 1978). Given the high degree of identity between cereolysin O and anthrolysin O, this data agrees well with the data in this work that suggests there is limited cross-reactivity between anthrolysin O and pneumolysin.

For each group, the protective capacity of the sera was mirrored by the anti-mALO IgG levels which were high in mALO and $\Delta 6$ mALO vaccinated groups but much lower in the PLY vaccinated group. Anti-PLY IgG levels were high in the PLY vaccinated group, indicating that the low anti-ALO titre was a result of a lack of cross-reactivity and not poor immunogenicity of PLY.

The lack of cross-reactivity was not reciprocated, however, as anti-PLY IgG levels were also high in mALO-vaccinated animals. Surprisingly, vaccination with $\Delta 6$ mALO did not give rise to high anti-PLY titres. One explanation for this is that the site altered in $\Delta 6$ mALO is highly conserved across the CDCs and this may be the main cross-reactive epitope between mALO and PLY. This region has previously been shown to be one of two highly antigenic sites by epitope scanning and was recognised by both convalescent human sera and hyper-immune rabbit sera (Salo *et al.*, 1993).

Serum from mALO and PLY immunised animals was found to neutralise the activity of the toxin used for vaccination but did not neutralise the activity of the

other CDC. This lack of cross-neutralisation correlated with the failure of vaccination with PLY to protect against challenge with mALO.

Despite the generation of high anti-mALO IgG levels, vaccination with mALO, $\Delta 6$ mALO and PLY failed to protect against challenge with *B. anthracis* in the i.p. challenge model. The positive control – immunisation with recombinant protective antigen – conferred full protection.

Anthrolysin O has been shown to be secreted by *B. anthracis* (Shannon *et al.*, 2003) and in this work it has been demonstrated that anthrolysin O causes peracute pathology when introduced to the bloodstream of mice. Vaccination with mALO or $\Delta 6$ mALO was protective against the lethality of i.v. injection with mALO but neutralisation of this activity was insufficient to protect against *B. anthracis* infection. Since the role of mALO in the pathogenesis of *B. anthracis* is currently undefined, it may be that the type of response generated was not appropriate to neutralise a critical activity of mALO, which may have an intracellular role (Wei *et al.*, 2005), or the activity of ALO may not be critical to the virulence of the organism. Alternatively, the role of ALO may be specific to a particular event in *B. anthracis* pathogenesis not simulated in this i.p. model, such as translocation of the bacterium across the alveolar barrier, so that an opportunity for protection was bypassed.

Conclusions

- ALO is lytic to both horse and human erythrocytes, and has a specific activity similar to that of other CDCs
- The $\Delta 6$ mALO deletion mutant of ALO was capable of cell binding but is not haemolytic and does not form pore structures on membranes. The effect of this mutation therefore mirrors that of the $\Delta 6$ PLY mutation.
- mALO forms pores on erythrocytes membranes. These are similar in appearance and size to those produced by other members of the CDCs.
- Anthrolysin O is toxic to mice by i.v. challenge with an estimated LD50 of 35mg kg^{-1} .
- Histological examination of mice that succumbed to ALO toxicity showed occlusion of the vascular lumen with acellular thrombi.
- Immunisation with a specific CDC does not necessarily confer good cross-reactivity, cross-protection or cross-neutralisation against other CDCs. Addition of the $\Delta 6$ mutation to ALO altered the cross-reactivity of the antibodies produced.
- Immunisation with mALO and $\Delta 6$ mALO was highly protective against challenge with mALO but did not protect against i.p. challenge with *B. anthracis*.

Appendix 1: Sequence Alignment of the CDCs

1
 (1) -----VKKSNHLKGRVLSLVSL
 (1) -----NKKNTKR-RKFACLVSL
 (1) -----NKKNTKR-RKFACLVSL
 (1) -----NKKNGKR-RKFTCVLVS
 (1) -----MIRFKTKLISLAML
 (1) MKDMSNKKTFKYSRVAGLLTAALIIGNLVTAESNKONTASTETTTTSEQPKESSEITTEKAGOKMDDMNNDMIK
 (1) -----MKNKVLKFSRSLIFSMTGLISNYNSNVLAKG
 (1) -----MKKIMLLMLTLLVSLPLAQ--EA0AD3VYSYO
 (1) -----MKKIMLVFITLILVSLPIA00TEAKDA3AFNK-E
 (1) -----MKIFGLVIMSLFVSLPIT00PEAR0VPLVDRSE
 (1) -----MKRKAFA5LVA5VAAAATVMTPTASFAAGIGNSS
 (1) -----MKTQNIARKLSRVVLSLVLSSAAPISAFVAFETP
 (1) -----
 (1) -----L I K LASL S
 (1) -----TRKSS

Alveolysin
 Anthrolysin 0
 Cereolysin 0
 Thuringiolysin 0
 Perfringiolysin 0
 Streptolysin 0
 Tetanolysin
 Ivanolysin 0
 Listeriolysin 0
 Seeligeriolysin 0
 Pyolysin
 Intermedilysin
 Pneumolysin
 Suilysin
 Consensus

80
 (22) OVFAFASISSAAPTEP-----NDIDMGTAGLNINRNEVLAI0G00ISSFVPKEGIOSNGKFIIVERDKKS
 (24) CTIHYSSISFAETOAGNATGAIKN---ASDINTGIANLKYSRDTLAVNGDKVESFIPKESINSNGKFIIVEREKKS
 (21) CTINYSSISFAETOASNATDVTKN---ASGIDTGANLKYNNQVAVAVGDKVESFVPKESINSNGKFIIVEREKKS
 (24) CTINYSSISFAETOAGHATDITKN---ASSIDTGINLTYNNQVAVAVGDKVESFVPKESINSNGKFIIVEREKKS
 (18) CLFS0PVYISFSKDIIDK-----NQSIDSGISSLYNNEVLASGDKTESFVPKEGKAGNKFIIVEROKRSL
 (81) LAPKEMPLESAEKEEKKSEDKKSEEDHTEFINDKIYSLNNELEVLAKNGETLENFVPKEGVKKADKFIIVERKKNIN
 (35) NVEEHSIINGQVTSNTKCNLAKDN---SSDIDKNIYGLSYPRKTLVYNGE0VENFVPAEGFENPKDFIIVKREKKSIS
 (33) GIISHMAPPASPPAKPKTPVEKKN---4A0ID0YI0GLDYDKNNLVYDGEAVKNVPPKAGYKEGN0YIIVERKKSIN
 (34) NSISSMAPPASPPASPPTPIEKKH---4DFIDKYI0GLDYKNNLVYHGGAVTNVPPKGYKDGNEYIIVERKKSIN
 (35) VTISPATPEAPPATPKTPVEKKH---4EEINKYI0GLDYKNNLVYDGEAVTNVPPKGYKDGSEYIIVERKKSIN
 (35) GLTDGLSAPRVSISPMDKVDLKS0A0ETDETSVDKYIRGLEYP5GVLAVKGESIENVPVTKD0LKDGTIVFKHERKSFN
 (37) TKPKA00TEKKTEKKPEN5EAA---KKAINDYI0GLDYKNNLVYDGEAVKNVPPKAGYKEGN0YIIVERKKSIN
 (1) -----NKAINDYI0GLDYKNNLVYDGEAVKNVPPKAGYKEGN0YIIVERKKSIN
 (6) HLILSSIVSLALVGVTPLSVLADS---KODIN0YF0SLTYE0EILVTHDGEKKNHSSREAFHRPGEYIVTEKKK0SIS
 (81) I SSI A K A DID YI GL YDKNEVLA NGE VENFVPEK GKFIIVEREKKSIT

Alveolysin
 Anthrolysin 0
 Cereolysin 0
 Thuringiolysin 0
 Perfringiolysin 0
 Streptolysin 0
 Tetanolysin
 Ivanolysin 0
 Listeriolysin 0
 Seeligeriolysin 0
 Pyolysin
 Intermedilysin
 Pneumolysin
 Suilysin
 Consensus

481

560

(403) Alveolysin
 (414) Anthrolysin 0
 (411) Cereolysin 0
 (414) Thuringiolysin 0
 (401) Perfringolysin 0
 (475) Streptolysin 0
 (427) Tetanolysin
 (425) Ivanolysin 0
 (426) Listeriolysin 0
 (427) See Ligeriolysin 0
 (434) Pyolysin
 (428) Intermedilysin
 (370) Pneumolysin
 (398) Suilysin
 (481) Consensus

AYVAQFEVYWDEFSDADGGEIIVTRKSWDGNWDPSSAHFSTEIPLPPNAKNIPIFARECTGLAWEWRTVDEIYNPLAS
 AYVAQFDVSMDEFIDONGKEVITHKITWEGSGDKTAHYSTVIPLPPNSKNIKIVARECTGLAWEWRTINEONPLTN
 AYVAQFDVSMDEFIDONGKEVITHKITWEGSGDKTAHYSTVIPLPPNSKNIKIVARECTGLAWEWRTINEONPLTN
 AYVAQFDVSMDEFIDONGKEVITHKITWEGSGDKTAHYSTVIPLPPNSKNIKIVARECTGLAWEWRTINEONPLTN
 AYVAQFEVAWDEVSYDKEGNEVITHKITWEGNYODKTAHYSTVIPLPPNSKNIKIVARECTGLAWEWRTVISEYDPLTN
 AYVAQVEI LWDEINYYDKGKEVITKPRWNNWYSKTPFSTVIPLGANSRNIPIARECTGLAWEWRTVIDERDKLSSK
 AYVAQFOVITWDEVSYDEKGEIIVEHKAWEGNNDRTAHFNIEIYKGNARNISVKIRECTGLAWEWRTVDVKNPLAK
 AYVARFNVITWDEVSYDANGNEVVEHKKVSENDKLAHFTBIYLPGNARNINHAARECTGLAWEWRTVDORNPLVK
 GYVAQFNISWDEVNYDPEGNEIIVOHKNVSENNSKLAHFTSSIYLPGNARNINYYARECTGLAWEWRTVDORNPLVK
 GYVAQFNISWDEVSYDENGNEIKVHKKVGENYSKLAHFTSSIYLPGNARNINYYARECTGLAWEWRTVDORNPLVK
 GYVAKFGKWDEISYDPOGKEIRTPKTVSGNWVGRLGFRREI IQLPANARNIHVEAGEATGLAWEPWTVINKNPLVP
 AEFARFYVYWEELGADAGYEITRSRWSVSGNGYNRGAHYSTLRFKGNVRNIPVKVLGATGLAWEPVRLYSKNDLPLVP
 AYVAQYITWDELSYDH0GKEVITPKAWDRNGODLTAHFTBIPLKGNVRNIPVKVLGATGLAWEWRTVYKTDLPLVR
 AYVAKNITWEEVSYNEAGEEIVWEPKAVDKNGVNLISHWSETIQIPGNARNIHNIARECTGLAWEWRTVYDK-DLPLVG
 AYVAQF VSWDEVSYD GNEVLTHKTDWGN KDKTAHFSTSIPLPGNARNIRI ARECTGLAWEWRTVIDE NLPLV

561

586

(483) Alveolysin
 (494) Anthrolysin 0
 (491) Cereolysin 0
 (494) Thuringiolysin 0
 (481) Perfringolysin 0
 (555) Streptolysin 0
 (507) Tetanolysin
 (505) Ivanolysin 0
 (506) Listeriolysin 0
 (507) See Ligeriolysin 0
 (514) Pyolysin
 (508) Intermedilysin
 (450) Pneumolysin
 (477) Suilysin
 (561) Consensus

DI NVSIWGTLLYPKSSITHH-----
 EIKVSI GGTTLYPTATISH-----
 EIKVSI GGTTLYPTASISH-----
 EIKVSI GGTTLYPTASISH-----
 NINVSIWGTLLYPGSSITYN-----
 EINVN SGGTLLSPYGSITLYK-----
 ERTFYIWGTLLYPKTSIETKM-----
 RPNVCIWGTLLYPAYSDIVDNPIK---
 RPNISIWGTLLYPKYSNKVDNPIE---
 RPNVSIWGTLLYPRHSNNVDNPIO---
 HREIVKGTLLNPWVEENKSKS-----
 ORNSTWGTLLPQFEDKVKKNDNTD--
 KRTISIWGTLLYPOVEDKVENDE----
 ORKTIWGTLLYPOYADEVIE-----
 RNVSIWGTLLYPSITV

Appendix 2: Oligonucleotides

Sequences of oligonucleotide primers

Primer Reference	Sequence (5' to 3')
08Y	CGGGATCCGGCAAATAAAGCAGTAAATGACTTT
09Z	GACGGAGCTCGACTAGTCATTTTCTACCTTATC
20G	GTCAGGCTAGCATGAGTAAAGGAGAAGAAC
20H	CCACGCAGATCTTTGTATAGTTCATCC
23B	GGTCAATAATGTCCCAATGCAGTATGAAAAATAACGGCTC
23C	GAGCCGTTATTTTTTCATACTGCATTGGGACATTATTGACC
24W	CACTTGTCACTACTCGACTTATGGTGTCAATGC
24X	GCATTGAACACCATAAGTCAGAGTAGTGACAAGTG
26C	TAATGTCCCAGCTAGAATGCAATATGAATCTA
26D	TTTTTTCATACTGCATTCTAGCTGGTACAGCA
26E	TGCTGTACCAGCTAGAATGCAGTATGAAAAA
26F	TAGATTCATATTGCATTCTAGCTGGGACATTA
26G	CAAGTTGGAAACCACGAGCAAGAGTACAAAAG
26H	CTTCATCACTCTTACTTGTAGTTTCAAATTC
26I	GAAATTTGAAACTACAAGTAAGAGTGATGAAG
26J	CTTTTGTACTCTTGCTCGTGGTTTTCCAAC TTG
26K	CTTGCCGATTTCCCTATACTTCTTTTGTGA
26L	GTAAAAAAGAAGTTGTGTAAGAGATTGGTACA
26M	TGTACCAATCTCTTACACAACCTTCTTTTTTAC
26N	TCACAAAAGAAGTAGTATAGGAAATCGGCAAG
26O	TCCTTTAAAAGGGAATGTTAGAAACATTGCGG
26P	CAGAGAGATTACGAAACATTTCCCTTGAAACGG
26Q	CCGTTTCAAGGGAAATGTTGTAATCTCTCTG
26R	CGCGAATGTTTCTAACATTCCCTTTTAAAGGA
26W	CGGGATCCGGAAACACCTACCAAACCAAAAGCA
26X	GACGGAGCTCGATTAATCAGTGTATCTTTCAC
30P	CCACGCAGATCTTATTTGTATAGTTCATCC
31T	GTCAGACTAGTATGAGTAAAGGAGAAGAAC
31U	GAACTATACAAAGATCCGGAAACACCTACCAAAAC
31V	GGTAGGTGTTTCCGGATCTTTGTATAGTTCATC
31W	CTAAAACCTCATGCTGTACCAATGCAATATGAATCTATTAGC
31X	GCTAATAGATTTCATATTGCATTGGTACAGCATGAGTTT TAG
32G	CTAAGGCGACGCAACCATTAG
32H	GAAGTGCTCATAGATTGTCTC
32U	GACGGAGCTCGACTAGTCATTTTCAACTTTATCTTCAAACCTGTGG
32V	GACGGAGCTCGATTAATCAGTGTATCTTCACTACCTTATCTCTACCTGAGG
32W	CGGGCTTGCCCTGGGAACCTTGGCGTACGGTTTATG
32X	CATAAACCGTACGCCAAGGTTCCAGGCAAGCCCG
32Y	CTGGACTAGCTTGGGAGTGGTGGAGACTGATCTATAG
32Z	CTATAGATCAGTCTCCACCACTCCCAAGCTAGTCCAG
33A	GTAATCTCTCTGTCAAAGTACTAGGAGCCACCGGGCTTGCCTGGG
33B	CCCAGGCAAGCCCGGTGGCTCCTAGTACTTTGACAGAGAGATTAC
33C	GAAACATTCGCGTAAAAATTAGAGAGTGTACTGGACTAGCTTGG
33D	CCAAGCTAGTCCAGTACACTCTCTAATTTTTACGCGAATGTTTC

Sequences of oligonucleotide primers

Primer Reference	Sequence (5' to 3')
35K	GAAACATTAGCATTGGGGAACAAC
35L	GAGCCTTGGAGAACGGTTTATAGCAAGAAC
35M	CCTAGTACTTTTACAGAGAGGTTTCTAACATTTT
35N	GAAATGTTAGAAACCTCTCTGTAAAAGTACTAGG
35O	GTTCTTGCTATAAACCGTTCTCCAAGGCTC
35P	GAGACTGATCTATGAAAAACCGATCTTCCTTTGG
35Q	CCAAAGGAAGATCGGTTTTTTCATAGATCAGTCTC
35R	CTTCTTTGGTTTCGTAAGCGGACGATTAGCACTTG
35S	GTTGTTCCCAAATGCTAATGTTTC
35T	CAAGTGCTAATCGTCCGCTTACGAACCAAAGGAAG
35U	GGGAACAACCCTTTATCCACAGTTTGAAG
35V	CTTCAAACGTGGATAAAGGGTTGTTCCC
35W	CCTTCATCCACAGGTAGAAGATAAAGTTG
35X	CAACTTATCTTCTACCTGTGGATGAAGG
35Y	CAGACCATGGAACACCTACCAAACCAAACCAAAC
35Z	TGCAGCCATGGCTTAATCAGTGTATCTTTCACTGTTATCTTTCAC
36C	GAACATACAAAGATCCGGCAAAAAAGCTCTGAATG
36D	GAGCTTTTTTGGCCGATCTTTGTATAGTTTCATC
38E	TCTAAAACATGCTGTACCAAT
40T	GGGGACAAGTTTGTACAAAAAGCAGGCTTACAAAAGTAACATCCTATAAAG
40U	GGGGACCACTTTGTACAAGAAAGCTGGGTCTTAATCAGTGTATCTTTCAC
41O	CGGGATCCGATTTTTCTGAATATTAAG
41P	GACGGAGCTCGACTAATGACTAATAGTAGCAG
42S	CAACACATACGTTACCTATGCAGTATACAGAATC
42T	GATTCTGTATACTGCATAGGTAACGTATGTGTTG
43L	CGGTCCGAACCTCATAACAACCTC
43M	GTAATTTCTGGCAAGGTAGAC
43Z	CGGGATCCGAAACACAAGCCGGTAATG
45L	CCACGCGAGCTCTTATTTGTATAGTTTCATCC
46Q	GTGCTTTCGTTGCACAATTCTATGTTTATTG
46R	CAATAAACATAGAATTGTGCAACGAAAG
46S	CACGCTTCTATGTTACTTGGGAAGAACTCGG
46T	CCGAGTTCTTCCCAAGTAACATAGAAGCGTG
46U	GATGGCTACGAACTTTGACTCCTAAGTCTTGGAGTGGAAATG
46V	CATTTCCACTCCAAGACTTAGGAGTCAAAGTTTCGTAGCCATC
46W	GTGGAAATGGCTACGATTTGGGTGCACACTATTC
46X	GAATAGTCTGCACCCAAATCGTAGCCATTTCCAC
46Y	CTACAACCTCCGTTTAAAGGGAAATGTTAG
46Z	CTAACATTTCCCTTTAAACGGAGAGTTGTAG
49O	CAAGGTAAGGAAGTCAATTCGCTCAAGAGCTTGGGACAGAAATG
49P	CATTTCTGTCCCAAGCTCTTGAGCGAATGACTTCCCTTACCTTG

Appendix 3: Buffers and Solutions

Phosphate Buffered Saline (PBS)

PBS was made using Dulbecco A PBS tablets (Oxoid) according to the manufacturer's recommended protocol. The final composition was:

	g/litre
NaCl	8.0
KCl	0.2
Na ₂ HPO ₄	1.15
KH ₂ PO ₄	0.2

pH 7.3

Erythrocyte Medium (ECM)

Dissolve in 2 litres ddH₂O then filter sterilise (0.2µM):

140mM NaCl	16.36g
5mM KCl	745mg
20mM Tris/HCl pH = 7.4	6.3g
2mM MgCl ₂	813mg
0.1mM EDTA	74.4mg
Dissolved in 2 litres dH ₂ O	

Terrific Broth

Terrific broth was made up according to the recipe of Tartof and Hobbs (Tartof & Hobbs, 1987).

For YTG base, to 900 ml of H₂O add:

- 12 g bacto-tryptone
- 24 g bacto-yeast extract
- 4 mL glycerol .

In a separate flask dissolve in 90 mL H₂O:

- 2.31 g KH₂PO₄ monobasic
- 12.54 g K₂HPO₄ dibasic (for trihydrate 16.45 g)
- Adjust volume to 100 mL with H₂O

Sterilize each separate volume by autoclaving for 20 min at 15 lb/square inch liquid cycle. Only add the potassium phosphate solution after the YTG base cools to 60°C.

YPAD Medium

Bacto-yeast extract	10 g
Bacto-peptone	20 g
Dextrose	20 g
Adenine sulphate	100 mg

Autoclaved, add distilled water to 1 litre.

ELISA bicarbonate coating buffer (pH 9.6)

1.59g Na₂CO₃
2.93g NaHCO₃
Dissolved in 1L dH₂O

1.0 M Lithium Acetate

Autoclave or filter sterilize
Final pH should be between 8.4 - 8.9

Synthetic Complete (SC) Drop Out Medium

12.0 g Glucose
Autoclave for 15 min.
Adjust pH to 5.6 with 10 N NaOH
600 ml ddH₂O
0.50 g Synthetic Complete Drop Out Mix
4.0 g Yeast Nitrogen Base w/o Amino Acids

Synthetic Complete (SC) Drop Out Medium Plates

10.0 g Bacto Agar
Adjust pH to 5.6 with 10 N NaOH
600 ml ddH₂O
0.50 g Synthetic Complete Drop Out Mix
12.0 g glucose
Autoclave the solution for 15 min.
4.0 g Yeast Nitrogen Base w/o Amino Acids

TE buffer

10 mM Tris-HCl, pH 8.0
1.0 mM EDTA

Single-Stranded Carrier DNA

Use 2 mg/ml Deoxyribonucleic acid Sodium Salt Type III from Salmon Testes (Sigma). Prior to use, boil an aliquot for at least 5 min and quickly cool in an ice water slurry. Disperse the DNA into solution by drawing it up and down repeatedly in a 10 ml pipette. Mix the solution vigorously on a magnetic stirrer for 2 to 3 hr or until fully dissolved. Prepare in TE.

Carrier DNA can be frozen after boiling and used 3 or 4 times. If transformation efficiencies begin to decrease with a specific aliquot of boiled carrier DNA, that aliquot should be boiled again or a new aliquot used. Store the aliquots in a -20°C freezer.

Uranyl Formate Negative Stain

Protocol obtained from Dr. Laurence Tetley, University of Glasgow

Use freshly prepared 1% uranyl formate for optimum results.

One millilitre aliquots of 1% uranyl acetate were dispensed into eppendorf tubes. 0.1mL of 1.0M NaOH was added, and the tubes were sealed and shaken. The precipitate was sedimented by centrifugation, and the supernatant was discarded. The pellet was dissolved in 100µl of 5% formic acid by vigorous mixing and used immediately.

Publications

Papers

Nagamune, H., Ohkura, K., Sukeho, A., Cowan, G., Mitchell, T. J., Ito, W., Ohnishi, O., Hattori, K., Yamato, M., Hirota, K., Miyake, Y., Maeda, T. & Kourai, H. (2004). The human-specific action of intermedilysin, a homolog of streptolysin O, is dictated by domain 4 of the protein. *Microbiol Immunol* 48, 677-692.

Fickl, H., Cockeran, R., Steel, H. C., Feldman, C., Cowan, G., Mitchell, T. J. & Anderson, R. (2005). Pneumolysin-mediated activation of NFkappaB in human neutrophils is antagonized by docosahexaenoic acid. *Clin Exp Immunol* 140, 274-281.

Beurg, M., Hafidi, A., Skinner, L., Cowan, G., Hondarrague, Y., Mitchell, T. J. & Dulon, D. (2005). The mechanism of pneumolysin-induced cochlear hair cell death in the rat. *J Physiol* 568, 211-227.

Cowan, G. J. M., Atkins, H. S., Johnson, L. S., Titball, R. W. & Mitchell, T. J. Immunisation with Anthrolysin O or a genetic toxoid protects against challenge with the toxin but not against *Bacillus anthracis*. Submitted to *Microbes and Infection*.

Patents

Kirkham, L. K., Mitchell, T. J. & Cowan, G. J. M. Mutant Cholesterol Binding Cytolysin Proteins. Patent Reference WO2005108419.

Mitchell, T. J., Douce, G. R., Cowan, G. J. M. & Kirkham, L. K. Novel adjuvant compositions. Filed with UK Patent office - reference BP6385215.

References

Adams, S. R., Campbell, R. E., Gross, L. A., Martin, B. R., Walkup, G. K., Yao, Y., Llopis, J. & Tsien, R. Y. (2002). New biarsenical ligands and tetracysteine motifs for protein labeling in vitro and in vivo: synthesis and biological applications. *J Am Chem Soc* **124**, 6063-6076.

Alcantara, R. B., Preheim, L. C. & Gentry, M. J. (1999). Role of Pneumolysin's complement-activating activity during pneumococcal bacteremia in cirrhotic rats. *Infect Immun* **67**, 2862-2866.

Alcantara, R. B., Preheim, L. C. & Gentry-Nielsen, M. J. (2001). Pneumolysin-induced complement depletion during experimental pneumococcal bacteremia. *Infect Immun* **69**, 3569-3575.

Alexander, J. E., Lock, R. A., Peeters, C. C., Poolman, J. T., Andrew, P. W., Mitchell, T. J., Hansman, D. & Paton, J. C. (1994). Immunization of mice with pneumolysin toxoid confers a significant degree of protection against at least nine serotypes of *Streptococcus pneumoniae*. *Infect Immun* **62**, 5683-5688.

Alexander, J. E., Berry, A. M., Paton, J. C., Rubins, J. B., Andrew, P. W. & Mitchell, T. J. (1998). Amino acid changes affecting the activity of pneumolysin alter the behaviour of pneumococci in pneumonia. *Microb Pathog* **24**, 167-174.

Alouf, J. E. (1980). Streptococcal toxins (streptolysin O, streptolysin S, erythrogenic toxin). *Pharmacol Ther* **11**, 661-717.

Altschul, S. F., Gish, W., Miller, W., Myers, E. W. & Lipman, D. J. (1990). Basic local alignment search tool. *J Mol Biol* **215**, 403-410.

Awad, M. M., Ellemor, D. M., Boyd, R. L., Emmins, J. J. & Rood, J. I. (2001). Synergistic effects of alpha-toxin and perfringolysin O in *Clostridium perfringens*-mediated gas gangrene. *Infect Immun* **69**, 7904-7910.

Baba, H., Kawamura, I., Kohda, C., Nomura, T., Ito, Y., Kimoto, T., Watanabe, I., Ichiyama, S. & Mitsuyama, M. (2001). Essential role of domain 4 of pneumolysin from *Streptococcus pneumoniae* in cytolytic activity as determined by truncated proteins. *Biochem Biophys Res Commun* **281**, 37-44.

Baba, H., Kawamura, I., Kohda, C., Nomura, T., Ito, Y., Kimoto, T., Watanabe, I., Ichiyama, S. & Mitsuyama, M. (2002). Induction of gamma interferon and nitric oxide by truncated pneumolysin that lacks pore-forming activity. *Infect Immun* **70**, 107-113.

Balachandran, P., Hollingshead, S. K., Paton, J. C. & Briles, D. E. (2001). The autolytic enzyme LytA of *Streptococcus pneumoniae* is not responsible for releasing pneumolysin. *J Bacteriol* **183**, 3108-3116.

Beedham, R. J., Turnbull, P. C. & Williamson, E. D. (2001). Passive transfer of protection against *Bacillus anthracis* infection in a murine model. *Vaccine* **19**, 4409-4416.

Benton, K. A., Everson, M. P. & Briles, D. E. (1995). A pneumolysin-negative mutant of *Streptococcus pneumoniae* causes chronic bacteremia rather than acute sepsis in mice. *Infect Immun* **63**, 448-455.

Benton, K. A., Paton, J. C. & Briles, D. E. (1997). Differences in virulence for mice among *Streptococcus pneumoniae* strains of capsular types 2, 3, 4, 5, and 6 are not attributable to differences in pneumolysin production. *Infect Immun* **65**, 1237-1244.

Berche, P., Gaillard, J. L. & Sansonetti, P. J. (1987). Intracellular growth of *Listeria monocytogenes* as a prerequisite for in vivo induction of T cell-mediated immunity. *J Immunol* **138**, 2266-2271.

Berry, A. M., Ogunniyi, A. D., Miller, D. C. & Paton, J. C. (1999). Comparative virulence of *Streptococcus pneumoniae* strains with insertion-duplication, point, and deletion mutations in the pneumolysin gene. *Infect Immun* **67**, 981-985.

Beurg, M., Hafidi, A., Skinner, L., Cowan, G., Hondarrague, Y., Mitchell, T. J. & Dulon, D. (2005). The mechanism of pneumolysin-induced cochlear hair cell death in the rat. *J Physiol* **568**, 211-227.

Bhakdi, S. & Trantum-Jensen, J. (1985). Complement activation and attack on autologous cell membranes induced by streptolysin-O. *Infect Immun* **48**, 713-719.

Bhakdi, S., Trantum-Jensen, J. & Sziegoleit, A. (1985). Mechanism of membrane damage by streptolysin-O. *Infect Immun* **47**, 52-60.

Bhakdi, S., Weller, U., Walev, I., Martin, E., Jonas, D. & Palmer, M. (1993). A guide to the use of pore-forming toxins for controlled permeabilization of cell membranes. *Med Microbiol Immunol (Berl)* **182**, 167-175.

Bielecki, J., Youngman, P., Connelly, P. & Portnoy, D. A. (1990). Bacillus subtilis expressing a haemolysin gene from Listeria monocytogenes can grow in mammalian cells. *Nature* **345**, 175-176.

Billington, S. J., Songer, J. G. & Jost, B. H. (2001). Molecular characterization of the pore-forming toxin, pyolysin, a major virulence determinant of Arcanobacterium pyogenes. *Vet Microbiol* **82**, 261-274.

Billington, S. J., Songer, J. G. & Jost, B. H. (2002). The variant undecapeptide sequence of the Arcanobacterium pyogenes haemolysin, pyolysin, is required for full cytolytic activity. *Microbiology* **148**, 3947-3954.

Boulnois, G. J., Paton, J. C., Mitchell, T. J. & Andrew, P. W. (1991). Structure and function of pneumolysin, the multifunctional, thiol-activated toxin of Streptococcus pneumoniae. *Mol Microbiol* **5**, 2611-2616.

Bradford, M. M. (1976). A rapid and sensitive method for the quantitation of microgram quantities of protein utilizing the principle of protein-dye binding. *Anal Biochem* **72**, 248-254.

Braun, J. S., Novak, R., Gao, G., Murray, P. J. & Shenep, J. L. (1999). Pneumolysin, a protein toxin of *Streptococcus pneumoniae*, induces nitric oxide production from macrophages. *Infect Immun* **67**, 3750-3756.

Braun, J. S., Sublett, J. E., Freyer, D., Mitchell, T. J., Cleveland, J. L., Tuomanen, E. I. & Weber, J. R. (2002). Pneumococcal pneumolysin and H₂O₂ mediate brain cell apoptosis during meningitis. *J Clin Invest* **109**, 19-27.

Burnette, W. N. (1981). "Western blotting": electrophoretic transfer of proteins from sodium dodecyl sulfate--polyacrylamide gels to unmodified nitrocellulose and radiographic detection with antibody and radioiodinated protein A. *Anal Biochem* **112**, 195-203.

Bushman, W., Thompson, J. F., Vargas, L. & Landy, A. (1985). Control of directionality in lambda site specific recombination. *Science* **230**, 906-911.

Camilli, A., Tilney, L. G. & Portnoy, D. A. (1993). Dual roles of *plcA* in *Listeria monocytogenes* pathogenesis. *Mol Microbiol* **8**, 143-157.

Chalfie, M., Tu, Y., Euskirchen, G., Ward, W. W. & Prasher, D. C. (1994). Green fluorescent protein as a marker for gene expression. *Science* **263**, 802-805.

Chalfie, M. & Kain, S. (1998). *Green fluorescent protein : properties, applications and protocols.* New York ; Chichester: Wiley-Liss.

Cockeran, R., Durandt, C., Feldman, C., Mitchell, T. J. & Anderson, R. (2002). Pneumolysin activates the synthesis and release of interleukin-8 by human neutrophils in vitro. *J Infect Dis* **186**, 562-565.

Cormack, B. P., Valdivia, R. H. & Falkow, S. (1996). FACS-optimized mutants of the green fluorescent protein (GFP). *Gene* **173**, 33-38.

Cornell, K. A., Bouwer, H. G., Hinrichs, D. J. & Barry, R. A. (1999). Genetic immunization of mice against *Listeria monocytogenes* using plasmid DNA encoding listeriolysin O. *J Immunol* **163**, 322-329.

Cossart, P., Vicente, M. F., Mengaud, J., Baquero, F., Perez-Diaz, J. C. & Berche, P. (1989). Listeriolysin O is essential for virulence of *Listeria monocytogenes*: direct evidence obtained by gene complementation. *Infect Immun* **57**, 3629-3636.

Cowell, J. L., Kim, K. S. & Bernheimer, A. W. (1978). Alteration by cereolysin of the structure of cholesterol-containing membranes. *Biochim Biophys Acta* **507**, 230-241.

Czajkowsky, D. M., Hotze, E. M., Shao, Z. & Tweten, R. K. (2004). Vertical collapse of a cytolysin prepore moves its transmembrane beta-hairpins to the membrane. *Embo J* **23**, 3206-3215.

Dang, T. X., Hotze, E. M., Rouiller, I., Tweten, R. K. & Wilson-Kubalek, E. M. (2005). Prepore to pore transition of a cholesterol-dependent cytolysin visualized by electron microscopy. *J Struct Biol* **150**, 100-108.

Decatur, A. L. & Portnoy, D. A. (2000). A PEST-like sequence in listeriolysin O essential for *Listeria monocytogenes* pathogenicity. *Science* **290**, 992-995.

Dixon, T. C., Fadi, A. A., Koehler, T. M., Swanson, J. A. & Hanna, P. C. (2000). Early *Bacillus anthracis*-macrophage interactions: intracellular survival and escape. *Cell Microbiol* **2**, 453-463.

Dubail, I., Autret, N., Beretti, J. L., Kayal, S., Berche, P. & Charbit, A. (2001). Functional assembly of two membrane-binding domains in listeriolysin O, the cytolysin of *Listeria monocytogenes*. *Microbiology* **147**, 2679-2688.

Duesbery, N. S., Webb, C. P., Leppla, S. H., Gordon, V. M., Klimpel, K. R., Copeland, T. D., Ahn, N. G., Oskarsson, M. K., Fukasawa, K., Paull, K. D. & Vande Woude, G. F. (1998). Proteolytic inactivation of MAP-kinase-kinase by anthrax lethal factor. *Science* **280**, 734-737.

Feldman, C., Munro, N. C., Jeffery, P. K., Mitchell, T. J., Andrew, P. W., Boulnois, G. J., Guerreiro, D., Rohde, J. A., Todd, H. C., Cole, P. J. & et al. (1991). Pneumolysin induces the salient histologic features of pneumococcal infection in the rat lung in vivo. *Am J Respir Cell Mol Biol* **5**, 416-423.

Fensterle, J., Grode, L., Hess, J. & Kaufmann, S. H. (1999). Effective DNA vaccination against listeriosis by prime/boost inoculation with the gene gun. *J Immunol* **163**, 4510-4518.

Ferreira, D. M., Areas, A. P., Darrieux, M., Leite, L. C. & Miyaji, E. N. (2006). DNA vaccines based on genetically detoxified derivatives of pneumolysin fail to protect mice against challenge with *Streptococcus pneumoniae*. *FEMS Immunol Med Microbiol* **46**, 291-297.

Fickl, H., Cockeran, R., Steel, H. C., Feldman, C., Cowan, G., Mitchell, T. J. & Anderson, R. (2005). Pneumolysin-mediated activation of NFkappaB in human neutrophils is antagonized by docosahexaenoic acid. *Clin Exp Immunol* **140**, 274-281.

Fish, D. C., Klein, F., Lincoln, R. E., Walker, J. S. & Dobbs, J. P. (1968). Pathophysiological changes in the rat associated with anthrax toxin. *J Infect Dis* **118**, 114-124.

Fouet, A., Sirard, J. C. & Mock, M. (1995). Virulence gene determinants. *Salisbury Medical Bulletin, Special Supplement* **87**, 84-85.

Funk, P. G., Staats, J. J., Howe, M., Nagaraja, T. G. & Chengappa, M. M. (1996). Identification and partial characterization of an *Actinomyces pyogenes* hemolysin. *Vet Microbiol* **50**, 129-142.

Gedde, M. M., Higgins, D. E., Tilney, L. G. & Portnoy, D. A. (2000). Role of listeriolysin O in cell-to-cell spread of *Listeria monocytogenes*. *Infect Immun* **68**, 999-1003.

Giddings, K. S., Johnson, A. E. & Tweten, R. K. (2003). Redefining cholesterol's role in the mechanism of the cholesterol-dependent cytolysins. *Proc Natl Acad Sci U S A* **100**, 11315-11320.

Giddings, K. S., Zhao, J., Sims, P. J. & Tweten, R. K. (2004). Human CD59 is a receptor for the cholesterol-dependent cytolysin intermedilysin. *Nat Struct Mol Biol* **11**, 1173-1178.

Gilbert, R. J., Rossjohn, J., Parker, M. W., Tweten, R. K., Morgan, P. J., Mitchell, T. J., Errington, N., Rowe, A. J., Andrew, P. W. & Byron, O. (1998). Self-interaction of pneumolysin, the pore-forming protein toxin of *Streptococcus pneumoniae*. *J Mol Biol* **284**, 1223-1237.

Gilbert, R. J., Jimenez, J. L., Chen, S., Tickle, I. J., Rossjohn, J., Parker, M., Andrew, P. W. & Saibil, H. R. (1999). Two structural transitions in membrane

pore formation by pneumolysin, the pore-forming toxin of *Streptococcus pneumoniae*. *Cell* **97**, 647-655.

Gilbert, R. J. (2002). Pore-forming toxins. *Cell Mol Life Sci* **59**, 832-844.

Gilbert, R. J. (2005). Inactivation and activity of cholesterol-dependent cytolysins: what structural studies tell us. *Structure (Camb)* **13**, 1097-1106.

Gill, D. M. (1982). Bacterial toxins: a table of lethal amounts. *Microbiol Rev* **46**, 86-94.

Glomski, I. J., Gedde, M. M., Tsang, A. W., Swanson, J. A. & Portnoy, D. A. (2002). The *Listeria monocytogenes* hemolysin has an acidic pH optimum to compartmentalize activity and prevent damage to infected host cells. *J Cell Biol* **156**, 1029-1038.

Grey, M. & Brendel, M. (1992). A ten-minute protocol for transforming *Saccharomyces cerevisiae* by electroporation. *Curr Genet* **22**, 335-336.

Griffin, B. A., Adams, S. R. & Tsien, R. Y. (1998). Specific covalent labeling of recombinant protein molecules inside live cells. *Science* **281**, 269-272.

Guidi-Rontani, C., Weber-Levy, M., Labruyere, E. & Mock, M. (1999). Germination of *Bacillus anthracis* spores within alveolar macrophages. *Mol Microbiol* **31**, 9-17.

Guidi-Rontani, C., Levy, M., Ohayon, H. & Mock, M. (2001). Fate of germinated *Bacillus anthracis* spores in primary murine macrophages. *Mol Microbiol* **42**, 931-938.

Hackett, S. P. & Stevens, D. L. (1992). Streptococcal toxic shock syndrome: synthesis of tumor necrosis factor and interleukin-1 by monocytes stimulated with pyrogenic exotoxin A and streptolysin O. *J Infect Dis* **165**, 879-885.

Hakansson, A., Bentley, C. C., Shakhnovic, E. A. & Wessels, M. R. (2005). Cytolysin-dependent evasion of lysosomal killing. *Proc Natl Acad Sci U S A* **102**, 5192-5197.

Harty, J. T. & Bevan, M. J. (1992). CD8⁺ T cells specific for a single nonamer epitope of *Listeria monocytogenes* are protective in vivo. *J Exp Med* **175**, 1531-1538.

Heuck, A. P., Hotze, E. M., Tweten, R. K. & Johnson, A. E. (2000). Mechanism of membrane insertion of a multimeric beta-barrel protein: perfringolysin O creates a pore using ordered and coupled conformational changes. *Mol Cell* **6**, 1233-1242.

Hirst, R. A., Yesilkaya, H., Clitheroe, E., Rutman, A., Dufty, N., Mitchell, T. J., O'Callaghan, C. & Andrew, P. W. (2002). Sensitivities of human monocytes and epithelial cells to pneumolysin are different. *Infect Immun* **70**, 1017-1022.

- Hoffmaster, A. R., Ravel, J., Rasko, D. A., Chapman, G. D., Chute, M. D., Marston, C. K., De, B. K., Sacchi, C. T., Fitzgerald, C., Mayer, L. W., Maiden, M. C., Priest, F. G., Barker, M., Jiang, L., Cer, R. Z., Rilstone, J., Peterson, S. N., Weyant, R. S., Galloway, D. R., Read, T. D., Popovic, T. & Fraser, C. M. (2004). Identification of anthrax toxin genes in a *Bacillus cereus* associated with an illness resembling inhalation anthrax. *Proc Natl Acad Sci U S A* **101**, 8449-8454.
- Hotze, E. M., Wilson-Kubalek, E. M., Rossjohn, J., Parker, M. W., Johnson, A. E. & Tweten, R. K. (2001). Arresting pore formation of a cholesterol-dependent cytolysin by disulfide trapping synchronizes the insertion of the transmembrane beta-sheet from a prepore intermediate. *J Biol Chem* **276**, 8261-8268.
- Hotze, E. M., Heuck, A. P., Czajkowsky, D. M., Shao, Z., Johnson, A. E. & Tweten, R. K. (2002). Monomer-monomer interactions drive the prepore to pore conversion of a beta-barrel-forming cholesterol-dependent cytolysin. *J Biol Chem* **277**, 11597-11605.
- Houldsworth, S., Andrew, P. W. & Mitchell, T. J. (1994). Pneumolysin stimulates production of tumor necrosis factor alpha and interleukin-1 beta by human mononuclear phagocytes. *Infect Immun* **62**, 1501-1503.
- Inouye, S. & Tsuji, F. I. (1994). Aequorea green fluorescent protein. Expression of the gene and fluorescence characteristics of the recombinant protein. *FEBS Lett* **341**, 277-280.

Ito, Y., Kawamura, I., Kohda, C., Baba, H., Nomura, T., Kimoto, T., Watanabe, I. & Mitsuyama, M. (2003). Seeligeriolysin O, a cholesterol-dependent cytolysin of *Listeria seeligeri*, induces gamma interferon from spleen cells of mice. *Infect Immun* **71**, 234-241.

Iwamoto, M., Ohno-Iwashita, Y. & Ando, S. (1987). Role of the essential thiol group in the thiol-activated cytolysin from *Clostridium perfringens*. *Eur J Biochem* **167**, 425-430.

Jacobs, A. A., Loeffen, P. L., van den Berg, A. J. & Storm, P. K. (1994). Identification, purification, and characterization of a thiol-activated hemolysin (sullysin) of *Streptococcus suis*. *Infect Immun* **62**, 1742-1748.

Jacobs, T., Darji, A., Frahm, N., Rohde, M., Wehland, J., Chakraborty, T. & Weiss, S. (1998). Listeriolysin O: cholesterol inhibits cytolysis but not binding to cellular membranes. *Mol Microbiol* **28**, 1081-1089.

Johnson, M. K. (1972). Properties of purified pneumococcal hemolysin. *Infect Immun* **6**, 755-760.

Johnson, M. K., Callegan, M. C., Engel, L. S., O'Callaghan, R. J., Hill, J. M., Hobden, J. A., Boulnois, G. J., Andrew, P. W. & Mitchell, T. J. (1995). Growth and virulence of a complement-activation-negative mutant of *Streptococcus pneumoniae* in the rabbit cornea. *Curr Eye Res* **14**, 281-284.

Jost, B. H., Songer, J. G. & Billington, S. J. (1999). An Arcanobacterium (Actinomyces) pyogenes mutant deficient in production of the pore-forming cytolyisin pyolysin has reduced virulence. *Infect Immun* **67**, 1723-1728.

Jost, B. H., Trinh, H. T., Songer, J. G. & Billington, S. J. (2003). Immunization with genetic toxoids of the Arcanobacterium pyogenes cholesterol-dependent cytolyisin, pyolysin, protects mice against infection. *Infect Immun* **71**, 2966-2969.

Kabat, E. A., Wu, T. T. & Bilofsky, H. (1977). Unusual distributions of amino acids in complementarity-determining (hypervariable) segments of heavy and light chains of immunoglobulins and their possible roles in specificity of antibody-combining sites. *J Biol Chem* **252**, 6609-6616.

Kawai, T. & Akira, S. (2005). Pathogen recognition with Toll-like receptors. *Curr Opin Immunol* **17**, 338-344.

Kayal, S., Lilienbaum, A., Poyart, C., Memet, S., Israel, A. & Berche, P. (1999). Listeriolysin O-dependent activation of endothelial cells during infection with *Listeria monocytogenes*: activation of NF-kappa B and upregulation of adhesion molecules and chemokines. *Mol Microbiol* **31**, 1709-1722.

Kehoe, M. A., Miller, L., Walker, J. A. & Boulnois, G. J. (1987). Nucleotide sequence of the streptolysin O (SLO) gene: structural homologies between SLO and other membrane-damaging, thiol-activated toxins. *Infect Immun* **55**, 3228-3232.

Kerr, A. R., Kirkham, L. A., Kadioglu, A., Andrew, P. W., Garside, P., Thompson, H. & Mitchell, T. J. (2005). Identification of a detrimental role for NK cells in pneumococcal pneumonia and sepsis in immunocompromised hosts.

Microbes Infect **7**, 845-852.

Kirkham, L. A., Jefferies, J. M., Kerr, A. R., Jing, Y., Clarke, S. C., Smith, A. & Mitchell, T. J. (2006a). Identification of invasive serotype 1 pneumococcal isolates that express nonhemolytic pneumolysin. *J Clin Microbiol* **44**, 151-159.

Kirkham, L. A., Kerr, A. R., Douce, G. R., Paterson, G. K., Dilts, D. A., Liu, D. F. & Mitchell, T. J. (2006b). Construction and immunological characterization of a novel nontoxic protective pneumolysin mutant for use in future pneumococcal vaccines. *Infect Immun* **74**, 586-593.

Klein, F., Hodges, D. R., Mahlandt, B. G., Jones, W. I., Haines, B. W. & Lincoln, R. E. (1962). Anthrax toxin: causative agent in the death of rhesus monkeys. *Science* **138**, 1331-1333.

Korchev, Y. E., Bashford, C. L. & Pasternak, C. A. (1992). Differential sensitivity of pneumolysin-induced channels to gating by divalent cations. *J Membr Biol* **127**, 195-203.

Korchev, Y. E., Bashford, C. L., Pederzoli, C., Pasternak, C. A., Morgan, P. J., Andrew, P. W. & Mitchell, T. J. (1998). A conserved tryptophan in pneumolysin is

a determinant of the characteristics of channels formed by pneumolysin in cells and planar lipid bilayers. *Biochem J* **329** (Pt 3), 571-577.

Lendrum, A. C., Fraser, D. S., Slidders, W. & Henderson, R. (1962). Studies on the character and staining of fibrin. *J Clin Pathol* **15**, 401-413.

Leppia, S. H. (1982). Anthrax toxin edema factor: a bacterial adenylate cyclase that increases cyclic AMP concentrations of eukaryotic cells. *Proc Natl Acad Sci U S A* **79**, 3162-3166.

Lety, M. A., Frehel, C., Dubail, I., Beretti, J. L., Kayal, S., Berche, P. & Charbit, A. (2001). Identification of a PEST-like motif in listeriolysin O required for phagosomal escape and for virulence in *Listeria monocytogenes*. *Mol Microbiol* **39**, 1124-1139.

Lety, M. A., Frehel, C., Berche, P. & Charbit, A. (2002). Critical role of the N-terminal residues of listeriolysin O in phagosomal escape and virulence of *Listeria monocytogenes*. *Mol Microbiol* **46**, 367-379.

Madden, J. C., Ruiz, N. & Caparon, M. (2001). Cytolysin-mediated translocation (CMT): a functional equivalent of type III secretion in gram-positive bacteria. *Cell* **104**, 143-152.

Malley, R., Henneke, P., Morse, S. C., Cieslewicz, M. J., Lipsitch, M., Thompson, C. M., Kurt-Jones, E., Paton, J. C., Wessels, M. R. & Golenbock,

D. T. (2003). Recognition of pneumolysin by Toll-like receptor 4 confers resistance to pneumococcal infection. *Proc Natl Acad Sci U S A* **100**, 1966-1971.

Meehl, M. A. & Caparon, M. G. (2004). Specificity of streptolysin O in cytolysin-mediated translocation. *Mol Microbiol* **52**, 1665-1676.

Menestrina, G., Bashford, C. L. & Pasternak, C. A. (1990). Pore-forming toxins: experiments with *S. aureus* alpha-toxin, *C. perfringens* theta-toxin and *E. coli* haemolysin in lipid bilayers, liposomes and intact cells. *Toxicon* **28**, 477-491.

Mengaud, J., Chenevert, J., Geoffroy, C., Gaillard, J. L. & Cossart, P. (1987). Identification of the structural gene encoding the SH-activated hemolysin of *Listeria monocytogenes*: listeriolysin O is homologous to streptolysin O and pneumolysin. *Infect Immun* **55**, 3225-3227.

Michel, E., Reich, K. A., Favier, R., Berche, P. & Cossart, P. (1990). Attenuated mutants of the intracellular bacterium *Listeria monocytogenes* obtained by single amino acid substitutions in listeriolysin O. *Mol Microbiol* **4**, 2167-2178.

Michos, A., Gryllos, I., Hakansson, A., Srivastava, A., Kokkotou, E. & Wessels, M. R. (2006). Enhancement of streptolysin O activity and intrinsic cytotoxic effects of the group A streptococcal toxin, NAD-glycohydrolase. *J Biol Chem* **281**, 8216-8223.

- Mitchell, T. J., Andrew, P. W., Saunders, F. K., Smith, A. N. & Boulnois, G. J. (1991).** Complement activation and antibody binding by pneumolysin via a region of the toxin homologous to a human acute-phase protein. *Mol Microbiol* **5**, 1883-1888.
- Mitsui, K., Sekiya, T., Okamura, S., Nozawa, Y. & Hase, J. (1979).** Ring formation of perfringolysin O as revealed by negative stain electron microscopy. *Biochim Biophys Acta* **558**, 307-313.
- Morgan, P. J., Hyman, S. C., Byron, O., Andrew, P. W., Mitchell, T. J. & Rowe, A. J. (1994).** Modeling the bacterial protein toxin, pneumolysin, in its monomeric and oligomeric form. *J Biol Chem* **269**, 25315-25320.
- Morgan, P. J., Hyman, S. C., Rowe, A. J., Mitchell, T. J., Andrew, P. W. & Saibil, H. R. (1995).** Subunit organisation and symmetry of pore-forming, oligomeric pneumolysin. *FEBS Lett* **371**, 77-80.
- Morise, H., Shimomura, O., Johnson, F. H. & Winant, J. (1974).** Intermolecular energy transfer in the bioluminescent system of *Aequorea*. *Biochemistry* **13**, 2656-2662.
- Mosmann, T. (1983).** Rapid colorimetric assay for cellular growth and survival: application to proliferation and cytotoxicity assays. *J Immunol Methods* **65**, 55-63.

Nagamune, H., Ohnishi, C., Katsuura, A., Fushitani, K., Whiley, R. A., Tsuji, A. & Matsuda, Y. (1996). Intermedilysin, a novel cytotoxin specific for human cells secreted by *Streptococcus intermedius* UNS46 isolated from a human liver abscess. *Infect Immun* **64**, 3093-3100.

Nagamune, H., Ohkura, K., Sukeno, A., Cowan, G., Mitchell, T. J., Ito, W., Ohnishi, O., Hattori, K., Yamato, M., Hirota, K., Miyake, Y., Maeda, T. & Kourai, H. (2004a). The human-specific action of intermedilysin, a homolog of streptolysin O, is dictated by domain 4 of the protein. *Microbiol Immunol* **48**, 677-692.

Nagamune, H., Ohkura, K., Umezumi, K., Shouji, H. & Kourai, H. (2004b). A cell membrane modification technique using domain 4 of intermedilysin for immunotherapy against cancer. *Anticancer Res* **24**, 3367-3372.

Nato, F., Reich, K., Lhopital, S., Rouyre, S., Geoffroy, C., Mazie, J. C. & Cossart, P. (1991). Production and characterization of neutralizing and nonneutralizing monoclonal antibodies against listeriolysin O. *Infect Immun* **59**, 4641-4646.

Nishibori, T., Xiong, H., Kawamura, I., Arakawa, M. & Mitsuyama, M. (1996). Induction of cytokine gene expression by listeriolysin O and roles of macrophages and NK cells. *Infect Immun* **64**, 3188-3195.

Nomura, T., Kawamura, I., Tsuchiya, K., Kohda, C., Baba, H., Ito, Y., Kimoto, T., Watanabe, I. & Mitsuyama, M. (2002). Essential role of interleukin-12 (IL-12) and IL-18 for gamma interferon production induced by listeriolysin O in mouse spleen cells. *Infect Immun* **70**, 1049-1055.

Ohkuni, H., Todome, Y., Okibayashi, F., Watanabe, Y., Ohtani, N., Ishikawa, T., Asano, G. & Kotani, S. (1997). Purification and partial characterization of a novel human platelet aggregation factor in the extracellular products of *Streptococcus mitis*, strain Nm-65. *FEMS Immunol Med Microbiol* **17**, 121-129.

Ohno-Iwashita, Y., Iwamoto, M., Mitsui, K., Ando, S. & Iwashita, S. (1991). A cytolysin, theta-toxin, preferentially binds to membrane cholesterol surrounded by phospholipids with 18-carbon hydrocarbon chains in cholesterol-rich region. *J Biochem (Tokyo)* **110**, 369-375.

Ohno-Iwashita, Y., Shimada, Y., Waheed, A. A., Hayashi, M., Inomata, M., Nakamura, M., Maruya, M. & Iwashita, S. (2004). Perfringolysin O, a cholesterol-binding cytolysin, as a probe for lipid rafts. *Anaerobe* **10**, 125-134.

Olofsson, A., Hebert, H. & Thelestam, M. (1993). The projection structure of perfringolysin O (*Clostridium perfringens* theta-toxin). *FEBS Lett* **319**, 125-127.

Oncu, S., Oncu, S. & Sakarya, S. (2003). Anthrax--an overview. *Med Sci Monit* **9**, RA276-283.

Owen, R. H., Boulnois, G. J., Andrew, P. W. & Mitchell, T. J. (1994). A role in cell-binding for the C-terminus of pneumolysin, the thiol-activated toxin of *Streptococcus pneumoniae*. *FEMS Microbiol Lett* **121**, 217-221.

Palmer, M., Harris, R., Freytag, C., Kehoe, M., Trantum-Jensen, J. & Bhakdi, S. (1998). Assembly mechanism of the oligomeric streptolysin O pore: the early membrane lesion is lined by a free edge of the lipid membrane and is extended gradually during oligomerization. *Embo J* **17**, 1598-1605.

Pamer, E. G., Harty, J. T. & Bevan, M. J. (1991). Precise prediction of a dominant class I MHC-restricted epitope of *Listeria monocytogenes*. *Nature* **353**, 852-855.

Park, J. M., Ng, V. H., Maeda, S., Rest, R. F. & Karin, M. (2004). Anthrolysin O and Other Gram-positive Cytolysins Are Toll-like Receptor 4 Agonists. *J Exp Med* **200**, 1647-1655.

Paton, J. C., Lock, R. A. & Hansman, D. J. (1983). Effect of immunization with pneumolysin on survival time of mice challenged with *Streptococcus pneumoniae*. *Infect Immun* **40**, 548-552.

Paton, J. C., Rowan-Kelly, B. & Ferrante, A. (1984). Activation of human complement by the pneumococcal toxin pneumolysin. *Infect Immun* **43**, 1085-1087.

Paton, J. C., Andrew, P. W., Boulnois, G. J. & Mitchell, T. J. (1993). Molecular analysis of the pathogenicity of *Streptococcus pneumoniae*: the role of pneumococcal proteins. *Annu Rev Microbiol* **47**, 89-115.

Peterson, W. D., Jr., Stulberg, C. S. & Simpson, W. F. (1971). A permanent heteroploid human cell line with type B glucose-6-phosphate dehydrogenase. *Proc Soc Exp Biol Med* **136**, 1187-1191.

Pinkney, M., Beachey, E. & Kehoe, M. (1989). The thiol-activated toxin streptolysin O does not require a thiol group for cytolytic activity. *Infect Immun* **57**, 2553-2558.

Polekhina, G., Giddings, K. S., Tweten, R. K. & Parker, M. W. (2005). Insights into the action of the superfamily of cholesterol-dependent cytolysins from studies of intermedilysin. *Proc Natl Acad Sci U S A* **102**, 600-605.

Portnoy, D. A., Jacks, P. S. & Hinrichs, D. J. (1988). Role of hemolysin for the intracellular growth of *Listeria monocytogenes*. *J Exp Med* **167**, 1459-1471.

Portnoy, D. A., Chakraborty, T., Goebel, W. & Cossart, P. (1992). Molecular determinants of *Listeria monocytogenes* pathogenesis. *Infect Immun* **60**, 1263-1267.

Prasher, D. C., Eckenrode, V. K., Ward, W. W., Prendergast, F. G. & Cormier, M. J. (1992). Primary structure of the *Aequorea victoria* green-fluorescent protein. *Gene* **111**, 229-233.

Prigent, D. & Alouf, J. E. (1976). Interaction of steptolysin O with sterols. *Biochim Biophys Acta* **443**, 288-300.

Ramachandran, R., Heuck, A. P., Tweten, R. K. & Johnson, A. E. (2002). Structural insights into the membrane-anchoring mechanism of a cholesterol-dependent cytolysin. *Nat Struct Biol* **9**, 823-827.

Ramachandran, R., Tweten, R. K. & Johnson, A. E. (2004). Membrane-dependent conformational changes initiate cholesterol-dependent cytolysin oligomerization and intersubunit beta-strand alignment. *Nat Struct Mol Biol* **11**, 697-705.

Ramachandran, R., Tweten, R. K. & Johnson, A. E. (2005). The domains of a cholesterol-dependent cytolysin undergo a major FRET-detected rearrangement during pore formation. *Proc Natl Acad Sci U S A* **102**, 7139-7144.

Ratner, A. J., Hippe, K. R., Aguilar, J. L., Bender, M. H., Nelson, A. L. & Weiser, J. N. (2006). Epithelial cells are sensitive detectors of bacterial pore-forming toxins. *J Biol Chem* **281**, 12994-12998.

Read, T. D., Peterson, S. N., Tourasse, N., Baillie, L. W., Paulsen, I. T., Nelson, K. E., Tettelin, H., Fouts, D. E., Eisen, J. A., Gill, S. R., Holtzapple, E. K., Okstad, O. A., Helgason, E., Rilstone, J., Wu, M., Kolonay, J. F., Beanan, M. J., Dodson, R. J., Brinkac, L. M., Gwinn, M., DeBoy, R. T., Madpu, R., Daugherty, S. C., Durkin, A. S., Haft, D. H., Nelson, W. C., Peterson, J. D., Pop, M., Khouri, H. M., Radune, D., Benton, J. L., Mahamoud, Y., Jiang, L., Hance, I. R., Weidman, J. F., Berry, K. J., Plaut, R. D., Wolf, A. M., Watkins, K. L., Nierman, W. C., Hazen, A., Cline, R., Redmond, C., Thwaite, J. E., White, O., Salzberg, S. L., Thomason, B., Friedlander, A. M., Koehler, T. M., Hanna, P. C., Kolsto, A. B. & Fraser, C. M. (2003). The genome sequence of *Bacillus anthracis* Ames and comparison to closely related bacteria. *Nature* **423**, 81-86.

Renart, J., Reiser, J. & Stark, G. R. (1979). Transfer of proteins from gels to diazobenzyloxymethyl-paper and detection with antisera: a method for studying antibody specificity and antigen structure. *Proc Natl Acad Sci U S A* **76**, 3116-3120.

Rossjohn, J., Feil, S. C., McKinstry, W. J., Tweten, R. K. & Parker, M. W. (1997). Structure of a cholesterol-binding, thiol-activated cytolysin and a model of its membrane form. *Cell* **89**, 685-692.

Rossjohn, J., Gilbert, R. J., Crane, D., Morgan, P. J., Mitchell, T. J., Rowe, A. J., Andrew, P. W., Paton, J. C., Tweten, R. K. & Parker, M. W. (1998). The molecular mechanism of pneumolysin, a virulence factor from *Streptococcus pneumoniae*. *J Mol Biol* **284**, 449-461.

Rubins, J. B., Charboneau, D., Paton, J. C., Mitchell, T. J., Andrew, P. W. & Janoff, E. N. (1995). Dual function of pneumolysin in the early pathogenesis of murine pneumococcal pneumonia. *J Clin Invest* **95**, 142-150.

Sacchetti, A., Cappetti, V., Marra, P., Dell'Arciprete, R., El Sewedy, T., Crescenzi, C. & Alberti, S. (2001). Green Fluorescent Protein variants fold differentially in prokaryotic and eukaryotic cells. *J Cell Biochem* **81**, 117-128.

Salo, P., Narvanen, A. & Leinonen, M. (1993). Mapping of immunoreactive sites of pneumococcal pneumolysin by use of synthetic peptides. *Infect Immun* **61**, 2822-2826.

Sato, K., Quartey, M. K., Liebeler, C. L., Le, C. T. & Giebink, G. S. (1996). Roles of autolysin and pneumolysin in middle ear inflammation caused by a type 3 *Streptococcus pneumoniae* strain in the chinchilla otitis media model. *Infect Immun* **64**, 1140-1145.

Saunders, F. K., Mitchell, T. J., Walker, J. A., Andrew, P. W. & Boulnois, G. J. (1989). Pneumolysin, the thiol-activated toxin of *Streptococcus pneumoniae*, does not require a thiol group for in vitro activity. *Infect Immun* **57**, 2547-2552.

Schnupf, P., Hofmann, J., Norseen, J., Glomski, I. J., Schwartzstein, H. & Decatur, A. L. (2006a). Regulated translation of listeriolysin O controls virulence of *Listeria monocytogenes*. *Mol Microbiol* **61**, 999-1012.

- Schnupf, P., Portnoy, D. A. & Decatur, A. L. (2006b).** Phosphorylation, ubiquitination and degradation of listeriolysin O in mammalian cells: role of the PEST-like sequence. *Cell Microbiol* **8**, 353-364.
- Schuerch, D. W., Wilson-Kubalek, E. M. & Tweten, R. K. (2005).** Molecular basis of listeriolysin O pH dependence. *Proc Natl Acad Sci U S A* **102**, 12537-12542.
- Schwandner, R., Dziarski, R., Wesche, H., Rothe, M. & Kirschning, C. J. (1999).** Peptidoglycan- and lipoteichoic acid-induced cell activation is mediated by toll-like receptor 2. *J Biol Chem* **274**, 17406-17409.
- Sekiya, K., Danbara, H. & Futaesaku, Y. (1993).** [Mechanism of pore formation on erythrocyte membrane by streptolysin-O]. *Kansenshogaku Zasshi* **67**, 736-740.
- Sekiya, K., Danbara, H., Yase, K. & Futaesaku, Y. (1996).** Electron microscopic evaluation of a two-step theory of pore formation by streptolysin O. *J Bacteriol* **178**, 6998-7002.
- Sekiya, K., Danbara, H., Futaesaku, Y., Haque, A., Sugimoto, N. & Matsuda, M. (1998).** Formation of ring-shaped structures on erythrocyte membranes after treatment with botulinolysin, a thiol-activated hemolysin from *Clostridium botulinum*. *Infect Immun* **66**, 2987-2990.

Shannon, J. G., Ross, C. L., Koehler, T. M. & Rest, R. F. (2003).

Characterization of Anthrolysin O, the *Bacillus anthracis* Cholesterol-Dependent Cytolysin. *Infect Immun* **71**, 3183-3189.

Shepard, L. A., Heuck, A. P., Hamman, B. D., Rossjohn, J., Parker, M. W.,

Ryan, K. R., Johnson, A. E. & Tweten, R. K. (1998). Identification of a membrane-spanning domain of the thiol-activated pore-forming toxin *Clostridium perfringens* perfringolysin O: an alpha-helical to beta-sheet transition identified by fluorescence spectroscopy. *Biochemistry* **37**, 14563-14574.

Shepard, L. A., Shatursky, O., Johnson, A. E. & Tweten, R. K. (2000). The

mechanism of pore assembly for a cholesterol-dependent cytolysin: formation of a large prepore complex precedes the insertion of the transmembrane beta-hairpins. *Biochemistry* **39**, 10284-10293.

Shimomura, O., Johnson, F. H. & Saiga, Y. (1962). Extraction, purification and properties of aequorin, a bioluminescent protein from the luminous hydromedusan, *Aequorea*. *J Cell Comp Physiol* **59**, 223-239.

Solovyova, A. S., Nollmann, M., Mitchell, T. J. & Byron, O. (2004). The solution structure and oligomerization behavior of two bacterial toxins: pneumolysin and perfringolysin O. *Biophys J* **87**, 540-552.

Stringaris, A. K., Geisenhainer, J., Bergmann, F., Balshusemann, C., Lee, U., Zysk, G., Mitchell, T. J., Keller, B. U., Kuhnt, U., Gerber, J., Spreer, A., Bahr,

- M., Michel, U. & Nau, R. (2002).** Neurotoxicity of Pneumolysin, a Major Pneumococcal Virulence Factor, Involves Calcium Influx and Depends on Activation of p38 Mitogen-Activated Protein Kinase. *Neurobiol Dis* **11**, 355-368.
- Sung, C. K., Li, H., Claverys, J. P. & Morrison, D. A. (2001).** An *rpsL* cassette, janus, for gene replacement through negative selection in *Streptococcus pneumoniae*. *Appl Environ Microbiol* **67**, 5190-5196.
- Tanabe, Y., Xiong, H., Nomura, T., Arakawa, M. & Mitsuyama, M. (1999).** Induction of protective T cells against *Listeria monocytogenes* in mice by immunization with a listeriolysin O-negative avirulent strain of bacteria and liposome-encapsulated listeriolysin O. *Infect Immun* **67**, 568-575.
- Tartof, K. D. & Hobbs, C. A. (1987).** Improved Media for Growing Plasmid and Cosmid Clones. *Bethesda Res Lab Focus* **9**, 14.
- Tilley, S. J., Orlova, E. V., Gilbert, R. J., Andrew, P. W. & Saibil, H. R. (2005).** Structural basis of pore formation by the bacterial toxin pneumolysin. *Cell* **121**, 247-256.
- Tsuchiya, K., Kawamura, I., Takahashi, A., Nomura, T., Kohda, C. & Mitsuyama, M. (2005).** Listeriolysin O-induced membrane permeation mediates persistent interleukin-6 production in Caco-2 cells during *Listeria monocytogenes* infection in vitro. *Infect Immun* **73**, 3869-3877.

Tweten, R. K. (1988). Nucleotide sequence of the gene for perfringolysin O (theta-toxin) from *Clostridium perfringens*: significant homology with the genes for streptolysin O and pneumolysin. *Infect Immun* **56**, 3235-3240.

Tweten, R. K., Parker, M. W. & Johnson, A. E. (2001). The cholesterol-dependent cytolysins. *Curr Top Microbiol Immunol* **257**, 15-33.

Van Epps, D. E. & Andersen, B. R. (1971). Streptolysin O II. Relationship of Sulfhydryl Groups to Activity. *Infection and Immunity* **3**, 648-652.

Walev, I., Hombach, M., Bobkiewicz, W., Fenske, D., Bhakdi, S. & Husmann, M. (2002). Resealing of large transmembrane pores produced by streptolysin O in nucleated cells is accompanied by NF-kappaB activation and downstream events. *Faseb J* **16**, 237-239.

Walker, J. A., Allen, R. L., Falmagne, P., Johnson, M. K. & Boulnois, G. J. (1987). Molecular cloning, characterization, and complete nucleotide sequence of the gene for pneumolysin, the sulfhydryl-activated toxin of *Streptococcus pneumoniae*. *Infect Immun* **55**, 1184-1189.

Watanabe, I., Nomura, T., Tominaga, T., Yamamoto, K., Kohda, C., Kawamura, I. & Mitsuyama, M. (2006). Dependence of the lethal effect of pore-forming haemolysins of Gram-positive bacteria on cytolytic activity. *J Med Microbiol* **55**, 505-510.

Wei, Z., Schnupf, P., Poussin, M. A., Zenewicz, L. A., Shen, H. & Goldfine, H. (2005). Characterization of *Listeria monocytogenes* Expressing Anthrolysin O and Phosphatidylinositol-Specific Phospholipase C from *Bacillus anthracis*. *Infect Immun* **73**, 6639-6646.

Weis, S. & Palmer, M. (2001). Streptolysin O: the C-terminal, tryptophan-rich domain carries functional sites for both membrane binding and self-interaction but not for stable oligomerization. *Biochim Biophys Acta* **1510**, 292-299.

Wellmer, A., Zysk, G., Gerber, J., Kunst, T., Von Mering, M., Bunkowski, S., Eiffert, H. & Nau, R. (2002). Decreased virulence of a pneumolysin-deficient strain of *Streptococcus pneumoniae* in murine meningitis. *Infect Immun* **70**, 6504-6508.

Yang, W. S., Park, S. O., Yoon, A. R., Yoo, J. Y., Kim, M. K., Yun, C. O. & Kim, C. W. (2006). Suicide cancer gene therapy using pore-forming toxin, streptolysin O. *Mol Cancer Ther* **5**, 1610-1619.

Yoshikawa, H., Kawamura, I., Fujita, M., Tsukada, H., Arakawa, M. & Mitsuyama, M. (1993). Membrane damage and interleukin-1 production in murine macrophages exposed to listeriolysin O. *Infect Immun* **61**, 1334-1339.

Yuntao, W. (2004). Targeting HIV-1 infected Brain Macrophages by a novel lentiviral vector carrying Anthrolysin O (Abstract). In *Crossing Boundaries: Medical Biodefense & Civilian Medicine*.